AD-A061 449 INCOSYM INC CALABASAS CA F/G 17/7
FAILURE MODES AND REDUNDANCY ANALYSIS FOR THE MULTIFUNCTION INE--ETC(U)
MAR 78 R J CRAIG, J RUSSELL F33615-77-C-3015
UNCLASSIFIED AFFDL-TR-78-25 NL

1 OF 2
AD A061449

AFFDL-TR-78-25

LEVEL II

(12) B.S.

FAILURE MODES AND REDUNDANCY ANALYSIS FOR THE MULTIFUNCTION INERTIAL REFERENCE ASSEMBLY (MIRA)

INCOSYM, INC.
780 Lakefield Rd.
Westlake Village, CA 91361

MARCH 1978

TECHNICAL REPORT AFFDL-TR-78-25

Final Report January 1977 - December 1977

Approved for public release; distribution unlimited

AIR FORCE FLIGHT DYNAMICS LABORATORY
AIR FORCE WRIGHT AERONAUTICAL LABORATORIES
AIR FORCE SYSTEMS COMMAND
WRIGHT-PATTERSON AFB, OHIO 45433

NOTICE

When Government drawings, specifications, or other data are used for any purpose other than in connection with a definitely related Government procurement operation, the United States Government thereby incurs no responsibility nor any obligation whatsoever; and the fact that the government may have formulated, furnished, or in any way supplied the said drawings, specifications, or other data, is not to be regarded by implication or otherwise as in any manner licensing the holder or any other person or corporation, or conveying any rights or permission to manufacture, use, or sell any patented invention that may in any way be related thereto.

This report has been reviewed by the Information Office (OI) and is releasable to the National Technical Information Service (NTIS). At NTIS, it will be available to the general public, including foreign nations.

This technical report has been reviewed and is approved for publication.

JOHN M. PERDZOCK
Project Manager

EVARD H. FLINN, Chief
Control Systems Development Branch
Flight Control Division

FOR THE COMMANDER

MORRIS A. OSTGAARD
Assistant for Research
and Technology
Flight Control Division

"If your address has changed, if you wish to be removed from our mailing list, or if the addressee is no longer employed by your organization please notify AFFDL/FGL *,W-PAFB, OH 45433 to help us maintain a current mailing list".*

Copies of this report should not be returned unless return is required by security considerations, contractual obligations, or notice on a specific document.

AIR FORCE/56780/3 November 1978 — 250

UNCLASSIFIED

SECURITY CLASSIFICATION OF THIS PAGE (When Data Entered)

(19) **REPORT DOCUMENTATION PAGE**

READ INSTRUCTIONS BEFORE COMPLETING FORM

(18) 1. REPORT NUMBER: AFFDL-TR-78-25

2. GOVT ACCESSION NO.

(9) 3. RECIPIENT'S CATALOG NUMBER

(6) 4. TITLE (and Subtitle): FAILURE MODES AND REDUNDANCY ANALYSIS FOR THE MULTIFUNCTION INERTIAL REFERENCE ASSEMBLY (MIRA).

5. TYPE OF REPORT & PERIOD COVERED: FINAL rept. 3 Jan - 22 Dec 1977,

6. PERFORMING ORG. REPORT NUMBER

(10) 7. AUTHOR(s): R.J. Craig, J. Russell

(15) 8. CONTRACT OR GRANT NUMBER(s): F33615-77-C-3015 New

9. PERFORMING ORGANIZATION NAME AND ADDRESS
INCOSYM, INC. Calabasas
780 Lakefield Rd.
Former ~~Westlake Village,~~ CA 91361

(16) 10. PROGRAM ELEMENT, PROJECT, TASK AREA & WORK UNIT NUMBERS: 24030224 (12) 02

62201F

11. CONTROLLING OFFICE NAME AND ADDRESS
Air Force Flight Dynamics Laboratory (FGL)
Air Force Systems Command
Wright-Patterson AFB, Ohio 45433

(11) 12. REPORT DATE: March 1978

13. NUMBER OF PAGES: 147

14. MONITORING AGENCY NAME & ADDRESS(if different from Controlling Office)
(12) 149p.

15. SECURITY CLASS. (of this report): Unclassified

15a. DECLASSIFICATION/DOWNGRADING SCHEDULE

16. DISTRIBUTION STATEMENT (of this Report)

Approved for public release, distribution unlimited

17. DISTRIBUTION STATEMENT (of the abstract entered in Block 20, if different from Report)

18. SUPPLEMENTARY NOTES

19. KEY WORDS (Continue on reverse side if necessary and identify by block number)

Gyroscope	Redundancy	Dodecahedron
Accelerometer	Fail-op/Fail-op	Failure
Skewed axes	Tetrahedron	Multisensor

20. ABSTRACT (Continue on reverse side if necessary and identify by block number)

This report analyzes potential failure modes for various gyroscope and accelercmeter designs and their associated electronics and considers the most appropriate mechanizations to accomplish a fail-operational/fail-operational Inertial Reference Assembly.

DD FORM 1 JAN 73 1473 EDITION OF 1 NOV 65 IS OBSOLETE

UNCLASSIFIED

SECURITY CLASSIFICATION OF THIS PAGE (When Data Entered)

LB

393 014 78 11 15 158

FOREWORD

The MIRA Failure Modes and Redundancy Analysis Program was started on 3 January 1977 and completed on 22 December 1978. This report presents the results.

This document was prepared by INCOSYM, Inc., Westlake Village, California, under U. S. Air Force Contract No. F33615-77-C-3015.

The program was sponsored and administered by the Air Force Flight Dynamics Laboratory, Wright-Patterson Air Force Base, Ohio. The Air Force Project Manager directing the technical and management aspects of the program was John M. Perdzock, AFFDL/FGL.

Principal contributors to this report are Mr. J. Russell and Mr. R. J. Craig of INCOSYM, Inc.

The authors wish to acknowledge the contributions to the content reported herein of the MIRA project personnel at the McDonnell Douglas Corporation (MDC) under the direction of Mr. R. C. Burns, MIRA Project Manager, MDC.

This Final Report was submitted by the authors in March 1978.

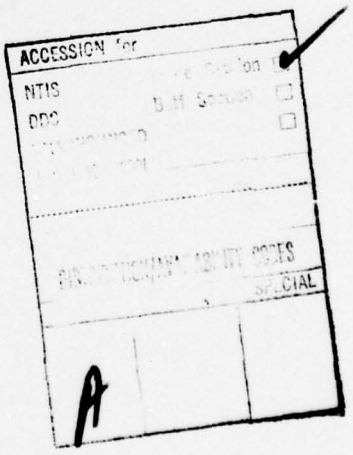

TABLE OF CONTENTS

TABLE OF CONTENTS (Continued)

TABLE OF CONTENTS (Continued)

LIST OF ILLUSTRATIONS

LIST OF TABLES

LIST OF TABLES (Continued)

SECTION I

INTRODUCTION

This report analyzes potential failure modes for various gyro and accelerometer designs and their associated electronics and considers the most appropriate redundant mechanizations for these sensors.

The intent is to establish optimum configurations for a Multifunction Inertial Reference Assembly (MIRA) using various sensors generally in a skewed axes array. The resultant MIRA system is intended to provide the required angular rate and translational acceleration measurements for flight control, navigation, weapon delivery, cockpit display and terminal area control.

The sensors considered are two-degrees-of-freedom tuned rotor gyros, single-degree-of-freedom floated gyros, laser gyros, single and two-degree-of-freedom accelerometers and a multisensor configuration based on a tuned rotor gyro. Failure rates were established for these types of sensors and their electronics. Then, system mechanizations were considered and their deficiencies were examined.

All systems are required to be fail-operational/fail-operational. The definition of fail-operational/fail-operational redundancy is that the system can DETECT and ISOLATE two separate failures of any of its component parts. Some consideration was initially given to system mechanizations that could detect two failures, but only isolate the first failure. These have been referred to in past literature as fail-op/fail-safe. However, for a fail-safe mode to be valid assumes that the redundant system is neither flight critical or mission critical. As the MIRA concept is to integrate avionics functions, there will be a high percentage of applications where the equipment is flight or mission critical. Therefore, a fail-op/fail-safe system was not considered appropriate for MIRA.

The failure detection and isolation in the mechanizations studied is all based on comparison of the outputs of the system sensors. The addition or implementation of Built-in-Test (BIT) to augment failure detection and

isolation was not part of the intent of this report. The addition of BIT to any system could possibly improve the probability of failure detection and isolation, but it does not alter the basic configuration. To obtain fail-op/fail-op redundancy, a minimum of four two-degree-of-freedom (the system must be configured to allow for both axes to fail) or six single-degree-of-freedom instruments must be implemented in some manner. Any increase in the instrument complement over the minimum is to improve packaging efficiency, survivability or performance rather than reliability. Therefore, there does not appear to be a viable trade-off between BIT and the number of instruments.

SECTION II

FAILURE RATES FOR VARIOUS INERTIAL INSTRUMENTS AND THEIR ASSOCIATED ELECTRONICS

The following section analyzes the failure rates for various instruments and their associated electronics. The methodology used was to analyze the probability of failure of typical instrument components, e.g., coils, bearings, suspensions, and apply these to various instrument configurations. For the electronics, a typical design was analyzed and then modified to fit various instruments.

The results show failure rates for accelerometers that approximate those observed in applications, although, in general, somewhat lower. The computed gyro failure rates were lower than present experience shows for aircraft applications. Further analysis, however, reveals two reasons for this.

First, the present gyros used in production configurations are heated, and for aircraft, high heat rates are used to improve reaction time. Also, it has been observed that a large percentage of failures are due to case leak problems. Our analysis suggests that the hermetic seals on gyros are being over stressed due to the high heat rates applied.

Secondly, all present gyros in aircraft operate at much higher rotational speeds than the gyros that are being used in the preproduction strapdown systems presently being designed. The present production systems are of course, gimbaled. This higher rotational speed greatly increases bearing wear, which affects gyro operation.

The following analysis only addresses catastrophic, i.e., complete failures. It does not address "out-of-tolerance" or recalibration occurrences. In production systems presently in the field, failure data is often contaminated by the inability to determine the difference between a catastrophic and "out-of-tolerance" failure.

One other factor that a redundant system should improve is the false indication of failure, that often occurs in present systems.

The definition of airborne-inhabited and airborne-uninhabited environment is from Reference I. Airborne-inhabited means the equipment is located in an area controlled for crew members, whereas airborne-uninhabited means that the location is outside the crew compartment.

2.1 Failure rates for the TDF gyro and associated electronics assembly. The failure rate for a two-degree-of-freedom, dry tuned gyro and its associated electronics in an uninhabited flight environment is estimated to be 76 per million hours for a two-axes failure and 8 per million hours for a single-axis failure. Table 1 lists the failure rates for the major sub-assemblies. The gyro failure rate accounts for approximately 11 out of the 76, while the electronics accounts for the other 65 for the two-axes failure case. For the single axis failure case, the gyro accounts for 0.104 and the electronics 8.028. From the relative numbers, it is obvious that a single axis failure can hardly ever happen in a gyro; both axes are nearly always effected. The only possibility of a single axis electronic failure is if the I/O for that axis fails. Any failure in one axis of the torquing electronics, for example, will cause an open loop condition which will affect the other axis.

TABLE 1. FAILURE RATES FOR THE TDF GYRO AND ASSOCIATED ELECTRONICS FOR UNINHABITED AIRBORNE ENVIRONMENT

Assembly	Failure Rates (Per 10^6 Hrs)	
	Single Axis	Two Axes
Gyro	0.104	10.500
Preamplifier	-	1.708
Digital Caging Amplifier	-	23.443
Spin Power Supply	-	18.635
I/O	8.028	-
Power Supply	-	21.548
Total	8.132	75.834

[I] Military Standardization Handbook. Reliability Prediction of Electronic Equipment, Military Handbook 217B, 20 September 1974, Department of Defense.

The one-and two-axis failures are calculated separately so that the axes orientation can be optimized for failure detection in Section III.

2.1.1 Failure rates for the electronics. Tables 2 through 9 show failure rates for typical electronics that are used with the TDF gyro. Digital pulse width binary torquing electronics were selected because this type would appear to be most commonly used in newer systems.

TABLE 2. RELIABILITY PREDICTION DATA FOR THE PREAMPLIFIER AIRBORNE UNINHABITED

Quant (η)	Part Type/Assembly		Stress Ratio	Individual Failure Rate $(\lambda)/10^6$ Hrs	Total Failure Rate $(\eta\lambda)/10^6$ Hrs
2	I.C. SSI/MSI	(LM118)	-	0.641	1.282
4	Capacitor Ceramic	(CKR)	0.4	0.022	0.088
4	Capacitor Glass	(CYR)	0.4	0.072	0.288
10	Resistor, Carbon	(RCR)	0.2	0.005	0.050

Assembly Failure Rate 1.708 Failures/10^6 Hours

Assembly MTBF 5.85×10^5 Hours

TABLE 3. RELIABILITY PREDICTION DATA FOR THE DIGITAL TORQUING ELECTRONICS AIRBORNE UNINHABITED

Quant (η)	Part Type/Assembly		Stress Ratio	Individual Failure Rate (λ)	Total Failure Rate ($\eta\lambda$)
2	I.C., SSI/MSI Digital	(CD4053)	-	0.263	0.526
2	I.C., SSI/MSI Digital	(AM1500)	-	0.071	0.142
1	I.C., SSI/MSI Linear (M38510/ 10304)	(LM111)	-	0.482	0.482
2	I.C., SSI/MSI Linear	(LM112)	-	0.533	1.066
4	I.C., SSI/MSI Linear	(LM118)	-	0.641	2.564
2	Transistor, NPN, Linear	(JANTX)	0.2	0.079	0.158
8	Transistor, PNP, Linear	(JANTX)	0.2	0.130	1.040
8	Transistor, Field Effect, Linear	(JANTX)	0.2	0.744	5.952
18	Diode, General Purpose	(JANTX)	0.2	0.120	2.160
2	Diode, Zener	(JANTX)	0.2	0.244	0.488
20	Capacitor, Ceramic	(CKR)	0.4	0.022	0.440
4	Capacitor, Tant. Solid	(CSR)	0.4	0.026	0.104
5	Resistor, Film	(RNC)	0.2	0.011	0.055
52	Resistor, Carbon Composition	(RCR)	0.2	0.005	0.260
2	Resistor, Variable	(RTR)	0.2	0.083	0.166
1	Connector, 90 Pin		-	7.840	7.840

Assembly Failure Rate 23.443 Failures/10^6 Hours

Assembly MTBF 42,656 Hours

TABLE 4. RELIABILITY PREDICTION DATA FOR THE GYRO MOTOR ELECTRONICS AIRBORNE UNINHABITED

Quant. (η)	Part Type/Assembly		Stress Ratio	Individual Failure Rate (λ)	Total Failure Rate (ηλ)
1	I.C., SSI/MSI Digital (M38510/05001)	(CD4011)	-	0.094	0.094
3	I.C., SSI/MSI Digital (M38510/05102)	(CD4027)	-	0.313	0.939
1	I.C., SSI/MSI Digital ( )	(CD4029)	-	0.330	0.330
3	I.C., SSI/MSI Digital (M38510/01306)	(SN54161)	-	0.246	0.738
3	I.C., SSI/MSI Digital	(DM7095)	-	0.119	0.357
2	I.C., SSI/MSI Digital	(SN54LS112)	-	0.126	0.252
2	I.C., SSI/MSI Digital (M38510/00104)	(SN5400)	-	0.103	0.206
2	I.C., SSI/MSI Digital (M38510/00105)	(SN5404)	-	0.111	0.222
1	I.C., SSI/MSI Digital (M38510/00102)	(SN5420)	-	0.082	0.082
1	I.C., SSI/MSI Digital (M38510/00901)	(SN5493)	-	0.224	0.224
1	I.C., SSI/MSI Digital (M38510/01403)	(SN54153)	-	0.150	0.150
5	I.C., SSI/MSI Digital (M38510/01304)	(SN54163)	-	0.246	1.230
1	I.C., SSI/MSI, Linear	(LM105)	-	0.395	0.395
1	I.C., SSI/MSI, Linear	(LM112)	-	0.533	0.533
1	I.C., SSI/MSI, Linear	(LM139)	-	0.482	0.482
1	Transistor, NPN, Logic Switch	(JANTX)	0.2	0.037	0.037
6	Transistor, NPN, Linear	(JANTX)	0.2	0.079	0.474
1	Transistor, PNP, Linear	(JANTX)	0.2	0.130	0.130
3	Diode, General Purpose	(JANTX)	0.2	0.120	0.360
12	Diode, SCR	(JANTX)	0.2	0.244	2.928
8	Capacitor, Ceramic	(CKR)	0.4	0.022	0.176
5	Capacitor, Tant. Solid	(CSR)	0.4	0.026	0.130
30	Resistor, Film	(RLR)	0.2	0.010	0.300
1	Resistor, W.W., Power	(RWR)	0.2	0.026	0.026
1	Connector, 90 Pin		-	7.840	7.840

Assembly Failure Rate 18.635 Failures/10^6 Hours

Assembly MTBF 53,662 Hours

TABLE 5. RELIABILITY PREDICTION DATA FOR THE I/O ELECTRONICS AIRBORNE UNINHABITED

Quant (η)	Part Type/Assembly		Stress Ratio	Individual Failure Rate (λ)	Total Failure Rate ($\eta\lambda$)
1	I.C., 1024 Bit PROM	(AM5300)	-	1.372	1.372
1	I.C., SSI/MSI Digital	(AM1500)	-	0.071	0.071
1	I.C., SSI/MSI Digital (M38510/ 00104)	(SN5400)	-	0.103	0.103
1	I.C., SSI/MSI Digital (M38510/ 00401)	(SN5402)	-	0.111	0.111
1	I.C., SSI/MSI Digital (M38510/ 01203)	(SN54123)	-	0.126	0.126
2	I.C., SSI/MSI Digital (M38510/ 01306)	(SN54161)	-	0.246	0.492
4	I.C., SSI/MSI Digital (M38510/ 00903)	(SN54164)	-	0.241	0.964
2	I.C., SSI/MSI Digital (M38510/ 07102)	(SN54LS112)	-	0.126	0.252
3	I.C., SSI/MSI Digital	(SN545257)	-	0.168	0.504
1	I.C., SSI/MSI Linear (M38510/ 10101)	(LM741)	-	0.420	0.420
4	Capacitor, Ceramic	(CKR)	0.4	0.022	0.088
1	Capacitor, Tant. Solid	(CSR)	0.4	0.026	0.026
10	Resistor, Film	(RLR)	0.2	0.010	0.100
20	Resistor, Carbon Composition	(RCR)	0.2	0.005	0.100
1	Connector, 45 Pin		-	3.299	3.299

Assembly Failure Rate 8.028 Failures/10^6 Hours

Assembly MTBF 124,564 Hours

TABLE 6. RELIABILITY PREDICTION DATA FOR THE POWER SUPPLY ASSEMBLY AIRBORNE UNINHABITED

Quant. (η)	Part Type/Assembly	See Page	Individual Failure Rate (λ)	Total Failure Rate (ηλ)
1	Power Supply Card	2-8	13.983	13.983
1	+5 Volt Supply Module	2-10	0.835	0.835
1	High Voltage Supply Card	2-9	6.730	6.730

Assembly Failure Rate 21.548 Failures/10^6 Hours

Assembly MTBF 46,408 Hours

TABLE 7. RELIABILITY PREDICTION DATA FOR THE POWER SUPPLY CARD AIRBORNE UNINHABITED

Quant. (η)	Part Type/Assembly		Stress Ratio	Individual Failure Rate (λ)	Total Failure Rate (ηλ)
1	I.C., SSI/MSI Linear	(LM105)	-	0.395	0.395
1	I.C., SSI/MSI Linear	(LM111)	-	0.482	0.482
3	I.C., SSI/MSI Linear	(LM139)	-	0.482	1.446
11	Transistor, NPN, Linear		0.2	0.079	0.869
4	Transistor, PNP, Linear		0.2	0.130	0.520
12	Diode, General Purpose		0.2	0.120	1.440
6	Diode, Zener		0.2	0.244	1.464
13	Diode, Rectifier		0.2	0.181	2.353
10	Capacitor, Tant. Solid	(CSR)	0.4	0.026	0.260
28	Capacitor, Ceramic	(CKR)	0.4	0.022	0.616
2	Capacitor, Polycarbonate	(CHR)	0.4	0.001	0.002
32	Resistor, Film	(RLR)	0.2	0.010	0.320
1	Resistor, Film	(RNC)	0.2	0.011	0.011
26	Resistor, Carbon Composition	(RCR)	0.2	0.005	0.130
8	Resistor, W.W., Power	(RWR)	0.2	0.026	0.208
1	Resistor, Variable	(RTR)	0.2	0.083	0.083
11	Coil, Power		-	0.101	1.111
2	Transformer, Power		-	0.101	0.201
1	Connector, 30 Pin		-	2.072	2.072

Assembly Failure Rate 13.983 Failures/10^6 Hours

Assembly MTBF 71,515 Hours

TABLE 8. RELIABILITY PREDICTION DATA FOR THE HIGH VOLTAGE SUPPLY AIRBORNE UNINHABITED

Quant (η)	Part Type/Assembly		Stress Ratio	Individual Failure Rate (λ)	Total Failure Rate ($\eta\lambda$)
1	I.C., SSI/MSI Linear	(LM124)	-	0.804	0.804
11	Transistor, NPN, Linear		0.2	0.079	0.869
1	Transistor, PNP, Linear		0.2	0.130	0.130
10	Diode, General Purpose		0.2	0.120	1.200
6	Diode, Rectifier		0.2	0.181	1.086
5	Capacitor, Tant. Solid	(CSR)	0.4	0.026	0.130
8	Capacitor, Ceramic	(CKR)	0.4	0.022	0.176
1	Capacitor, Polycarbonate	(CHR)	0.4	0.001	0.001
12	Resistor, Film	(RLR)	0.2	0.010	0.120
25	Resistor, Carbon Composition	(RCR)	0.2	0.005	0.125
4	Resistor, W.W., Power	(RWR)	0.2	0.026	0.104
3	Coil, Power		-	0.101	0.303
2	Transformer, Power		-	0.101	0.202
1	Connector, 20 Pin		-	1.480	1.480

Assembly Failure Rate 6.730 Failures/10^6 Hours

Assembly MTBF 148,588 Hours

TABLE 9. RELIABILITY PREDICTION DATA FOR THE +5 VOLT SUPPLY MODULE AIRBORNE UNINHABITED

Quant (n)	Part Type/Assembly		Stress Ratio	Individual Failure Rate (λ)	Total Failure Rate ($n\lambda$)
1	I.C., SSI/MSI Linear	(LM107)	-	0.451	0.451
2	Transistor, NPN, Linear		0.2	0.079	0.158
1	Transistor, PNP, Linear		0.2	0.130	0.130
1	Capacitor, Tant. Solid	(CSR)	0.4	0.026	0.026
4	Capacitor, Ceramic	(CKR)	0.4	0.022	0.088
3	Resistor, Film	(RLR)	0.2	0.010	0.030
8	Resistor, Carbon Composition	(RCR)	0.2	0.005	0.040

Assembly Failure Rate 0.835 Failures/10^6 Hours

Assembly MTBF 1,197,605 Hours

2.1.2 Failure rates for the two-degree-of-freedom dry tuned rotor gyro. Table 10 lists the TDF gyro failure rates for eight different environments for 10,000 hours of gyro operation. Table 11 lists these rates for 100,000 hours of operation. The base failure rate for 10,000 hours of operation is 1.129 per million hours, and for 100,000 hours of operation is 6.139 per million hours. The gyro bearings cause this difference in failure rates as a function of operating time, since bearing failure is a wear-out phenomena. Thus, for 100,000 hours of operation, the bearing failure rate of 5.0 per million hours is the dominant rate; while, for 10,000 hours of operation the feedthrough failure rate of 0.710 per million hours is the dominant rate.

The failure rate for a single axis only, of 0.0112 per million hours, is the result of shorted turns in the torquer coils.

Table 12 lists the base failure rates for the gyro components.

TABLE 10. TWO-DEGREE-OF-FREEDOM DRY TUNED ROTOR GYRO FAILURE RATES VERSUS ENVIRONMENTS FOR 10,000 HOUR OPERATION

Environment	Multiplier	Single Axis Failure Rate (Per 10^6 Hrs)	Two Axis Failure Rate (Per 10^6 Hrs)
Base Rate	1.0	0.0112	1.129
Ground, Fixed	1.5	0.0168	1.694
Space, Flight	2.0	0.0224	2.258
Airborne, Inhabited	2.5	0.0280	2.823
Naval, Sheltered	4.5	0.0504	5.081
Ground, Mobile	6.0	0.0672	6.774
Naval, Unsheltered	7.7	0.0862	8.693
Airborne, Uninhabited	9.3	0.1041	10.500
Missile, Launch	10.0	0.1120	11.290

TABLE 11. TWO-DEGREE-OF-FREEDOM DRY TUNED ROTO..
FAILURE RATES VERSUS ENVIRONMENTS FOR
100,000 HOUR OPERATION

Environment	Multiplier	Single Axis Failure Rate (Per 10^6 Hrs)	Two Axis Failure Rate (Per 10^6 Hrs)
Base Rate	1.0	0.0112	6.139
Ground, Fixed	1.5	0.0168	9.209
Space, Flight	2.0	0.0224	12.278
Airborne, Inhabited	2.5	0.0280	15.348
Naval, Sheltered	4.5	0.0504	27.626
Ground, Mobile	6.0	0.0672	36.834
Naval, Unsheltered	7.7	0.0862	47.270
Airborne, Uninhabited	9.3	0.1041	57.093
Missile, Launch	10.0	0.1120	61.390

TABLE 12. TWO-DEGREE-OF-FREEDOM DRY TUNED ROTOR GYRO BASE FAILURE RATES FOR COMPONENTS FOR 10,000 HOUR OPERATION AND 100,000 HOUR OPERATION

Gyro Component	Base Rate For 10^4 Hours Operation (Per 10^6 Hrs)	Base Rate For 10^5 Hours Operation (Per 10^6 Hrs)
Coils Single Axis Fail	0.0112	0.0112
Coils Two Axis Fail	0.0218	0.0218
Bearings Two Axis Fail	0.000002	5.0
Suspension Two Axis Fail	0.00008	0.00008
Cement Joints Two Axis Fail	0.0002	0.0002
Feedthrus Two Axis Fail	0.71	0.71
Solder Connections	0.396	0.396
Total Single Axis Fail	0.0112	0.0112
Total Two Axes Fail	1.129	6.139

2.1.2.1 Base failure rate from shorts and opens in coils. The base failure rate of a TDF gyro from a coil failure is 0.0112 per million hours for a single-axis failure and 0.0218 per million hours for a two-axis failure. Table 13 shows the individual coil failure rates.

TABLE 13. FAILURE RATES FROM COIL FAILURES

	Pickoff- 8 Coils (Per 10^6 Hrs)	Torquer- 4 Coils (Per 10^6 Hrs)	Motor- 3 Coils (Per 10^6 Hrs)
Shorts (0.0028/Coil)	No Failure 0	Single Axis Failure 0.0112	Two Axis Failure 0.0008
Opens (0.0014/Coil)	Two Axis Failure 0.0112	Two Axis Failure 0.0056	Two Axis Failure 0.0042

2.1.2.2 Coils. The dry tuned gyro has three types of coils:

a. Pickoff

b. Torquer

c. Motor

The pickoff coils consist of four primary coils and four secondary coils. There are four torquer coils - two for each input axis. The motor coils consist of three coils for a three phase motor (the most commonly used) and four coils for a two phase motor.

Coil failures consist of shorts and opens with shorts occurring about two thirds of the time and opens one third of the time. Shorts generally occur between adjacent turns which has the effect of reducing the effective number of turns in the coil by one or more. When this occurs, the coil may continue to perform its function depending on the number of turns shorted, and the coil function. When a coil fails due to an open circuit, it can no longer perform its function. The following discussion considers the effects of shorts on the three types of gyro coils.

2.1.2.3 Shorted turns in pickoff coils. Pickoff coils typically consist of 200 to 400 turns - 10 layers of 20 to 40 turns each; the worst possible short between adjacent turns would be between two end turns that effectively removed both layers, thus reducing the number of turns in the coil by 20 percent. If this occurred in one of the primary coils, the effect would be

to increase the pickoff scale factor on that axis by one half of 20 percent, or 10 percent since there are two primary coils on each axis. If this occurred in one of the secondary coils, the effect would be to reduce the pickoff scale factor by 10 percent. The effect of changing the pickoff scale factor by $\pm$10 percent would be to change the open loop gain of the gyro capture loop by the same percent. Since capture loops typically operate with 10 dB to 20 dB of gain margin, a change of 10 percent (approximately 1.0 dB) is of little consequence and the gyro will continue to function normally.

2.1.2.4 Shorted turns in torquer coils. Torquer coils typically consist of 100 to 200 turns. The worst case short between adjacent turns would effectively remove two of the 10 layers thereby reducing the torquer scale factor by 10 percent for that axis. By the same rationale as presented in the paragraph on shorted turns in the pickoff coils, the gyro would continue to function normally except that the rate information coming from the affected axis would be in error by as much as 10 percent. Thus, the effect of shorted turns in a torquer coil would be to cause a single axis failure.

2.1.2.5 Shorted turns in motor coils. Motor coils for a dry tuned gyro typically consist of 20 coils per phase with 20 to 30 turns per coil. If adjacent coils in the same phase were to short, the worst case effect would be to lose about 10 turns out of 500 turns, in that phase. The effect of this would be a slight unbalance in phases and a slight change in motor power and the gyro would continue to function normally. If the short were to occur between phases, the result would likely be to overload the motor supply or overheat the gyro and thereby constitute a failure of both axes. However, the number of turns adjacent to each other from one phase to another phase is approximately 10 percent of the number of adjacent turns within a phase; thus, only about 10 percent of the shorted turns occurrences in a motor coil would constitute a gyro failure.

2.1.2.6 Occurrence of shorts and opens in coils. Reference I gives the failure rate model for high speed motors as:

$$\lambda_P = (\lambda_E + \lambda_W)\ \pi_E \text{ failures}/(10)^6 \text{ hours}$$

where:

λ_E = electrical failure rate = $\lambda_b(\pi_F)$

λ_W = mechanical failure rate = $\frac{P_{pop}(10)^4}{t_{op}}$

λ_b = electrical base failure rate (Tables 2.8.1-1 and -3 of Ref. I)

π_F = motor family and quality factor (Table 2.8.1-2 of Ref. I)

t_{op} = motor operating time (hr) for which λ_P is to be calculated

P_{pop} = percentage of motor mechanical failures during operating period, t_{op}

π_E = environmental factor (Table 2.8.1-4 of Ref. I)

The base electrical failure rate for high quality synchronous motors with a hot spot temperature of 140°C and insulation rated at 155°C is listed as 0.0043 failures per million hours. Since, as shown in the preceding paragraph, a shorted turn would not generally cause a motor failure, this base failure rate will be assumed to be entirely from "opens" and not from "shorts"; thus, the base rate for the occurrence of an open in a coil is established as one third of 0.0043 or 0.0014 per million hours (since the typical synchronous motor has three coils). To establish the occurrence of shorts, it is assumed that shorts occur twice as often as opens. The justification for this assumption is "Handbook of Piece Part Failure Rates", Martin-Marietta Report Number T-70-48891-007. This then establishes the base rate of occurrence of shorts in coils as 0.0028 per million hours.

2.1.2.7 Base failure rate from bearings. The problem of modeling the failure rate of the lightly loaded instrument bearing is made difficult by a lack of failure data because the mean time to failure (MTTF) is so long. The experience within the gyro industry has been that the lightly loaded instrument bearing spinning at relatively low speed (6,000 RPM) has an MTTF in excess of 100,000 hours. The calculated MTTF utilizing equations from the bearing industry is approximately 1,000,000 hours.

Since the bearing failure is a wear out phenomena, the failure rate is not constant but increases with operation time. For this reason, failure rates have been derived as a function of operation time and this data is presented in Figure 1. This derived failure rate varies from 2×10^{-6} per million hours for a 10,000 hour operation, to 5 per million hours for a 100,000 hour operation.

To derive a failure rate for a wearout phenomena, an MTTF and a wearout distribution are needed. For the failure rates of Figure 1, a conservative MTTF of 100,000 hours and a wearout distribution based on three sigma at 50 percent of MTTF (Figure 2) is used.

As a check on these derived failure rates, the MIL-HDBK-217B (Reference I) section on mechanical failure of high speed motors yields approximately the same failure rate for a 10,000 hour operation.

For purposes of this analysis, it is assumed that the mechanical failure of a motor is a bearing failure.

The bearings used in any inertial grade gyro are of the highest quality, and the lubrication used is a high quality, long lasting, non-oxidizing type such as Kendall KG-80. Also, the bearing loads are quite light (typically less than 10 percent of rated load). Therefore, the use of the high quality options in MIL-HDBK-217B is easily justified.

An MTTF for the bearing of 14,000 hours is derived from Figure 2.8.1-1 of 217B for operation at 6,000 RPM and 85°C. A wear out population of approximately one motor out of one hundred million is derived from Figure 2.8.1-4 for a 10,000 hour operation time and a bearing load of 10 percent of rated load. This yields a failure rate during the 10,000 hour operation of 1×10^{-6} failures per million hours.

The failure rate model used in Reference I for bearing failure assumes that the MTTF is not increased by decreasing the bearing load and that the bearing load decrease only decreases the failure rate for operating times less than the calculated MTTF. The experience of the gyro industry has been that the

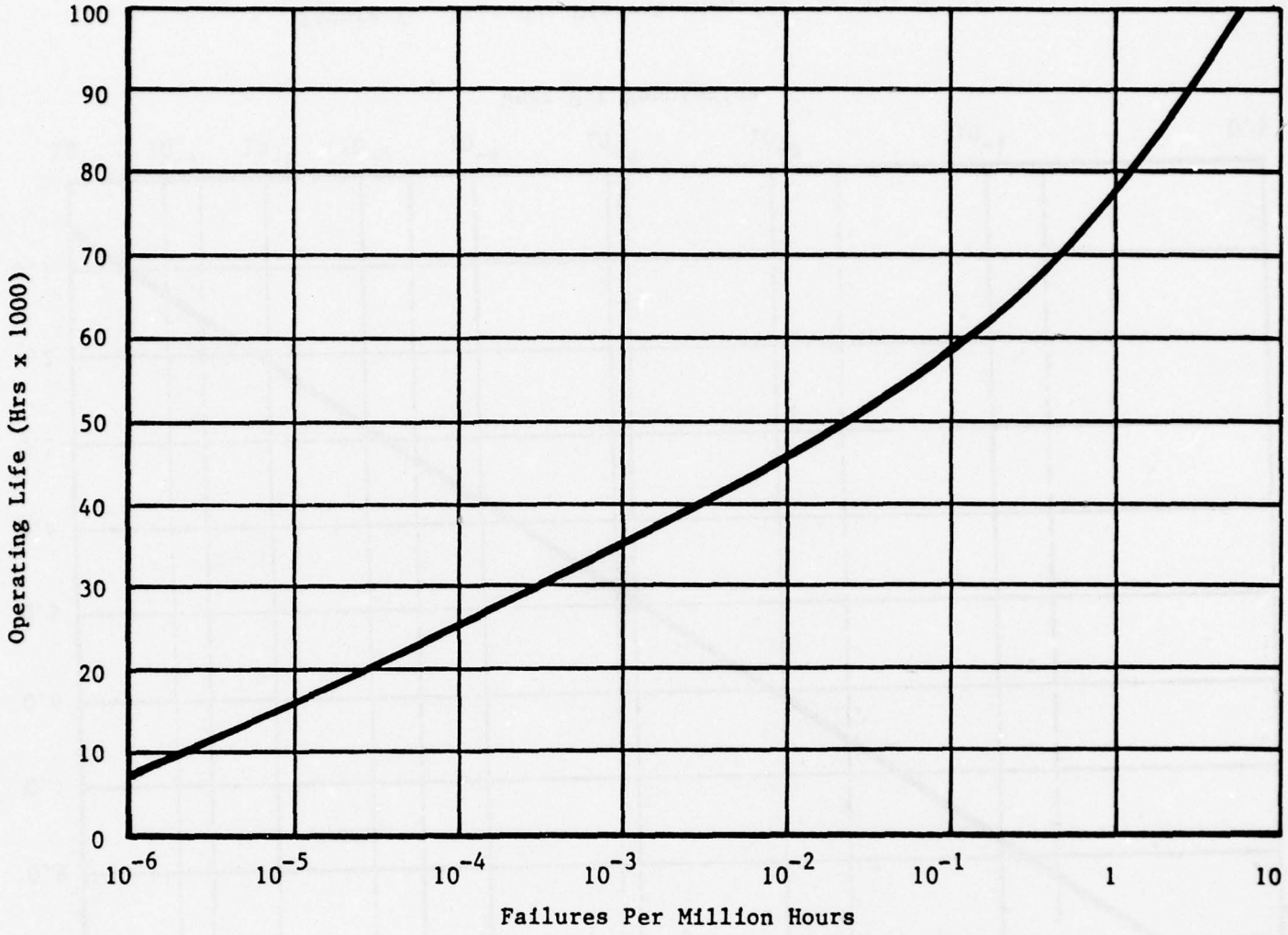

Figure 1. Bearing Failure Rate versus Operating Time

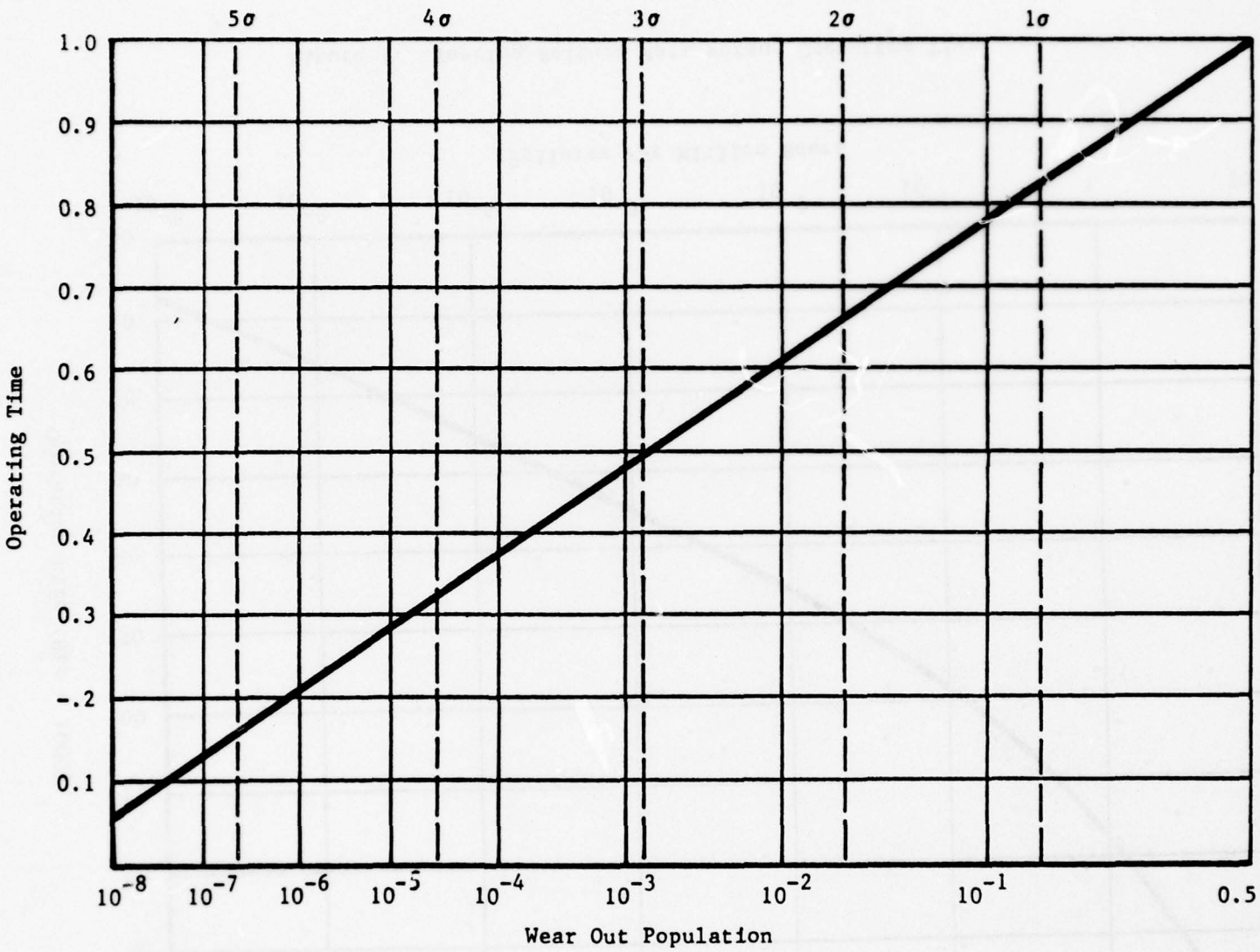

Figure 2. Wear Out Distribution (3σ at 50% MTTF)

lightly loaded instrument bearing spinning at relatively low speed (6,000 RPM) has an MTTF in excess of 100,000 hours of operation. The problem of modelling the failure rate of the lightly loaded instrument bearing is made difficult by a lack of failure data because the MTTF's are so long.

2.1.2.8 Base failure rate for the suspension system. The weakest part of the suspension system for a two-degree-of-freedom dry tuned rotor gyro is typically the flexure. If the flexure strength is assumed to have a normal distribution, then a failure model can be developed. The nominal strength of a flexure is determined by the design and the material while the variation from the nominal is determined by tolerances and heat treat conditions. The tolerances are typically ± 5 percent on flexure thickness, which is the most critical dimension, and the heat treat conditions are closely controlled; thus, the flexure strength deviation from nominal should be small.

Two assumptions are needed to be able to complete the failure model, they are:

a. the nominal value of flexure strength.
b. the deviation from the nominal.

Reasonable values that are in the direction of worst case are:

a. a nominal strength of twice the rated value or maximum service value (i.e., a safety factor of 2) for the worst case shock and vibration.
b. a deviation of 30 percent for the 3 sigma value.

Using these two values, the population of flexures with less than one half the nominal strength is one out of 3×10^{7}.

The number of flexures in a two-degree-of-freedom, dry tuned gyro varies from eight to twenty four. If the larger number is used the probability of gyro failure from a flexure failure becomes 8.0×10^{-7}. Using a 10,000 hour life time for the gyro this yields a failure rate of 0.00008 per million hours.

2.1.2.9 Base failure rate from an epoxy bond joint failure. The probability of a gyro failure from an epoxy bond joint failure was calculated to be very low (2×10^{-6}), and the resulting failure rate, then, is very low; 0.0002 failures per million hours based on a 10,000 hour life time.

The epoxy bond joints in a typical gyro are:

a. torquer coil to coil support.
b. pickoff coil to pickoff core.
c. pickoff core to pickoff support.
d. spin motor stator to case.
e. permanent magnets to rotor.
f. suspension to rotor.
g. wire tack-down to case.
h. balance weight tacks.

All of these epoxy joints typically have a large area of contact for the weight they support, therefore the strength to weight ratio is very large. The determining factor in the reliability of these joints will likely be other factors than strength to weight, such as;

a. bonding procedures
b. the epoxy used
c. the characteristics of the materials being bonded.

For purposes of this analysis it was assumed that the bonding procedures and the epoxies used were adequate for the materials being joined. However, it was reasonable to assume that the bonding procedures were not followed perfectly. As a result, the effective area of some of the bond joints is less than 100 percent. From this assumption, a failure model can be developed. Since the quality control on gyros is normally stringent, it is reasonable to assume a narrow normal distribution of bond area. A distribution with the three sigma value at 50 percent of bond area would yield a population of one joint in 5×10^{7}, with 10 percent or less bond area. If this is assumed to be the bond area that would eventually cause a failure of the joint, then the probability of gyro failure from bond joint failure is:

P(G/B) = Probability of gyro failure from bond joint failure

P(B) = Probability of bond joint failure

= 2×10^{-8}

N(B/G) = Number of bond joints in gyro

= 100 (typically)

P(G/B) = 2×10^{-6}

The purpose of this analysis is to show that the failure of a gyro, or any other high grade inertial instrument, from a bond joint failure is quite low, which agrees with the general experience in the industry in the last few years. Ten years ago, bond joint failures were more common. However, epoxies have been improved and experience gained in procedures and controls.

2.1.2.9.1 Torquer coil to coil support. The most susceptible bond joint failure is the torquer coil to coil support, since it is frequently cantilevered as shown below.

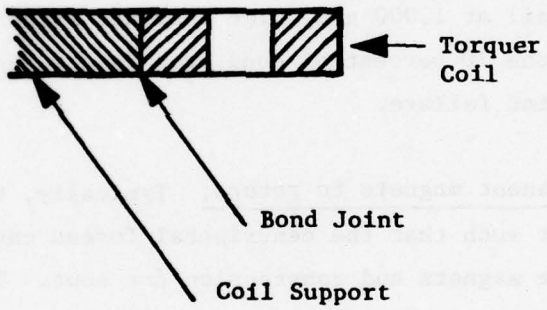

The maximum stress on this joint is:

$$S(T) = \frac{6 \times M \times \ell}{b \times t^2}$$

where

M = mass of coil

= 7 grams

= 0.015 lbs

ℓ = displacement from joint to GC of coil
= 0.20 in.
b = width of joint
= 0.50 in.
t = thickness of coil
= 0.15 in.
= 1.6 PSI/G

This is tensile stress.

With a 10 percent of area bond joint and a 5,000 PSI tensile strength cement this joint would fail at 312 g's. The stress in shear is:

$$S(s) = \frac{M}{b \times t}$$

$$= 0.20 \text{ PSI/G}$$

With a 10 percent of area bond joint and a 2,000 PSI shear strength cement, this joint would fail at 1,000 g's. The combined stress failure level would be 237 g's; thus, the 10 percent of bond area is a reasonable approximation to yield a bond joint failure.

2.1.2.9.2 Permanent magnets to rotors. Typically, there are magnets bonded to the rotor such that the centripetal forces cause tension in the bond joint for some magnets and compression for some. This stress tends to increase with the overall size of the gyro and is approximately 60 PSI of tension and 90 PSI of compression for the largest two-degree-of-freedom dry tuned rotor gyro in the industry. With a 5,000 PSI tensile strength cement, and a 10 percent of bond area joint, there is a factor of eight safety margin.

2.1.2.10 Base failure rate from feedthrough. A failure rate of 0.0237 per million hours is derived for a single pin feedthrough, and the typical gyro has 20 to 40 such feedthroughs. This yields a gyro failure rate from a feedthrough failure of 0.71 per million hours, if the median value of 30 feedthroughs is used.

The only failure rate data found on hermetically sealed connectors is in the FARADA handbook (Reference II) and lists a failure rate of 0.176×10^{-6}/ hour. This is for a 55 pin connector used in the Titan II Missile Guidance Computer and is based on zero failures in 5.668×10^{6} hours.

The failure rate for a single pin connector would be expected to be lower than a 55 pin header, but not by the ratio of 55:1. A compromise ratio would be 7.4:1 based on the square root of 55. For lack of a better model or better data, the following relationship is used for the failure rate of a hermetically sealed connector with N pins -

$$F_R = 0.176 \times 10^{-6} \sqrt{\frac{N}{55}} \text{ per hour}$$

On the gyros, the feedthroughs are considered to be a 1 pin connector. The failure rate per feedthrough is:

$$N = 1$$
$$F_R = 0.0237 \times 10^{-6} \text{ failures per hour}$$

2.1.2.11 Cover to case joint and hermetic seal. The typical cover to case joint is shown in Figure 3. For this joint to fail from acceleration loading would require 2×10^{6} g's. To fail from differential pressure would require 800 PSI inside to outside. However, the maximum inside to outside difference is about 5 PSI. Therefore, the probability of failure of this joint in service from acceleration or pressure is insignificant.

There are means of causing failure in the cover to case joint that have been experienced in the industry, however. By attaching a heater to the cover and using it for rapid warmup, the low heat capacity of the cover and poor thermal conductivity from the cover to the case will cause a large

---

II "Failure Rate Data" from the Government and Industry Data Exchange Program.

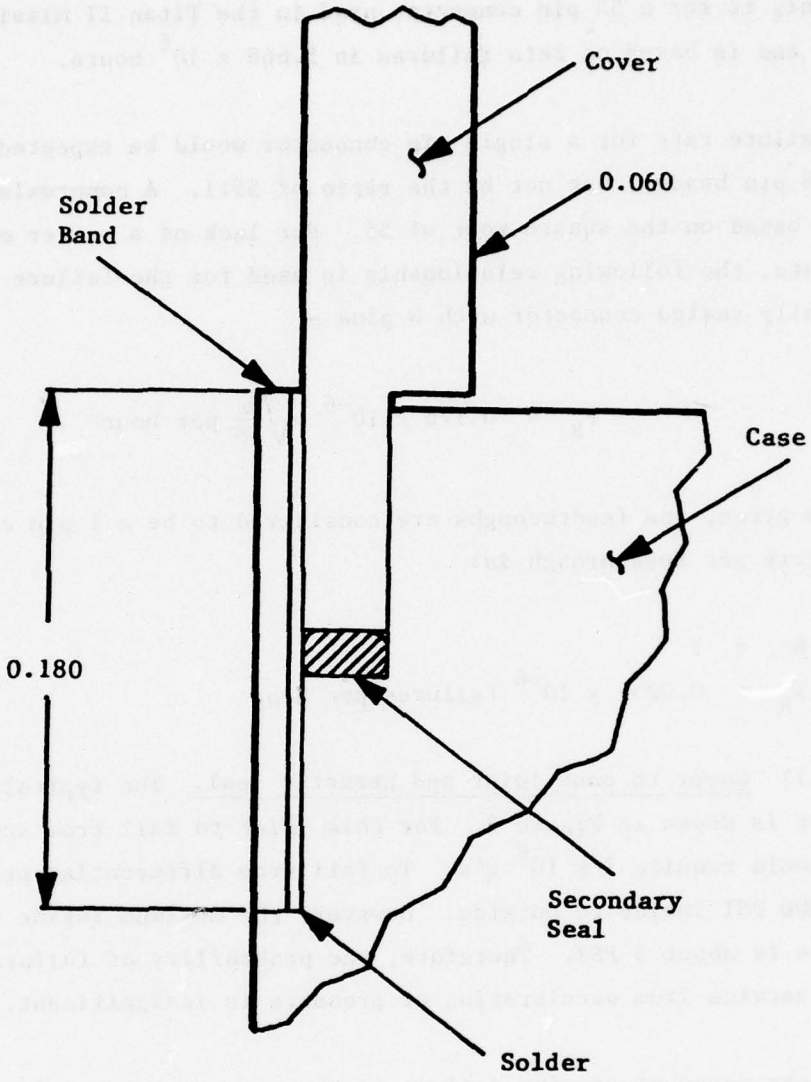

Figure 3. Solder Band Seal

differential temperature between cover and case. This large differential temperature will cause a stress in the solder joint, and the 5,000 PSI strength of the solder will be exceeded by a differential temperature of approximately $50^{o}F$. For fast reaction systems, where the heating time for the gyros is in the order of two or three minutes, a differential temperature of $50^{o}F$ can easily be generated, especially when the ambient temperature is low. High heating rates can also have an effect on the feedthrough failure rate (previous section). Thus, using the cover for heat input will lower the reliability of this joint. For purposes of this analysis it was assumed that the cover was not used for heat input, or that gyro heaters were not employed.

2.1.2.12 Base failure rate from solder connections. The base failure rate as listed in Reference I from solder connections is 0.0044 per hour per connection for hand made connections. The estimated number of connections for the two axes gyro is 90 and the resulting failure rate is 0.396 per million hours.

2.2 Failure rates for the pendulous single-axis, two-axes and three-axes dry accelerometers and associated electronics. The failure rates for the single axis, two axes, and three axes accelerometers and the associated electronics in a uninhabited airborne environment are:

a.	Single-axis	$45.474/10^{6}$ hrs
b.	Two-axes	$58.726/10^{6}$ hrs
c.	Three-axes	$80.400/10^{6}$ hrs

Table 14 lists the failure rates for the major subassemblies, which are the basis for the above numbers.

The failure rates for the electronics assemblies were derived by similarity to the electronics assemblies for the two-degree-of-freedom gyro. This assumes pulse torquing for the accelerometers that is similar to that used for the gyro.

TABLE 14. FAILURE RATES FOR SINGLE-AXIS, TWO-AXES AND THREE-AXES ACCELEROMETERS AND ASSOCIATED ELECTRONICS FOR AN UNINHABITED AIRBORNE ENVIRONMENT

Assembly	Failure Rates (Per 10^6 Hrs)		
	Single Axis	Two Axes	Three Axes
Accelerometer, Dry	2.093	3.943	5.794
Preamp	1.025	1.703	2.215
Digital Caging Amp	14.066	23.450	32.720
I/O	6.045	8.028	13.210
Power Supply	17.111	21.548	26.461
Total	45.474	58.726	80.400

2.2.1 Failure rates for the single-axis, two-axes, and three-axes dry accelerometers. The base failure rates for the single-axis, two-axes and three-axes unfloated accelerometers are:

a. Single-axis $0.225/10^6$ hrs

b. Two-axes $0.424/10^6$ hrs

c. Three-axes $0.623/10^6$ hrs

Table 15 lists the failure rates for these accelerometers for eight different environments. Table 16 lists the base failure rates from the accelerometer components.

TABLE 15. FAILURE RATES FOR THE SINGLE-AXIS, TWO-AXES AND THREE-AXES, DRY ACCELEROMETERS VERSUS ENVIRONMENTS

Environment	Multiplier	Failure Rates (Per 10^6 Hrs)		
		Single Axis	Two Axes	Three Axes
Base Rate	1.0	0.225	0.424	0.623
Ground, Fixed	1.5	0.338	0.636	0.935
Space, Flight	2.0	0.450	0.848	1.246
Airborne, Inhabited	2.5	0.563	1.060	1.558
Naval, Sheltered	4.5	1.013	1.908	2.804
Ground, Mobile	6.0	1.350	2.544	3.738
Naval, Unsheltered	7.7	1.733	3.265	4.897
Airborne, Uninhabited	9.3	2.093	3.943	5.794
Missile, Launch	10.0	2.225	4.240	6.230

TABLE 16. BASE FAILURE RATES FOR THE SINGLE-AXIS, TWO-AXES, AND THREE-AXES, DRY ACCELEROMETERS BY COMPONENTS

Accelerometer Component	Base Failure Rates (Per 10^6 Hrs)		
	Single Axis	Two Axes	Three Axes
Coils	0.0140	0.0280	0.0420
Pivot/Flexure	0.00003	0.00006	0.00009
Cement Joints	0.0001	0.0002	0.0003
Solder Connections	0.211	0.396	0.581
Total	0.225	0.424	0.623

2.2.2 Base failure rates from shorts and opens in coils. The base rates of the single-axis, two-axes, and three-axes dry accelerometers are:

a. Single-axis $0.0140/10^6$ hrs
b. Two-axes $0.0280/10^6$ hrs
c. Three-axes $0.0420/10^6$ hrs

Table 17 shows the individual coil failure rates.

TABLE 17. COIL FAILURE RATES IN ACCELEROMETERS

	Pickoff 4 Coils/Axis (Per 10^6 Hrs)			Torquer 2 Coils/Axis (Per 10^6 Hrs)		
	Single Axis	Two Axes	Three Axes	Single Axis	Two Axes	Three Axes
Shorts (0.0028/Coil)	No Failure 0	0	0	0.0056	0.0112	0.0168
Opens (0.0014/Coil)	0.0056	0.0112	0.0168	0.0028	0.0056	0.0084

2.2.3 Base failure rate from jewel and pivot or flexure. The probability of a pivot failure or a single flexure failure is the same as the probability of a flexure failure in a two-degree-of-freedom gyro, if the same assumptions are used. This yields failure rates from pivot/flexure failure for the dry accelerometers of:

a. Single-axis $0.00003/10^6$ hrs
b. Two-axes $0.00006/10^6$ hrs
c. Three-axes $0.00009/10^6$ hrs

2.2.4 Base failure rate from an epoxy bond joint failure. The dry accelerometers have approximately one half the number of bond joints per axis as a gyro; thus the failure rates are:

a. Single-axis $0.0001/10^6$ hrs
b. Two-axes $0.0002/10^6$ hrs
c. Three-axes $0.0003/10^6$ hrs

2.2.5 Base failure rate from feedthroughs and cover seal. The typical dry accelerometer does not require a hermetic seal. Therefore, the hermeticity failure of a feedthrough or cover seal does not produce an accelerometer failure. This is significant for fast warm-up systems where the accelerometer is heated at a fast rate (see paragraph 2.1.2.11).

2.2.6 Base failure rate from solder connections. The base failure rate from solder connections is 0.0044 from Reference I per connection for hand-made connections. The estimated numbers of connections and resulting failure rates for the dry accelerometers are listed in Table 18.

TABLE 18. FAILURE RATE FOR ACCELEROMETER SOLDER CONNECTIONS

Accelerometer	Connections	Failure Rates (Per 10^6 Hrs)
Single Axis	48	0.211
Two Axes	90	0.396
Three Axes	132	0.581

2.3 Failure rates for the single-axis, floated accelerometer and associated electronics. The failure rate for a single-axis, floated accelerometer and the associated electronics in the uninhabited airborne environment is approximately 60 per million hours. Table 19 lists the failure rates for the major subassemblies.

The failure rates for the electronics assemblies were derived by similarity to the electronics assemblies for the two-degree-of-freedom gyro.

TABLE 19. FAILURE RATES FOR SINGLE-AXIS, FLOATED ACCELEROMETER AND ASSOCIATED ELECTRONICS FOR A UNINHABITED AIRBORNE ENVIRONMENT

Assembly	Failure Rate (Per 10^6 Hrs)
Accelerometer, SA/Floated	16.563
Preamplifier	1.025
Digital Caging Amplifier	14.066
I/O	11.181
Power Supply	17.111
Total	59.946

2.3.1 Failure rates for the single-axis, floated accelerometer. Table 20 lists the single-axis, floated accelerometer failure rates for eight different environments. The base failure rate is 1.570 per million hours.

TABLE 20. SINGLE-AXIS, FLOATED ACCELEROMETER FAILURE RATES VERSUS ENVIRONMENTS

Environment	Multiplier	Failure Rate (Per 10^6 Hrs)
Base Rate	1.0	1.781
Ground, Fixed	1.5	2.672
Space, Flight	2.0	3.562
Airborne, Inhabited	2.5	4.453
Naval, Sheltered	4.5	8.015
Ground, Mobile	6.0	10.686
Naval, Unsheltered	7.7	13.714
Airborne, Uninhabited	9.3	16.563
Missile, Launch	10.0	17.810

Table 21 lists the base failure rates from the accelerometer components.

TABLE 21. BASE FAILURE RATES FOR A SINGLE-AXIS FLOATED ACCELEROMETER BY COMPONENTS

Accelerometer Component	Base Failure Rate (Per 10^6 Hrs)
Coils	0.0140
Jewel and Pivot	0.00003
Cement Joints	0.0001
Feedthrus	0.355
Solder Connections	0.211
Bellows	1.20
Total	1.781

2.3.2 Base failure rates from shorts and opens in coils. The base failure rate of a single-axis floated accelerometer from a coil failure is 0.0140 per million hours. Table 22 below shows the individual coil failure rates.

TABLE 22. FAILURE RATES FOR COILS IN A FLOATED ACCELEROMETER

	Pickoff- 4 Coils (Per 10^6 Hrs)	Torquer 2 Coils (Per 10^6 Hrs)
Shorts (0.0028/Coil)	No Failure 0	0.0056
Opens (0.0014/Coil)	0.0056	0.0028

2.3.3 Base failure rate from jewel and pivot failure. The probability of a jewel and pivot failure in an accelerometer is the same as the probability of a jewel and pivot failure in single-degree-of-freedom gyro. This yields an accelerometer base failure rate of 0.00003 per million hours.

2.3.4 Base failure rate from an epoxy bond joint failure. The base failure rate for an accelerometer is 0.0001 per million hours from a bond joint failure. This is half of the value for a gyro since it has half the number of bond joints.

2.3.5 Base failure rate from feedthroughs and bellows. The base failure rate from feedthroughs for an accelerometer is 0.355 per million hours. An accelerometer has about half the number of feedthroughs as a gyro, therefore, half the failure rate.

The failure from the bellows is the same as for the floated gyro bellows, 1.20 per million hours.

The total failure rate from feedthroughs and bellows is 1.555 per million hours.

The fact that leak proof seals and bellows are required, is the major difference between floated and unfloated accelerometers.

2.3.6 Base failure rate from solder connections. The base failure rate from solder connections is 0.0044 per connection for handmade connections. The estimated number of connections for the single-axis accelerometer is 48 and the resulting failure rate is 0.211 per million hours.

2.4 Failure rates for the multisensor and associated electronics. The type of multisensor considered here is the rotating wheel variety that gives two axes of rate and two axes of acceleration measurement.

The failure rate for a multisensor and the associated electronics in an uninhabited flight environment is approximately 123 per million hours. Table 23 lists the failure rates for the major subassemblies.

The failure rates for the electronics assemblies were derived by similarity to the electronics assemblies for the two-degree-of-freedom gyro.

TABLE 23. FAILURE RATES FOR MULTISENSOR AND ASSOCIATED ELECTRONICS FOR AN UNINHABITED AIRBORNE ENVIRONMENT

Assembly	Failure Rate (Per 10^6 Hrs)
Multisensor	11.774
Preamps	3.416
Digital Caging Amp	35.165
Spin Supply	18.635
I/O	32.120
Power Supply	21.548
Total	122.658

2.4.1 Failure rates for the multisensor. Table 24 lists the failure rates for the multisensor for eight different environments and for two different periods of operation, 10,000 hours and 100,000 hours. The base failure rate for 10,000 hours of operation is 0.826 per million hours and 5.826 per million hours for 100,000 hours of operation. The spin bearings cause this increase in failure rate as a function of operating time since bearing failure is a wearout phenomena.

TABLE 24. FAILURE RATES VERSUS ENVIRONMENTS FOR A MULTISENSOR

Environment	Multiplier	10,000 Hour Operation Failure Rate (Per 10^6 Hrs)	100,000 Hour Operation Failure Rate (Per 10^6 Hrs)
Base Rate	1.0	1.266	6.266
Ground, Fixed	1.5	1.899	9.399
Space, Flight	2.0	2.532	12.532
Airborne, Inhabited	2.5	3.165	15.665
Naval, Sheltered	4.5	5.697	28.197
Ground, Mobile	6.0	7.596	37.596
Naval, Unsheltered	7.7	9.748	48.248
Airborne, Uninhabited	9.3	11.774	58.274
Missile, Launch	10.0	12.660	62.660

Table 25 lists the base failure rates for the multisensor components.

TABLE 25. BASE FAILURE RATES FOR A MULTISENSOR BY COMPONENT

Component	10,000 Hour Operation (Per 10^6 Hrs)	100,000 Hour Operation (Per 10^6 Hrs)
Coils	0.0442	0.0442
Bearings	0.000002	5.0
Suspension	0.0007	0.0007
Bond Joints	0.0002	0.0002
Feedthroughs	0.781	0.781
Solder Connections	0.440	0.440
Total	1.266	6.266

2.4.2 Base failure rate from shorts and opens in coils. The base failure rate of a multisensor from a coil failure is 0.0442 per million hours.

Table 26 shows the individual coil failure rates.

TABLE 26. COIL FAILURE RATES FOR A MULTISENSOR

	Pickoff- 16 Coils (Per 10^6 Hrs)	Torquer- 4 Coils (Per 10^6 Hrs)	Motor 3 Coils (Per 10^6 Hrs)
Shorts (0.0028/Coil)	No Failure 0	0.0112 (Single Axis)	0.0008
Opens (0.0014/Coil)	0.0224	0.0056	0.0042

2.4.3 Base failure rate from bearing failure. The base failure rate or a multisensor from bearing failure is the same as for the two-degree-of-freedom gyro if the same low spin speed is used (6,000 RPM). Since bearing failure is a wearout phenomena, the failure rate varies from a very low

$0.000002/10^6$ hrs for 10,000 hours of operation to $5.0/10^6$ hrs for 100,000 hours of operation.

2.4.4 Base failure rate from suspension system failure. The base failure rate of a multisensor from a suspension system failure is the same as for the two-degree-of-freedom gyro - 0.0007 per million hours. This is using the maximum number of flexures as was used for a gyro.

2.4.5 Base failure rate from an epoxy bond joint failure. The probability of a multisensor failure from an epoxy bond joint failure is the same as for the two-degree-of-freedom gyro - 0.0002 failures per million hours.

2.4.6 Base failure rate from feedthrough failure. The base failure rate from feedthroughs for a multisensor will be slightly higher because there will be about 10 percent more feedthroughs; thus, the failure rate is 0.781 per million hours.

2.4.7 Base failure rate from solder connections. The base failure rate from handmade solder connections is $0.0044/10^6$ hrs per connection per MIL-STD-217B. The estimated numbers of connections for the multisensor is 100 and the resulting failure rate is $0.440/10^6$ hrs.

2.5 Failure rates for single-degree-of-freedom floated gyro and associated electronics. The failure rate for a single-degree-of-freedom floated gyro and the associated electronics in an uninhabited flight environment is approximately 8.2 per million hours. Table 27 lists the breakdown for the major subassemblies.

The failure rates for the electronics assemblies were derived by similarity to the electronics assemblies for the two-degree-of-freedom gyro, i.e., pulse torqued.

TABLE 27. FAILURE RATES FOR SINGLE-DEGREE-OF-FREEDOM FLOATED GYRO AND ASSOCIATED ELECTRONICS FOR UNINHABITED AIRBORNE ENVIRONMENT

Assembly	Failure Rate (Per 10^6 Hrs)
Gyro, SDF/Floated	20.972
Preamp	1.025
Digital Caging Amp	14.066
Spin Supply	18.635
I/O	6.045
Power Supply	21.548
Total	82.291

2.5.1 Failure rates for the single-degree-of-freedom, floated gyro. Table 28 lists the SDF gyro failure rates for eight different environments and for two different periods of operation, 10,000 hours and 100,000 hours. The base failure rate for 10,000 hours of operation is 2.25 per million hours and 7.26 per million hours for 100,000 hours of operation. The gyro bearings cause this increase in failure rate as a function of operating time since bearing failure is a wearout phenomena. For low speeds (approximately 100 Hz), it is assumed that a ball-bearing and air bearing have the same failure rates.

Table 28 shows the failure rates for different environments and Table 29 gives the base failure rates for the gyro components.

TABLE 28. FAILURE RATES VERSUS ENVIRONMENTS FOR SINGLE-DEGREE-OF-FREEDOM FLOATED GYRO

Environment	Multiplier	10,000 Hour Operation Failure Rate (Per 10^6 Hrs)	100,000 Hour Operation Failure Rate (Per 10^6 Hrs)
Base Rate	1.0	2.255	7.255
Ground, Fixed	1.5	3.383	10.883
Space, Flight	2.0	4.510	14.510
Airborne, Inhabited	2.5	5.638	18.138
Naval, Sheltered	4.5	10.148	32.648
Ground, Mobile	6.0	13.530	43.530
Naval, Unsheltered	7.7	17.364	55.864
Airborne, Uninhabited	9.3	20.972	67.472
Missile, Launch	10.0	22.550	72.550

TABLE 29. BASE FAILURE RATES FOR A SINGLE-DEGREE-OF-FREEDOM FLOATED GYRO

Gyro Component	Base Failure Rates (Per 10^6 Hrs)	
	10,000 Hour Operation	100,000 Hour Operation
Coils	0.0266	0.0266
Bearings	0.000002	5.0
Pivot and Jewel	0.0007	0.0007
Bond Joints	0.0002	0.0002
Feedthrus	0.710	0.710
Solder Connections	0.317	0.317
Bellows	1.2	1.2
Total	2.255	7.255

2.5.2 Base failure rate from shorts and opens in coils. The base failure rate of a SDF gyro from a coil failure is 0.0190 per million hours. Table 30 shows the individual coil failure rates.

TABLE 30. FAILURE RATE OF COILS FOR A SDF GYRO

	Pickoff- 4 Coils (Per 10^6 Hrs)	Torquer- 2 Coils (Per 10^6 Hrs)	Motor- 3 Coils (Per 10^6 Hrs)
Shorts (0.0028/Coil)	No Failure 0	0.0056	0.0084
Opens (0.0014/Coil)	0.0056	0.0028	0.0042

2.5.3 Base failure rate from bearing failure. The base failure rate of a SDF gyro from bearing failure is the same as for a TDF gyro if the same low spin speed (6,000 RPM) is used. Since bearing failure is a wear out phenomena, the failure rate varies from a low $0.000002/10^6$ hrs for 10,000 hours of operation to $5/10^6$ hrs for 100,000 hours of operation.

2.5.4 Base failure rate from pivot and jewel failure. The probability of failure of the pivot or jewel in a SDF gyro is comparable to the suspension system failure in a TDF gyro - both are very low. The failure rate is 0.0007 per million hours.

2.5.5 Base failure rate from an epoxy bond joint failure. The probability of a SDF gyro failure from a bond joint failure was estimated to be the same as for the TDF gyro - 0.0002 failures per million hours.

2.5.6 Base failure rate from feedthroughs and bellows. The base failure rate from feedthroughs for a SDF gyro is the same as a TDF gyro; 0.710 per million hours. The SDF gyro also has bellows which yields a failure rate of 1.2 per million hours. The total for feedthroughs and bellows is 1.91 failures per million hours.

2.5.7 Base failure rate from solder connections. The base failure rate from hand solder connections is $0.0044/10^6$ hrs per connection from Reference I. The estimated number of connections for the single axis gyro is 72 and the resulting failure rate is $0.317/10^6$ hrs.

2.6 Failure rate for the ring laser gyro in an uninhabited airborne environment. The failure rate for the ring laser gyro in an uninhabited airborne environment is 11.54 per million hours for 10,000 hours of operation, and 57.02 per million hours for 100,000 hours of operation. The failure rates by component are listed in Table 31.

TABLE 31. FAILURE RATE OF RING LASER GYRO BY COMPONENT IN AN UNINHABITED AIRBORNE ENVIRONMENT

Ring Laser Gyro Component	Failure Rate (Per 10^6 Hrs)	
	10,000 Hrs Operation	100,000 Hrs Operation
Laser	1.02	46.50
Readout Assembly	0.72	0.72
Path Length Transducer	1.86	1.86
Dither Mechanism	0.0045	0.0045
Electronics	7.942	7.942
Total	11.54	57.02

2.6.1 Failure rate for the laser. The section on lasers from Reference I 217B follows:

> "At the present time there is very little failure rate data, must less failure rate models for laser devices. Some quantitative life information is available and is shown in Table 2.4-1. For the most part, this data resulted from laboratory testing and indicates reasonable values of lifetime that can

be expected under these conditions. Caution is advised in using these values for field conditions since no data is presently available. For the time being, the tabulated values should be considered as an upper limit for field values with actual field values probably lower. These values do not include peripheral apparatus such as power supplies, pumps, cooling systems, etc. Quality control problems exist and, if not carefully attended to, can seriously reduce the lifetimes shown."

TABLE 2.4-1

LASER LIFE CHARACTERISTICS

Material	Life Characteristics
Helium Cadmium	1500 hours
Krypton	2000 hours
Helium Neon	12,000 hours
Argon Blue	2,000 hours
Solid State (Ruby, Neodymium YAG, Neodymium Glass)	Limited by Xenon flash lamps = $(10)^7$ pulses (low power)
Heterojunction (Gallium Arsenide)	2,000 hours
Sealed CO_2	2,000 hours
Flowing CO_2	No lifetimes available but should be better than sealed CO_2 type.

Although, as pointed out in Reference I, there is limited data on lasers, there is some significant lifetime data. The ring laser gyro utilizes the helium-neon lasing medium, and the primary failure modes for this type of laser are leaks and outgassing. By utilizing the best available vacuum seal technology, lasers have been built and operated continuously for 100,000 hours.

Although relatively low laser lifetimes could be used and justified by Reference I, it must be realized that the ring laser gyro is a developing technology, and that, in general, the latest techniques for achieving the best laser lifetimes will tend to be used. Therefore, a more optimistic assumption about laser lifetimes than is presented in Reference I can be justified.

This analysis, then, makes the following optimistic assumptions:

a. The lasing medium is sealed, utilizing the best available vacuum sealing techniques.

b. The lasers are given adequate initial operation to screen out any gross failures.

c. The MTTF for the laser is 100,000 hours, with a 3 sigma value at 10 percent of the MTTF.

This last assumption yields a failure rate that varies from 0.11 per million hours for the first 10,000 hours of operation to 5.0 per million hours for 100,000 hours of operation.

The environmental multipliers for the laser are:

Ground, Base	1.0
Space, Flight	1.5
Ground, Fixed	2.0
Airborne, Inhabited	2.5
Naval, Sheltered	4.5
Ground, Mobile	6.0
Naval, Unsheltered	7.7
Airborne, Uninhabited	9.3
Missile, Launch	10.0

Thus, the failure rate for the laser in an uninhabited airborne environment for 10,000 hours of operation is 1.02 per million hours, and $46.5/10^6$ hrs for 100,000 hours of operation.

2.6.2 Failure rate of the laser readout assembly. The readout assembly consists of the readout substrate, the dielectric mirror, and the photosensor. The photosensor is the only element that has a significant failure rate and it is the same as a JANTX zener diode at 50 percent stress and 100°C. The failure rate is 0.018 per million hours. The environmental multipliers are as follows:

Ground, Base	1
Space, Flight	1
Ground, Fixed	5
Airborne, Inhabited	25
Naval, Sheltered	25
Ground, Mobile	25
Naval, Unsheltered	25
Airborne, Uninhabited	40
Missile, Launch	40

Thus, the airborne uninhabited failure rate for this assembly is 0.72 per million hours.

2.6.3 Failure rate of the laser path length transducer. The transducer that is used for the laser path length control typically consists of a piezoelectric element and a mechanical diaphragm. The piezoelectric element was given the same failure rate as a quartz crystal from Reference I, 0.2 per million hours. The mechanical element will be given the same failure rate as a single flexure in a dry tuned gyro, 0.00003 per million hours.

The environmental multipliers are:

Ground, Base	1.0
Space, Flight	1.5
Ground, Fixed	2.0
Airborne, Inhabited	2.5
Naval, Sheltered	4.5
Ground, Mobile	6.0

Naval, Unsheltered	7.7
Airborne, Uninhabited	9.3
Missile, Launch	10.0

Therefore, the airborne, uninhabited failure rate for this transducer is 1.86 per million hours.

2.6.4 Failure rate of the dither mechanism. The dither mechanism is only one of the methods used to eliminate phase lock. However, it is presently the most commonly used and the most successful.

The typical dither mechanism consists of a relatively stiff single rotational degree-of-freedom suspension with piezoelectric drivers. There are 6 to 16 blades or flexures in the suspension with two piezoelectrics on each blade. The geometry is such that a failure of any one flexure would constitute a failure, while approximately half of the piezoelectrics would have to fail to constitute a failure.

The failure rate of a single flexure for the dither mechanism is the same as the failure rate of a single flexure for the dry tuned gyro, 0.00003 per million hours.

If 16 blades are assumed this yields a failure rate of 0.00048 per million hours.

The piezoelectric has the same failure rate as a quartz crystal, 0.2 per million hours. For any 16 out of 32 to fail has a very small probability.

$$P(16/32) = \frac{32!}{16!\ 16!} \times P^{16}$$

Where P = failure rate x time for 100,000 hours

$$P = 0.02$$

$$P(16/32) = 3.94 \times 10^{-19}$$

for a failure rate of 3.94×10^{-18} per million hours.

Thus, the base failure rate for the dither mechanism is 0.00048 per million hours. The environmental multipliers are:

Ground, Base	1.0
Space, Flight	1.5
Ground, Fixed	2.0
Airborne, Inhabited	2.5
Naval, Sheltered	4.5
Ground, Mobile	6.0
Naval, Unsheltered	7.7
Airborne, Uninhabited	9.3
Missile, Launch	10.0

The uninhabited airborne environment failure rate for this mechanism is 0.0045 per million hours.

2.6.5 Failure rate for the ring laser gyro electronics. The failure rate for the typical ring laser gyro electronics in an uninhabited airborne environment is 7.942 per million hours. The breakdown by component is shown in Table 32.

TABLE 32. LASER GYRO ELECTRONICS FAILURE RATES

Quant. (η)	Part Type/Assembly		Stress Ratio	Individual Failure Rate $(\lambda)/10^6$ Hrs	Total Failure Rate $(\eta\lambda)/10^6$ Hrs
1	I.C., SSI/MSI Digital	(CD4053)	-	0.263	0.263
2	I.C., SSI/MSI Digital (M38510/ 01303)	(SN54160)	-	0.246	0.492
2	I.C., SSI/MSI Linear (M38510/10101)	(LM741)	-	0.420	0.840
3	I.C., SSI/MSI Linear	(LM112)	-	0.533	1.599
3	I.C., SSI/MSI Linear	(LM118)	-	0.641	1.523
17	Capacitor, Ceramic	(CKR)	0.4	0.022	0.374
25	Resistor, Film	(RLR)	0.2	0.010	0.250
1	Inductor, Power		-	0.101	0.101
1	Crystal Oscillator		-	2.100	2.100

SECTION III

MECHANIZATION OF REDUNDANT INERTIAL REFERENCE ASSEMBLIES

The major items in the consideration of a redundant system mechanization for aircraft are: ability to detect and isolate failures; the cost to acquire the desired redundancy level; the cost to maintain a system with the required redundancy level; the size and weight for the required redundancy level; survivability of the system; and the affects of the mechanization on accuracy.

These considerations will be examined in greater detail below:

a. Ability to Detect and Isolate Failures. There are two considerations in detection. The first is the probability that a failure will be detected, and the second is the time it takes to detect the failure. The probability of detection is dependent on the level of redundancy i.e., the number of channels, but, it will be shown in later sections that the orientation of the sensors can also affect the probability of detection. However, even after detection has occurred, the ability to isolate the failed channel also must be established. This ability to isolate the failure is also dependent on the level of redundancy and, for the TDF gyro, on the type of failure. This will be examined in section 3.1.4.

b. The Cost in Dollars of Acquiring the Required Redundancy. Redundancy costs money. However, the potential cost advantage over non-skewed axes approaches is the primary motivation for the consideration of skewed axes redundancy. The intent is to minimize the number of sensors (and consequently associated electronics) to reach a specified level of reliability.

c. The Life-Cycle (Cost-of-Ownership) of the System. The acquisition cost is only part of the cost-of-ownership of the system. The system needs to be mechanized so that spares are not excessively expensive. This means that complete system replacement, if a failure occurs, is uneconomical. Therefore submodules, such as individual gyros or accelerometers, should be carried as spares and replaced

when necessary. It is generally not economical to have to carry as a spare, for example, a two gyro module. The spare would be used to replace a failed two gyro module, but invariably only one of the gyros caused the failure. This results in the removal of one good gyro, and also doubles the cost of the spare used to replace the failed gyro. To make the most efficient use of logistics money, each submodule should also be designed so that spares are interchangeable between channels.

The ease with which submodules can be changed is also important in the skewed axes redundant system. If it is difficult to replace the submodule, or if it takes a considerable amount of recalibration of the system after replacement, then the acquisition cost advantage of skewed axes redundancy will be negated.

d. Size and Weight. Size and weight have always been a problem for inertial systems and redundancy requires more size and weight than nonredundant systems, and the higher the order of redundancy the larger and heavier the system. The size and weight will be mainly affected by the sensors used, i.e., single or two-degrees-of-freedom, and the sensor orientation.

e. Survivability. One of the reasons for using redundancy is to improve survivability and increase the probability of mission success. However, the simplest solution to survivability is to disperse the sensors and allied electronics in the aircraft. This increases the cost and size of the system, because either difficult sensor alignment mechanizations are required or extra sensors added to eliminate sensor-to-sensor alignment requirements. However, survivability is very important where the MIRA is Flight Critical or Mission Critical.

f. The Affects of Redundancy on Performance. A skewed axes mechanization can have adverse affects on the potential accuracy of a system. One affect could be the reduced sensitivity to motions about the aircraft axes. Another is that in some mechanizations, all axes of the gyros have gravity sensitive error terms. In systems mechanized to date, only the heading axes had a gravity sensitive error term. The level axes were immune from gravity sensitive errors, resulting in much better accuracy, especially for flights of only a few hours duration.

As gravity sensitive errors are the major errors in most of the gyros so far produced, the affect of the redundancy mechanization on performance is significant.

3.1 Two-degree-of-freedom fault isolation singularities. In a redundant system consisting of three two-degree-of-freedom (TDF) gyros, there are certain failure modes that cannot be isolated using conventional parity checks. The purpose of this section is to discuss, in general, the method by which parity equations are formulated and subsequently establish the unique conditions which result in fault isolation singularities in TDF gyros.

3.1.1 Parity equations. Failure status of the redundant system is indicated by the results obtained from parity equations. Parity equations are equations that are formed using the outputs of the various sensors in such a way as to expose the measurement error of these sensors. As the error detection scheme must be a continuous process, that is unaffected by the outside environment, the parity equations must expose measurement errors in the presence of quantity being measured. This means that the parity equations must be formed in such a way as to cancel out the quantity being measured.

The following simple examples illustrates the use of parity equations in the process of failure detection and isolation. Assume a quantity, V, is measured simultaneously by three instruments A, B and C. The outputs of these instruments are V_A, V_B and V_C respectively. Failure status of the system is indicated by the truth table (Table 33) formed using parity equations.

TABLE 33. TRUTH TABLE FOR FAILURE DETECTION

Instrument Failed	Parity Equations		
	$K_{AB} = V_A - V_B$	$K_{AC} = V_A - V_C$	$K_{BC} = V_B - V_C$
None	0	0	0
A	1	1	0
B	1	0	1
C	0	1	1

The output of the parity equation other than zero represents a failure and the inspection of the truth table reveals a unique sequence of "ones" and "zeros" representing specific instrument failures. Next, let us consider three TDF gyros arranged with their spin axes and sensing axes mutually orthogonal. This is shown in Figure 4 where X, Y, Z is the reference coordinate set along which angular rates, ω_X, ω_Y and ω_Z, are assumed to exist. The X-gyro with its spin axis along the X axis measures rates ω_Z^Y and ω_Y^X, the Y-gyro with its spin axis along the Y axis measures rates ω_X^Y and ω_Z^Y and the Z-gyro with its spin axis along the Z axis measures rates ω_X^Z and ω_Y^Z. Because at least two gyros measure the same angular rate we can write the three parity equations by inspection as follows:

$$K_{XY} = \omega_Z^X - \omega_Z^Y \tag{1}$$

$$K_{XZ} = \omega_Y^X - \omega_Y^Z \tag{2}$$

$$K_{YZ} = \omega_X^Y - \omega_X^Z \tag{3}$$

Table 33 is formed using equations (1), (2) and (3). It is noted that if both axes of any gyro fail, this failure can be detected and isolated. It is observed also that if only one axis fails, such a failure can be detected, but cannot be isolated. This is illustrated by the following example. Assume the output ω_Z^X is in error. When this output is processed by the parity equation the sequence is 1-0-0. It is noted that the same sequence would result if the output ω_Z^Y were in error.

3.1.2 Concept of a measurement plane of a TDF gyro. A TDF rate gyro is sensitive only to angular input rates whose vectors lie in the plane that is perpendicular to the spin axis of the gyro. This plane is referred to as the measurement plane of the gyro and is shown in Figure 5. Unit vector, $\hat{S}_i$, is coincident with the spin axis of the gyro and the component of the total angular rate vector in measurement plane is $\bar{\omega}_i'$. $\bar{\omega}$ is the total angular rate vector. The angular rate sensed by the ith gyro is

$$\bar{\omega}_i' = \bar{\omega} - \hat{S}_i (\bar{\omega} \cdot \hat{S}_i) \tag{4}$$

Note that single axis failure can be detected but cannot be isolated

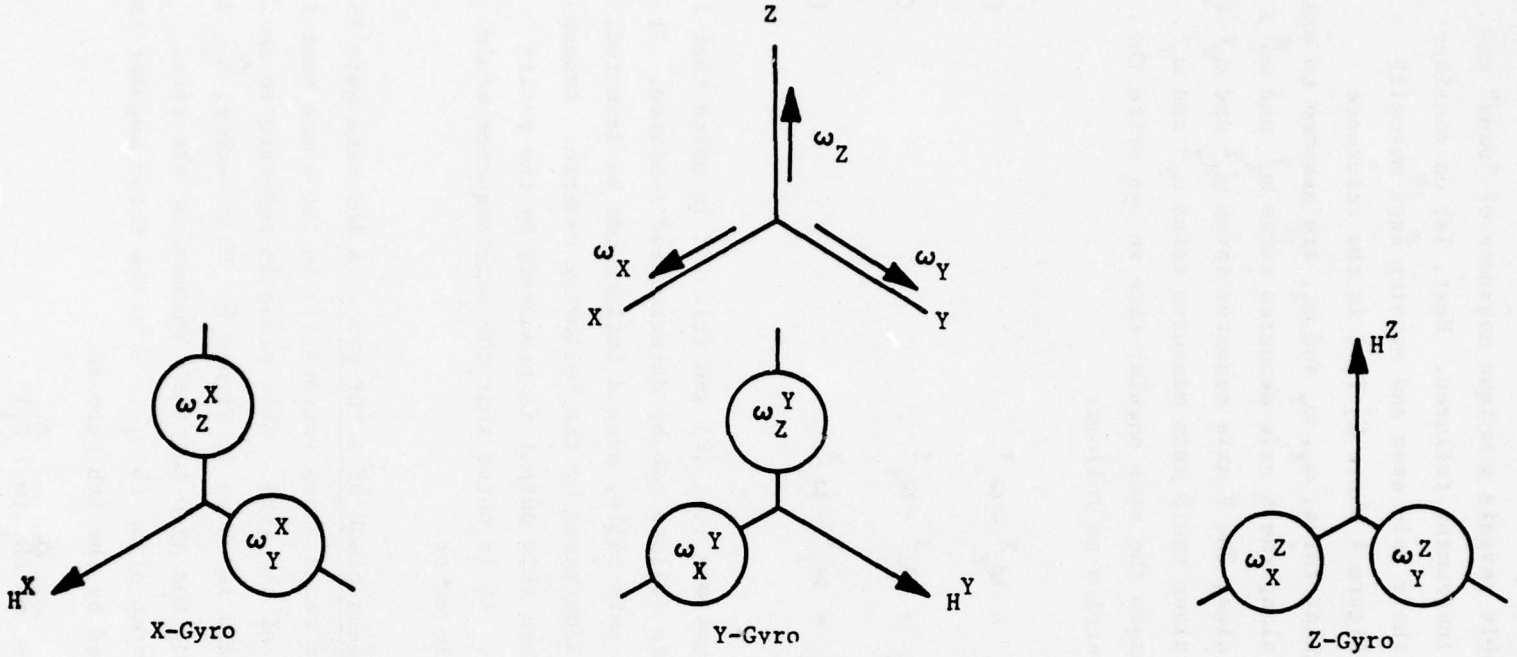

Gyro Failed	Parity Equations		
	$K_{XY} = \omega_Z^X - \omega_Z^Y$	$K_{XZ} = \omega_Y^X - \omega_Y^Z$	$K_{YZ} = \omega_X^Y - \omega_X^Z$
None	0	0	0
X-Gyro	1	1	0
Y-Gyro	1	0	1
Z-Gyro	0	1	1

Figure 4. Basic Redundant Rate Measuring System Utilizing Three TDF Gyros

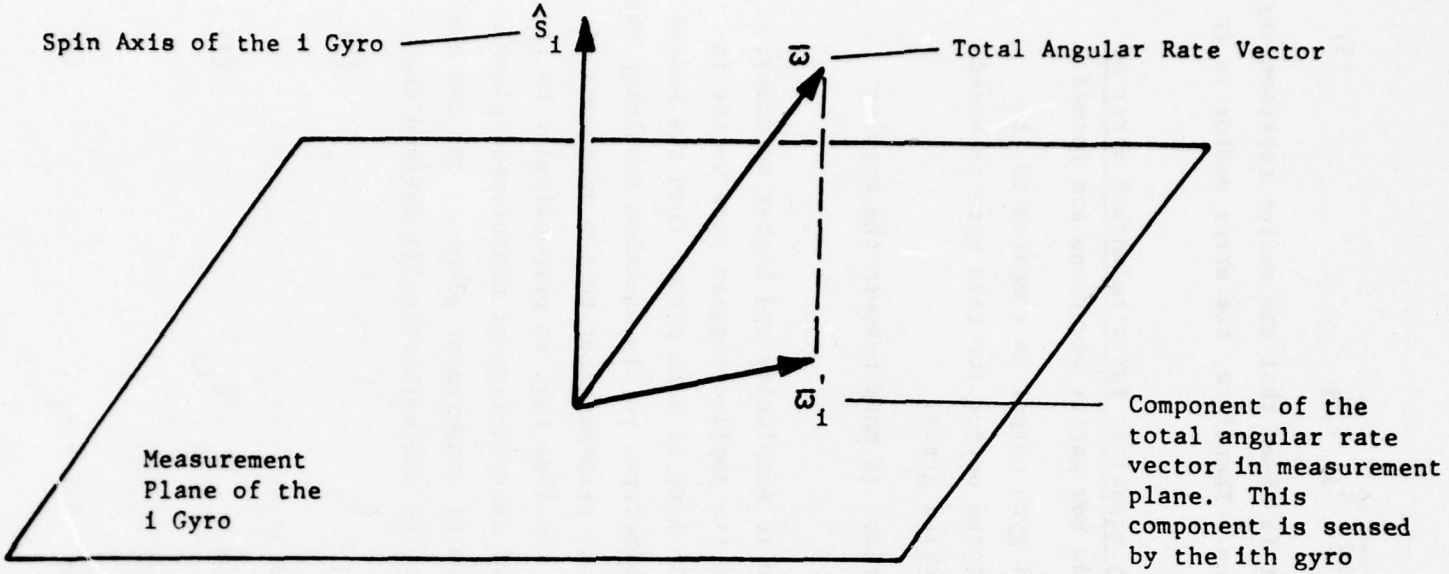

Sensed Input Angular Rate:

$$\bar{\omega}_i' = \bar{\omega} - \hat{S}_i \, (\bar{\omega} \cdot \hat{S}_i)$$

Gyro Output:

$$\bar{\omega}_i = \bar{\omega} - \hat{S}_i \, (\bar{\omega} \cdot \hat{S}_i) + \bar{e}_i$$

$\bar{e}_i$ = ith Gyro Error Vector (This Vector is in the Measurement Plane)

Figure 5. Concept of Measurement Plane of a TDF Gyro

while the gyro output is

$$\bar{\omega}_i = \omega - \hat{S}_i (\bar{\omega} \cdot \hat{S}_i) + \bar{e}_i \tag{5}$$

where $\bar{e}_i$ is the ith gyro error vector. It is noted that the vector representing the gyro output is in the measurement plane. Therefore, the error vector is in the same plane.

3.1.3 Methods of formulation of parity equations for a redundant array of TDF gyros. There are basically two methods how parity equations are formed.

Method 1. In this method an individual gyro output is compared to the predicted output for this gyro. The predicted output for this gyro is based on measurements of all the remaining nonfailed gyros.

Method 2. In this method direct comparison is made between the angular rates measured by any two gyros.

Method 2 is preferred over Method 1 due to simplicity and higher accuracy, and it is based on the observation that if the applied angular rate vector is orthogonal to the plane containing the spin axes of both gyros, then the sensed angular rates by both gyros are equal. Therefore, parity equation involving the two gyros is formulated along a line that is perpendicular to the spin axes of both gyros. Further, it is observed that the line that is perpendicular to the spin axes of both gyros is also the line of intersection of measurement planes of the two gyros. The line of intersection of measurement plane of the two gyros will be denoted as the line of parity equation and mathmetically defined as

$$\hat{P}_{ij} = \hat{S}_i \times \hat{S}_j \tag{6}$$

The parity equations for the i and j gyros is

$$K_{ij} = \bar{\omega}_i \cdot \hat{P}_{ij} - \bar{\omega}_j \cdot \hat{P}_{ij} \tag{7}$$

Substituting from (5) and recognizing that

$$\bar{\omega}_j = \omega - S_j (\bar{\omega} \cdot S_j) + e_j \, , \tag{8}$$

hence

$$K_{ij} = \left[- \hat{S}_i \, (\bar{\omega} \cdot \hat{S}_i) + \hat{S}_j \, (\bar{\omega} \cdot \hat{S}_j) + \bar{e}_i - \bar{e}_j \right] \cdot \hat{P}_{ij} \qquad (9)$$

As the unit vectors $\hat{S}_i$ and $\hat{S}_j$ are orthogonal to the unit vector $\hat{P}_{ij}$, therefore, $\hat{S}_i \cdot \hat{P}_{ij} = \hat{S}_j \cdot \hat{P}_{ij} = 0$ and the parity equation (9) becomes

$$K_{ij} = (\bar{e}_i - \bar{e}_j) \cdot \hat{P}_{ij} \, . \qquad (10)$$

In a fail/op-fail/op system four gyros are used resulting in six parity equations as follows.

$$\left.\begin{aligned} K_{12} &= (\bar{e}_1 - \bar{e}_2) \cdot \hat{P}_{12} \\ K_{13} &= (\bar{e}_1 - \bar{e}_3) \cdot \hat{P}_{13} \\ K_{14} &= (\bar{e}_1 - \bar{e}_4) \cdot \hat{P}_{14} \\ K_{23} &= (\bar{e}_2 - \bar{e}_3) \cdot \hat{P}_{23} \\ K_{24} &= (\bar{e}_2 - \bar{e}_4) \cdot \hat{P}_{24} \\ K_{34} &= (\bar{e}_3 - \bar{e}_4) \cdot \hat{P}_{34} \end{aligned}\right\} \qquad (11)$$

3.1.4 Orthogonal failure. Orthogonal failure is defined as one that is not detected by the parity equation. As discussed in paragraph 3.1.1, if the output of the parity equation is equal to zero, then this equation indicates that the axes, whose outputs are involved in this equation, did not fail. It is noted from Equation (11) that any of the parity equations will yield zero value for either $\bar{e}_i - \bar{e}_j = 0$, i.e., there is no error, or when the resultant error vector $(\bar{e}_i - \bar{e}_j)$ is orthogonal to the line of parity equation whose unit vector is $\hat{P}_{ij}$. Figure 6 describes the orthogonal failure vector.

For the purpose of isolation of the faulty gyro, we must have at least two parity equations to indicate that a failure has occurred. This is because the failure isolation scheme considered here depends upon a voting principle involving at least three voters.

When the first failure occurs in a four gyro system, and if this failure can be detected, then the faulty gyro can be isolated irrespective of whether the failure was orthogonal or not. The reason for this is that there is a sufficient number of parity equations to do so.

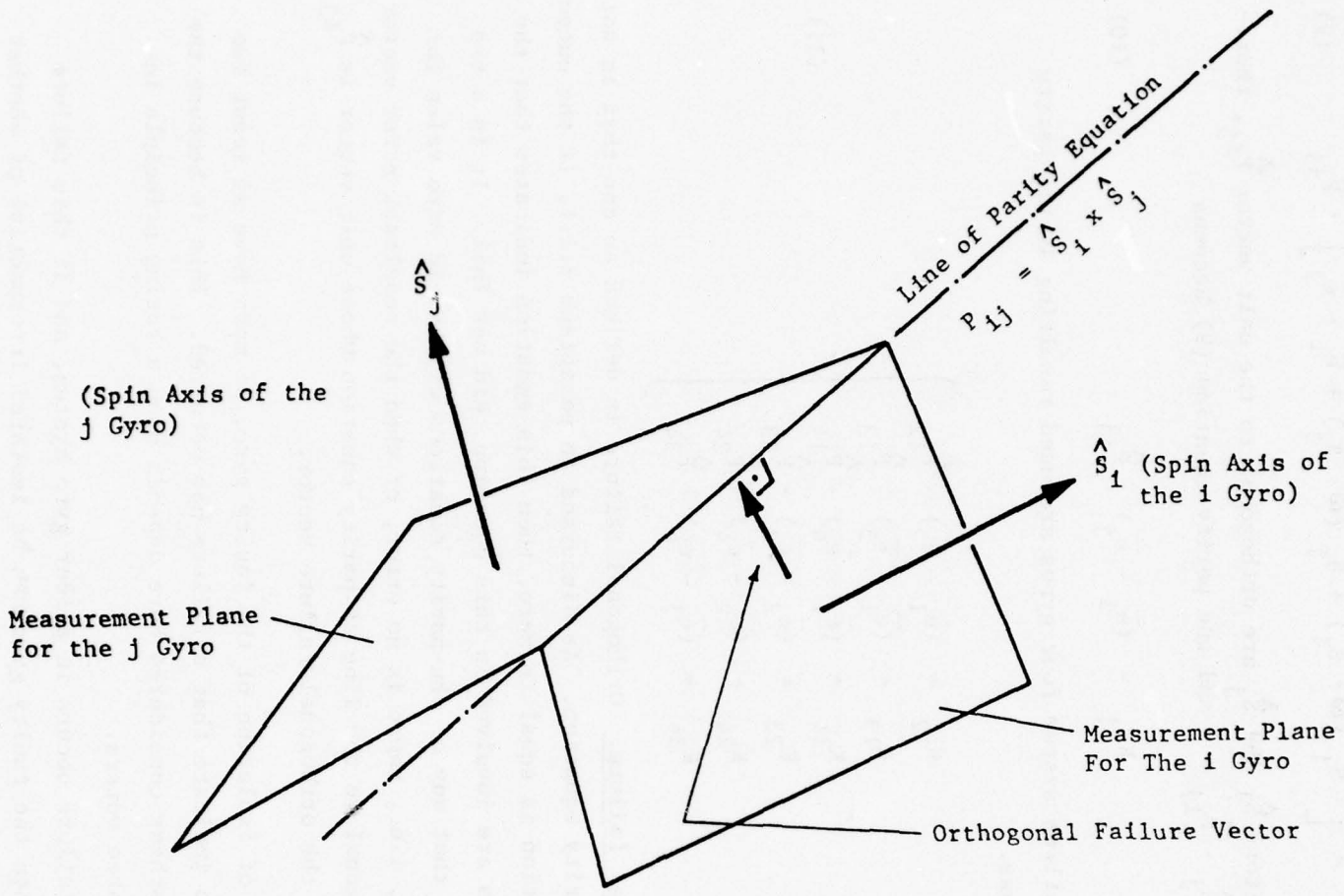

Parity Equation: $K_{ij} = (\bar{e}_i - \bar{e}_j) \cdot \hat{P}_{ij}$

Figure 6. Orthogonal Failure (Orthogonal Failure is not Detected by Parity Equation)

When the second failure occurs in a four gyro system, only a non-orthogonal failure can be isolated. Orthogonal failures can be detected but cannot be isolated. With the three gyro system we have only three parity equations, and so that the failed gyro can be isolated, two of the equations must indicate that the failure has occurred. When the failure is not orthogonal, this condition is satisfied. When the failure is orthogonal, this condition is not satisfied because there is only one equation indicating that failure has occurred.

An orthogonal failure can occur for any skewed axes gyroscopic arrangement. It should also be remembered that in any detection mechanization, the detection level will have to be set above the system noise level, so the vehicle may traverse a fairly considerable angle (or a rate, if rate detection is used) where the detection can be triggered and isolation occur. In a strapdown system, because of high bandwidth electronic requirements, the gyro noise level (which has low frequency components) is in the order of 10^{o}/hr. The electronic noise level, which for a digital torquing loop occurs at the limit cycle rate (generally 1K to 2K Hz), is in the order of 1^{o} to 2^{o}/second. The sensitivity of detection is also considerably affected, if an input rate is close to the spin axis of any gyro. However, the more serious problem is the failure of an axis or a gyro that cannot be detected because the apparent rate produced by a failure is orthogonal to a parity equation line. The orientation of the gyros determines the probability of this occurring and this will be considered in sections 3.2 and 3.3 where gyro orientations are examined.

3.1.5 Failure tables. Using Equation (11), a failure table (Table 34) for four TDF gyros was constructed. It is noted that both orthogonal and non-orthogonal failures were considered and inspection of this table shows that both orthogonal and nonorthogonal failures can be detected and isolated.

Let us assume that one gyro failed and the system now uses three good gyros; #1, #2 and #3. We can construct Table 35 for three gyros and note that only nonorthogonal failures can now be isolated. Nonorthogonal failures are represented by two "ones" and one "zero", while the orthogonal failures are represented by only one "one". The system knows what type of failure has occurred, but it cannot isolate the failed gyro when an orthogonal failure has occurred. This situation gives rise to the TDF fault isolation singularity.

TABLE 34. FAILURE TABLE FOR FOUR TDF GYROS

Failure		Parity Equation					
		K_{12}	K_{13}	K_{14}	K_{23}	K_{24}	K_{34}
Gyro 1	Nonorthogonal	1	1	1	0	0	0
	Orthogonal to gyro 2	0	1	1	0	0	0
	Orthogonal to gyro 3	1	0	1	0	0	0
	Orthogonal to gyro 4	1	1	0	0	0	0
Gyro 2	Nonorthogonal	1	0	0	1	1	0
	Orthogonal to gyro 1	0	0	0	1	1	0
	Orthogonal to gyro 3	1	0	0	0	1	0
	Orthogonal to gyro 4	1	0	0	1	0	0
Gyro 3	Nonorthogonal	0	1	0	1	0	1
	Orthogonal to gyro 1	0	0	0	1	0	1
	Orthogonal to gyro 2	0	1	0	0	0	1
	Orthogonal to gyro 4	0	1	0	1	0	0
Gyro 4	Nonorthogonal	0	0	1	0	1	1
	Orthogonal to gyro 1	0	0	0	0	1	1
	Orthogonal to gyro 2	0	0	1	0	0	1
	Orthogonal to gyro 3	0	0	1	0	1	0
Non Failed		0	0	0	0	0	0

Two or more "ones" indicate isolated failures

The above table provides fail-op operation with 100 percent probability because all failures can be detected and isolated.

TABLE 35. FAILURE TABLE FOR THREE TDF GYROS

Failure		Parity Equation		
		K_{12}	K_{13}	K_{23}
Gyro 1	Nonorthogonal	1	1	0
	Orthogonal to gyro 2	0	1	0
	Orthogonal to gyro 3	1	0	0
Gyro 2	Nonorthogonal	1	0	1
	Orthogonal to gyro 1	0	0	1
	Orthogonal to gyro 3	1	0	0
Gyro 3	Nonorthogonal	0	1	1
	Orthogonal to gyro 1	0	0	1
	Orthogonal to gyro 2	0	1	0
None Failed		0	0	0
Orthogonal failures cannot be isolated				

Two or more "ones" indicate isolated failures

The above table provides for fail-op operation for 90.3 percent of all failures where the gyro orientation is such that single axis failures are orthogonal. Fail-safe operation is provided for 100 percent of all failures as all failures, including orthogonal, can be detected.

3.2 Architecture for four redundant TDF gyros. This section briefly surveys the most likely instrument geometries for a four TDF gyro redundant system and points out some advantages and disadvantages of the proposed configurations. It is recognized that in order that the system reliability criteria be met, none of the spin axes of the gyros must be coincident. Once this condition is accomplished, the requirements for system reliability are achieved, but then a question arises as to what is the optimum architecture of the gyro such that the system will also have maximum accuracy and will be characterized by ease of packaging and computations. First, let us consider the architecture proposed by Teledyne and described in Reference III. Figure 7 shows this architecture when the three gyro spin axes H_1, H_2 and H_3 are mutually orthogonal, with the fourth gyro spin axis, H_4, bisecting the orthogonal set. The major disadvantage of this configuration is difficulty of packaging and inability to separate the system into two identical self contained subsystems.

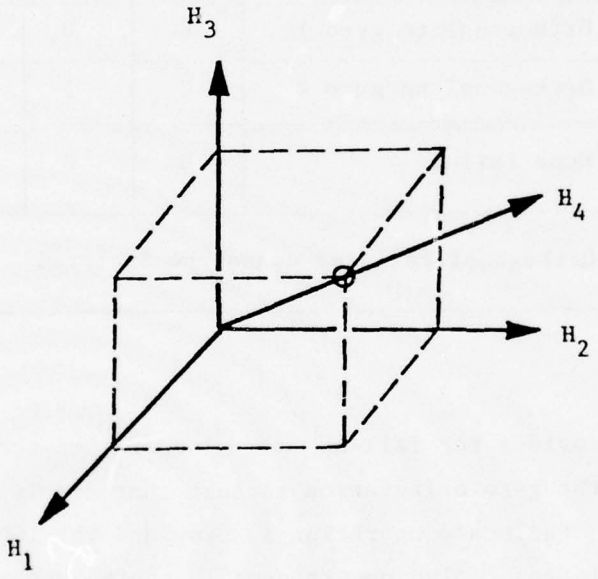

Figure 7. Four Gyro Arrangement with Three Gyros Mutually Orthogonal

III "Investigation of Applications of Two-Degrees-of-Freedom Dry-Tuned Gyroscopes to Strapdown Navigation Systems", Final Report, NASA CR-132419, April 1974 Teledyne Systems Company, Northridge, CA.

Figure 8 shows the architecture proposed by Litton, and described in Reference IV. In this configuration, the four gyro spin axes are normal to the surfaces of a regular tetrahedron. This architecture is characterized by two major advantages, i.e., ease of packaging, and ability to separate the system into two identical self contained subsystems.

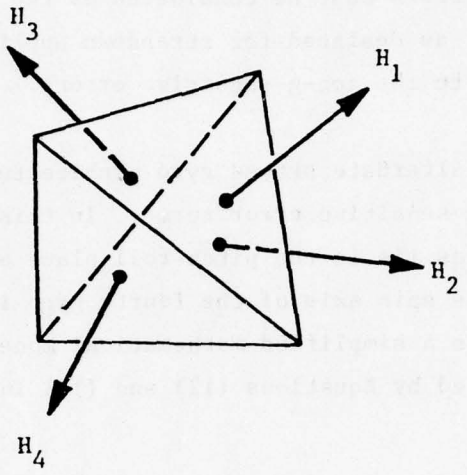

Figure 8. Four Gyro Tetrahedron Arrangement

Each subsystem generates enough information to formulate an attitude matrix independently, so navigation can be performed without requiring precise alignment between sensors on different halves of the tetrahedron. However, if both axes of a gyro fail on one half of the tetrahedron, attitude information is now required from the other half to keep the first half operating, if fail-op/fail-op operation is to be accomplished. Now, very precise alignment or knowledge of the misalignment for software compensation, (e.g., 10 to 20 arcseconds) is required between the gyro axes on different halves of the tetrahedron if accurate navigation is required. There does not appear to be any practical way to achieve this in an operational application. Such accurate alignment is not necessary for flight control.

IV "Preliminary Design of a Redundant Strapped Down Inertial Navigation Unit using Two-Degree-of-Freedom Tuned Gimbal Gyroscopes". Final Report, NASA CR-145305, October 1976, Litton Guidance and Control Systems, Woodland Hills, CA.

All the other four TDF and six SDF gyro configurations suffer from the same problem if the gyros are not mounted on a common base.

Both Litton and Teledyne system configurations suffer from the disadvantage of accuracy reduction due to the coupling of the g-sensitive gyro error terms into the horizontal plane. When considering the use of dynamically tuned gyros, these effects must be considered as the g-sensitive error terms in this type of gyro, as designed for strapdown applications, is typically larger than that due to the non-g-sensitive errors.

Figure 9 shows an alternate skewed gyro architecture which has reduced sensitivity to gyro g-sensitive error terms. In this arrangement the spin axes of the three gyros lie in the pitch-roll plane and are separated by 120^{o} from one another. The spin axis of the fourth gyro is along the yaw axis. For reference purposes a simplified mathematical model of a TDF Dynamically Tuned gyro is presented by Equations (12) and (13) in terms of torque to balance.

$$M_{fx} = \dot{\phi}_y H - Ma_y - Qa_x - Aa_y a_z + B_x \tag{12}$$

$$M_{fy} = -\dot{\phi}_x H + Ma_x - Qa_y + Aa_x a_z + B_y \tag{13}$$

Where

M_f = Torque to balance moment

$\dot{\phi}$ = Input angular rate about gyro axes

a = Linear acceleration along gyro axes

M = Spin axis mass unbalance-direct component

Q = Quadrature mass unbalance

A = Anisoelastic coefficient

B = Non-g-sensitive bias

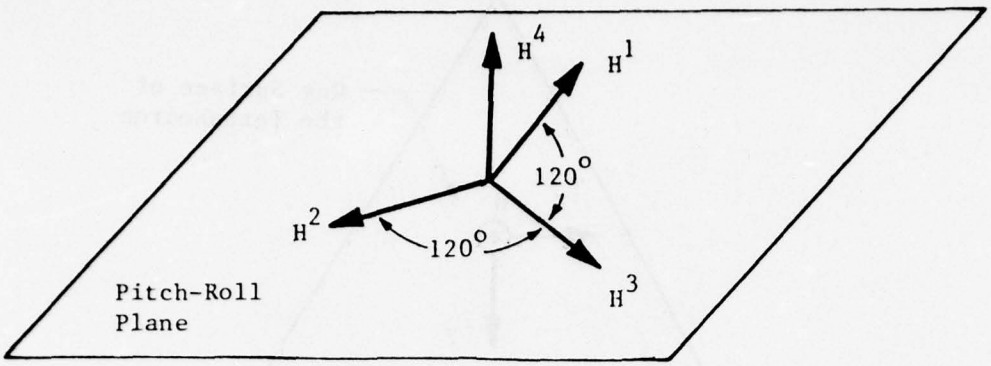

Figure 9. Skewed Arrangement of Four Gyros

The typical magnitudes of the g-sensitive error coefficients for the dynamically tuned gyros, designed for strapdown applications, are briefly discussed in the following paragraphs. The g-sensitive bias (direct component) day-to-day instability ranges from 0.01°/Hr/g to 1.0°/Hr/g with a temperature sensitivity of this term ranging from 0.005°/Hr/g/$^{\circ}$F to 0.05°/Hr/g/$^{\circ}$F. The g-sensitive bias (quadrature component) has an excellent short term and long term stability with negligibly small temperature sensitivity.

For comparison purposes, the non-g-sensitive bias day-to-day instability ranges from 0.005°/Hr to 0.1°/Hr, with a temperature sensitivity in the range of 0.003°/Hr/$^{\circ}$F to 0.01°/Hr/$^{\circ}$F. The anisoelastic coefficient has an excellent short term and long term stability, with negligibly small temperature sensitivity. The complete error model of a dynamically tuned gyro is presented in Appendix A.

The most important aspect of the configurations shown is the orientation of the torquer axes to the mounting base. The deciding factor for torquer axes orientation is the probability of failure of both axes, versus the probability of failure of a single axes. As the probability is considerably higher for both axes to fail (76 failures per million hours for two axes and 8 failures per million hours for one axis) the torquer axes should be orientated orthogonally to the parity equation line. This is shown in Figure 10 for the tetrahedron configuration. One of the axes cannot be exactly orthogonal as can be

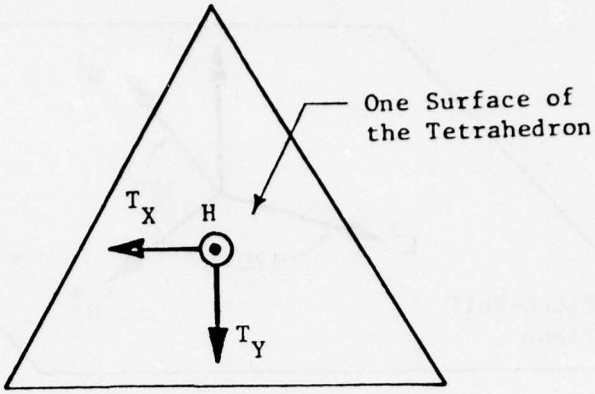

Figure 10. Preferred Orientation of Torquer Axes
T_X and T_Y are the X and Y torquer axes
and H is the spin axis

seen from the figure, but the arrangement shown is the closest possible to making all torquer axes orthogonal to the parity equation line.

Although only six accelerometers are essential, if correctly orientated, for fail-op/fail-op reliability, the mechanical configurations shown do not lend themselves readily to a six accelerometer package. The six accelerometers would ideally be mounted on a dodecahedron, but this would require a separate mounting structure for gyros and accelerometers. Axes alignment between the gyros and accelerometers needs to be accurate for navigation purposes, and would be costly to accomplish on separate structures. Also the size and weight of the total system would be greatly increased. If the alignment equations are carried as software coefficients instead of being mechanically established, then the whole system has to be recalibrated each time an instrument is replaced. This causes the whole system to become a Line Replaceable Item (LRU), greatly increasing the Life Cycle Cost because of the inherent cost of the spares.

Therefore, it is recommended that two axes of acceleration measurement, i.e., either two single-axes or one two-axes accelerometer, be utilized on each mounting surface with each gyro. The accelerometer sensitive axes are mounted parallel to each torquer axes of the gyro.

The extra two axes of acceleration measurement over that essential for fail-op/fail-op will not increase acquisition cost when compared to precise alignments between two mounting structures, and will obviously save considerably on size and weight. The acquisition cost is also justified when compared to the alternative of having a complete system as an LRU.

The associated electronics for both gyros and accelerometers would be packaged with their respective instruments. This would allow a modular approach to all instruments and would allow complete interchangeability of instrument types. This assumes the unique coefficients for each instrument, e.g., biases, are carried in the electronics. This modular approach would be desirable for all types of instruments, including single-degree-of-freedom gyros, lasers, multisensors etc., that will be discussed later.

Power supplies are generally not considered as electronics associated with any one instrument and are not, in fact, unique to any instrument. They therefore can be shared and be made common to more than one instrument. However, to meet the criteria of fail-op/fail-op, i.e., no single failure can cause a complete system to fail, then three power supplies in parallel are always necessary. To detect and isolate failures Built-In-Test (BIT) is required. However, if such a shared mechanization is used, a short in any instrument (including any cabling), must be disconnected at the output of the power supply. This would not be difficult if a current sense is used as the BIT at each output port, and if each instrument has a separate output port from each supply. Voltage levels from the supply would also need to be monitored, although with the power supplies in parallel, a diode gate at each instrument could also be used. To be sure that operation can continue after two failures, each supply has to be able to generate enough power to carry the entire system by itself.

The power supply failure rates, computed in Section II, suggest that such a mechanization of three parallel supplies would allow the system to meet a mission reliability of .99999.

Another attractive alternative is to have a power supply for each gyro, and share with the allied (parallel) two axes of acceleration. This eliminates reliance on BIT tests, and reduces the power requirements for each supply. However, it means that if the supply fails, then both axes of gyro and accelerometer also fail. This means that the failure rates for both the gyros and accelerometers and their associated electronics must have the power supply failure rate added. This increases the gyro failure rate by approximately 30 percent and the accelerometer by approximately 40 percent. However, in a fail-op/fail-op mechanization, this has little affect on the reliability. As an illustration, the probability of failure for three power supplies in parallel, four TDF gyros and four TDF accelerometers can be written

$$P \cong 3(F_p t)^2 - 3(F_p t)^3 - 9(F_p t)^4 + 4(F_G t)^3 - 9(F_G t)^4 + 4(F_A t)^3 - 9(F_A t)^4$$

Where

F_p = Failure rate for a power supply

F_G = Failure rate for a gyro and its electronics

F_A = Failure rate for an accelerometer and its electronics

t = Operational (mission) time

The above is the system failure rate to the first order, and to simplify things, it has been assumed that both axes of gyro and accelerometer fail. We shall also assume that the power supplies for both cases have equal failure rates.

The equation is written for up to and including two power supplies and two instrument failures of either type. Using the same assumptions, the equation for the base of a power supply shared between a TDF gyro and TDF accelerometer is

$$P \cong 4\,(F_G t + F_P t)^3 - 9\,(F_G t + F_P t)^4 + 4\,(F_A t + F_P t)^3$$

$$- 9\,(F_A t + F_P t)^4$$

$$\cong 2\left[4\,(F_P t)^3 - 9\,(F_P t)^4\right] + 4\,(F_G t)^3 - 9\,(F_G t)^4$$

$$+ 4\,(F_A t)^3 - 9\,(F_A t)^4$$

In other words, the latter case has reduced the sensitivity of the system to power supply failures.

There will be some impact on cost, size and weight however. Power supplies costs and size and weight tend to vary directly in proportion to their wattage capability. The power capability of each of those in parallel will be equivalent to all four of the individual supplies. Therefore, we can safely assume that the three in parallel configuration will be considerably larger and cost more. Our estimate is that there will be a decrease in cost, size and weight - in favor of the four supply configurations. The individual four supply configurations also eliminates any dependency on BIT, which was an original ground rule, and increases the options that can be exercised in designing for modularity. The decrease in size and weight for the four supply configuration will be by the same ratio as the power capability requirement, i.e., 4 to 12 or 66 percent.

A block diagram of the four gyro configuration is shown in Figure 11.

As all the instruments are mounted on one common base, the survivability of this system is low. One solution is possibly to armor plate the instruments and cables. However, this would add at least 20 percent to the weight, assuming only the instruments and cables and not the complete package was protected. A more viable solution may be to disperse the sensors throughout the aircraft, and such a mechanization is outlined in the next section.

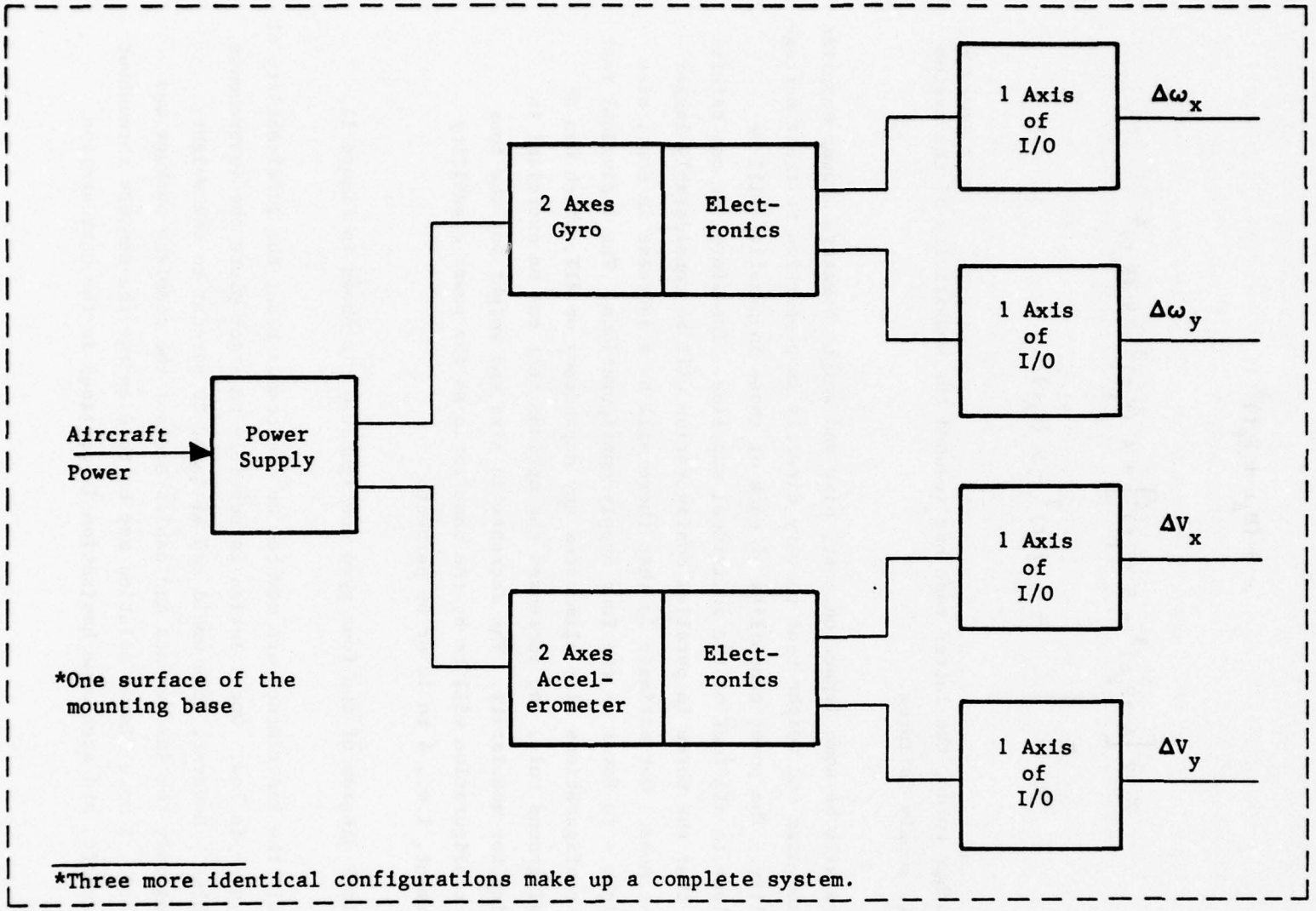

Figure 11. Four Two-Degree-Of-Freedom System Configuration

3.3 Architecture for six redundant TDF gyros. If the sensors are to be dispersed throughout the aircraft for maximum survivability, it appears that a mechanization using only four gyros is not practical. The problem would be mainly in establishing alignment of the sensor axes to each other, as explained earlier. The most convenient mechanization would appear to be six 2 axes gyros orientated to give three identical Inertial Reference Assemblies (see Figure 12). Each IRA would have one gyro with its spin axis vertical and the other gyro would have its spin axis horizontal and orthogonal to the first. This approach results in three Inertial Reference Assemblies that are stand-alone strapdown navigation systems. There are now six gyros in the system, giving twelve axes of rate sensing. Now four of these axes can be coincident for each of the pitch, roll and yaw sensing of vehicle motion and still give a fail-op, fail-op system with voting capability. If the three Inertial Reference Assemblies are identical, then mounting provisions must be made so that one of the assemblies can be mounted with a 90^{o} rotation about vertical to the other, which is no problem. However, the third assembly must be rotated 90^{o} about a horizontal axes from the second, which means mounting surfaces must be provided on orthogonal sides of the box that houses the instruments. This would not be particularly difficult, however, as the mounting alignments do not have to be precise. This is because a complete three axes attitude matrix can be formulated by any one IRA. Now, failure detection can be performed in a common reference frame between IRA's and navigation accuracy is unaffected by the separation of IRA's even after a complete (both axes) failure. However, to introduce all four gyro axes of any IRA into the failure detection matrix, the attitude needs to be computed twice. The second time, the "redundant" axis of the IRA is utilized. For example, in Figure 12 T_Y^1 is used first and then T_Y^2 in IRA No. 1, etc. Now, if any two complete gyros or if any two single axes fail, in any combination in any of the IRA's, the system is still fully operational. As soon as a complete gyro has failed, that particular IRA is inoperative for navigation purposes. Depending on which axes fail, the system can still operate fully with up to four single-axis failures; and up to three complete gyro failures, again depending on which gyros fail. The system can always detect and isolate two failures of any kind making it a fail-op/fail-op system.

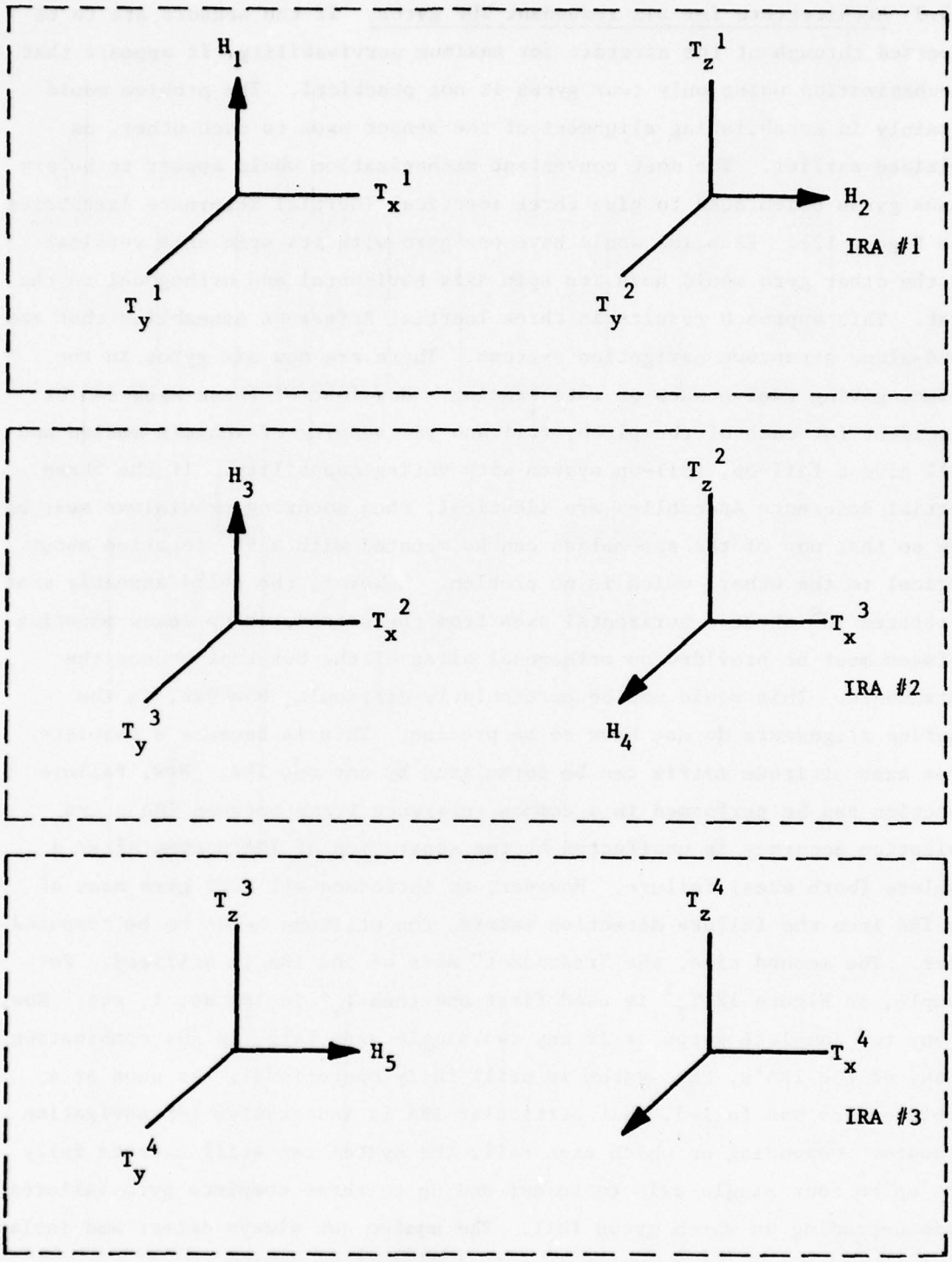

H_1 through H_6 are gyro spin axes and T_x and T_y are the associated torquer axes.

Figure 12. Six TDF Gyro Configuration

Two 3 gyro IRA's could be utilized with 3 spin axes orthogonal to each other, if one was rotated by 90^{o} about two of its axes. However, survivability would be better for three 2 gyro IRA's. Both approaches shown above eliminate the isolation singularities for the 4 gyro mechanizations, and provide good failure detection sensitivity. The cost is of course greater than for any of the four gyro configurations. The increase in cost for six gyro configuration will be approximately a 20 percent increase over the four gyro configuration for the complete MIRA fail-op/fail-op system. It should also be noted that the mass unbalance term only affects the azimuth axis in IRA No.'s 1 and 2, so the accuracy obtained from level axes is not contaminated by skewing of axes.

If the accelerometer axes are skewed with reference to each other, then the same problem of alignment between the IRA's exists. Therefore, it is best to align the accelerometer input axes parallel to the gyro torquer axes. This will result in six 2-axes accelerometers or twelve single-axes accelerometers.

Although this mechanization requires six TDF gyros and six TDF (or twelve SDF) accelerometers, it has no orthogonal failures for fail-op/fail-op operation and it has sensors dispersed throughout the aircraft for maximum survivability.

It would be appropriate in this mechanization to use only three power supplies as each supply would only have to service one IRA. It would not have to be designed to carry any excess load if one of the supplies in the other two IRA's failed.

The six TDF gyro and six TDF accelerometer mechanizations outlined above would increase the acquisition cost of the system by approximately 40 percent over the four TDF gyro and four TDF accelerometer configuration outlined in the previous section. The estimated total weight of the three IRA's would be approximately 45 pounds.

One problem with dispersed sensors is that the vehicle body bending motions and lever arm affects can add to the noise on the outputs of the sensors, especially the gyros, relative to each other. This can affect the stabilization of the vehicle if the IRA's are used for this purpose. A very significant problem is the affect of body bending motions on the time to detect and isolate failures, although failure detection sensitivity is not affected over a longer period as filtering occurs. As the IRA's will be comparing outputs for failure detection, the added noise on the output will slow the failure detection response time. Navigation performance will be unaffected.

3.4 Single-degree-of-freedom gyro orientation. Five single-degree-of-freedom gyros - either rotating wheel or lasers - can be mounted to perform fail-operational performance by software parity equation comparison.

However, such an array cannot isolate a second failure. The second failure can be detected, but cannot be isolated because of the lack of parity equations.

Six single-degree-of-freedom gyros are therefore the minimum number that can be utilized to provide fail-operational/fail-operational performance. In principal, various six gyro skewed configurations possess the required level of redundancy. The most advantageous configuration, however, is the dodecahedron array because of its symmetry, whereby the six measurement axes are spherically distributed with equal angles between them.

The input axes are orientated to be normal to the faces of the dodecahedron, with an angle of 63.4 degrees between any axes (see Reference V).

This configuration gives equal sensitivity to all axes for failure detection and isolation and the greatest likelihood of operational accuracy compared to any other mechanization.

[V] "A Redundant Strapdown Inertial Reference Unit (SIRU)", Jerald P. Gilmore and Richard A. McKern; Journal of Spacecraft and Rockets, Vol. 9, No. 1, January 1972.

This system could operate with only three gyros operational. However, a maximum of two of the six can be isolated by gyro output comparisons.

One convenience of this mechanization is that the minimum number of accelerometers i.e., six, can be conveniently packaged on the same mounting surface as the gyros. The most convenient location for the associated electronics would also be on the same surface. In this way, a separate module could be designed for both the gyro and accelerometer, each with their own electronics.

The same tradeoff for the power supply configuration can be made as shown for the TDF gyros. It is true that now six individual power supplies will be necessary, but the same general effect on reliability, size/weight and cost still hold. This makes the individual supply servicing a gyro and accelerometer attractive.

The dodecahedron approach using single-degree-of-freedom gyros will be fairly large. The size will be somewhat larger for laser gyros due to their inherently larger size and the complexity of mounting requirements needed to eliminate case stresses, especially for fast reacting and unheated systems. For the six single-degree-of-freedom floated gyro array, with six accelerometers and all required electronics, the size is estimated to be 1900 cubic inches and the weight approximately 65 pounds. For the laser array, the size is expected to be 2330 cubic inches and the weight 80 pounds.

A major deficiency of the dodecahedron array is that the complete system is packaged together, therefore being vulnerable to complete failure if the aircraft suffers damage during an operation. If the sensors are separated, the same problem of sensor alignment occurs as explained earlier for two-degree-of-freedom gyros. If the sensors are distributed, twelve single-degree-of-freedom gyros and twelve single-degree-of-freedom accelerometers will be required to obtain fail-op/fail-op reliability. This will of course increase the acquisition cost, size and weight considerably. The other alternative is to armor plate the system and connecting cables. If 1/4 inch armor plating

is used to protect the instrument modules the system will weigh approximately 20 pounds more for the system using either single-degree-of-freedom or laser gyros.

The increased cost, size and weight for the dispersed single axis sensor configuration, i.e., twelve gyros and twelve accelerometers, makes this approach non-competitive. Therefore, it has not been considered a viable candidate.

3.5 Multisensor. The multisensor considered in this document consists of two axes of rate measurement with two axes of acceleration all encased in the same housing with the rate measurement and acceleration measurement axes in parallel. Therefore, the multisensor can be considered as a TDF gyro and TDF accelerometer from a redundancy viewpoint, so all the analysis for the four TDF gyro configurations is valid for the multisensor.

As with the TDF gyro, the optimum configuration would appear to consist of four multisensors mounted on the faces of a tetrahedron. The only difference from the TDF gyro case would be that the Line Replaceable Unit would consist of a module that contained both axes of rate and acceleration measurement, rather than a separate module for rate and acceleration. This will increase the sensor spares costs by a factor of 2.

3.6 Synopsis of preferred configurations. It was concluded that the most practical configurations are the tetrahedron, dodecahedron and three identical Inertial Reference Assemblies.

The tetrahedron can only be mechanized using two-degree-of-freedom gyros and accelerometers, or multisensors. The dodecahedron can best be configured with single-degree-of-freedom instruments, although two-degree-of-freedom instruments could be used. The tetrahedron configuration requires four TDF gyros and four TDF accelerometers, or four multisensors. The dodecahedron requires six gyros and six accelerometers of whatever type.

As the tetrahedron requires the least number of instruments, it would be the smallest. Also, it will have the lowest acquisition cost. This is because for equivalent performance, the cost of two axes instruments has historically been the same as that for single axis instruments. Therefore, the four gyro/four accelerometer combination is lower in cost than a six gyro/six accelerometer approach.

The tetrahedron configuration suffers from an inability to isolate a second failure, if it is an orthogonal failure. This is true of any mechanization using four TDF sensors. By orientating the sensing axes as shown in Figure 10, single axes failures will be orthogonal to the parity equation line. The failure rate for a single axis for the TDF gyro and its electronics has been estimated to be eight per million hours. However, this would be a second failure. The worst case probability of an undetectable single axis failure would be a complete gyro failure followed by a single axis failure. For a 10 hour mission the probability of failure for this dual occurrence would be 6×10^{-9}/Hr, using the failure rates from Section II, resulting in a mission probability of success (Mission Reliability) in excess of .99999. This certainly would seem to make the tetrahedron a useable configuration.

One problem that plagues both the tetrahedron and dodecahedron is the impracticality of dispersing the instruments within the aircraft for survivability. To eliminate this problem, a six TDF gyro/six TDF accelerometer system was configured as shown in Section 3.3. This configuration allows dispersed sensors, can detect and isolate any two failures (i.e., fail-op/fail-op), and has no mass unbalance coupling into the level axes.

SECTION IV

DIRECTIONAL PROBABILITY OF FAILURE IN A TDF TUNED-GIMBAL GYRO

Let us start the discussion of directional probability of failure in a TDF gyro with a simple case of two single-degree-of-freedom (SDF) gyros. Thus, let us assume that a SDF gyro can only fail to operate satisfactorily along one axis in space, where it is tacitly assumed that the gyro/s in question are stationary relative to the reference space. When we consider two entirely independent[1] and identical SDF gyros, each having a probability of failure equal to P, then the probability that either one or the other gyro fails is equal to $2P(1-P)$, and the probability that both of these gyros fail simultaneously is equal to P^2 as this condition is characterized by the criterion of independent events. Let us consider that the SDF gyros are mounted orthogonally to each other with their sensing axes along the X and Y axes as shown in Figure 13.

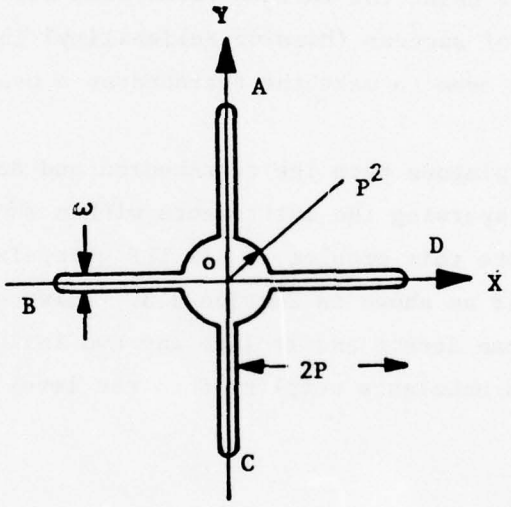

Figure 13. Directional Probability of Failure in Two Independent Single-Degree-of-Freedom Gyros Mounted Orthogonally to Each Other

---

1) Independent, here, means that each gyro is self contained and does not share any components with any other gyro. For example, each gyro is assumed to have its own voltage and power supplies and its mounting structure is independent of the mounting structure of any other gyro.

Since the gyro errors can be either positive or negative, and the probability of occurrence of such errors is equal, therefore we can plot four points denoted A, B, C and D along X and Y axes such that AO = BO = CO = DO equal to the probability of failure of either one or the other axis. It is assumed that $P << 1$. When both gyros fail simultaneously, the error vector that characterizes this failure has an equal probability of occurrence at any angle, and relative to any axis. Thus, the probability of failure in the quadrants can be represented by a circle whose radius is equal to P^2. It is, of course, noted that the magnitude of the resultant error vector may assume any value. Since $P << 1$ then $2P >> P^2$ by several orders of magnitude. In Figure 13 the finite width, ω, is only used for illustrative purposes because in actuality $\omega = 0$.

Next, let us consider the same two SDF gyros, but, let us assume that they share between them one power supply. Let us assume that the probability of failure of the power supply is equal to P_P, and let us further assume that if the power supply fails, then both gyros will cease to function properly. The probability of failure of both axes, P_2, can be obtained with the help of Table 36

TABLE 36. TRUTH TABLE FOR *POWER SUPPLY AND GYRO FAILURES*

Power Supply	Gyro No. 1	Gyro No. 2	Probability
Fails	Not Fails	Not Fails	P_P (1-P) (1-P)
Fails	Not Fails	Fails	P_P (1-P) P
Fails	Fails	Not Fails	$P_P P$ (1-P)
Fails	Fails	Fails	$P_P P^2$
Not Fails	Fails	Fails	$(1-P_P)$ P^2

$$P_2 = P_P (1-P)^2 + 2P_P P (1-P) + P_P P^2 + (1-P_P) P^2 \quad (14)$$

Assuming

$$P << 1$$

and

$$P_P << 1$$

Then equation (1) becomes

$$P_2 = P_P + 2P_P P + P_P P^2 + P^2$$

$$= P_P (1 + 2P + P^2) + P^2$$

$$\cong P_P + P^2 \quad (15)$$

Equation (15) states the probability of failure of both axes. The probability of failure of either one or the other axis P_1, is obtained with the help of Table 37.

TABLE 37. TRUTH TABLE FOR THE PROBABILITY OF A SINGLE AXIS FAILURE

Power Supply	Gyro No. 1	Gyro No. 2	Probability
Not Failed	Not Failed	Failed	$(1-P_P)(1-P)P$
Not Failed	Failed	Not Failed	$(1-P_P)(1-P)P$

$$P_1 = 2 (1-P_P) (1-P_P)P$$

Assuming again $P_P << 1$

$$P_1 = 2P \tag{16}$$

Equation (16) represents the probability of failure of a single axis. For the cases considered above, the probability of simultaneous failure of both gyros may be smaller or greater than the probability of failure of a single axis. This, of course depends on the relative magnitudes of P_P and P.

If the probability of failure of the power supply is larger than that of the gyro, then

$$P_2 \cong P_P$$

and

$$P_1 \cong 2P \text{ (where } P << 1)$$

and therefore, probability of failure of both gyros is larger than the probability of failure of either one or the other gyro. If one assumes that a failure of the power supply would affect the performance of both gyros equally then the maximum probability of failure would occur at 45^o, 135^o, 225^o and 315^o relative to the X axis. Under this condition the directional probability of failure would assume a general form shown in Figure 14. The exact shape of the directional probability of failure could be obtained from the analysis of modes of failure.

Now, let us consider a two-degree-of-freedom gyro. Figure 15 shows the functional block diagram of a TDF gyro and its associated electronics and supplies. Both axes are supplied by a common power supply. Under these conditions the TDF gyro directional probability of failure would also assume the shape of Figure 14.

Prior to the more detailed discussion of directional probability of failure in a TDF gyro, let us briefly review the functions of the various subassemblies of the gyro and its associated electronics.

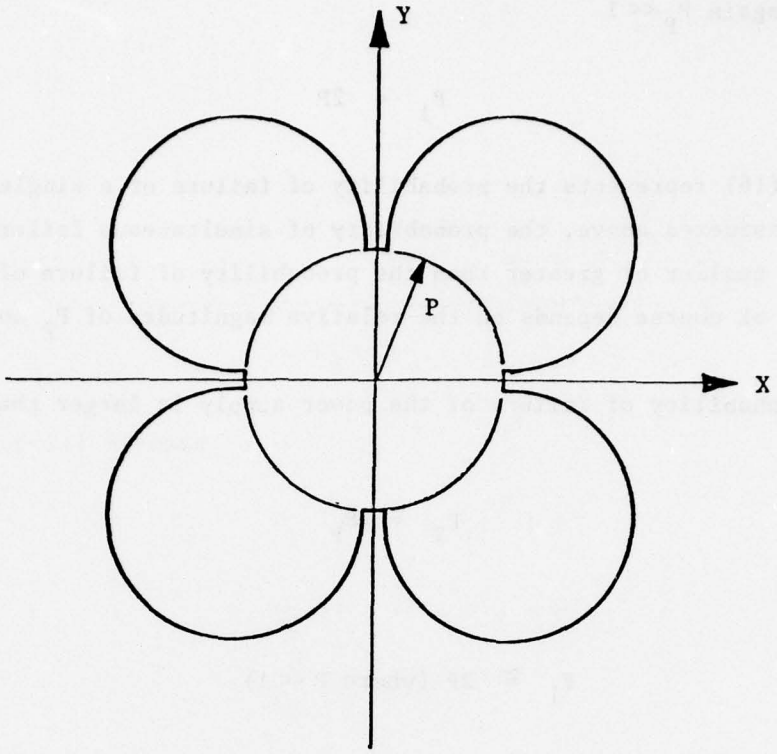

Figure 14. Hypothetical Directional Probability of Failure of Two SDF Gyros

4.1 Functions of TDF gyro subassemblies

Pickoff and Torquer Assemblies

The function of the pickoffs and torquers is to control the attitude of the rotor relative to the gyro housing. When an input rate is applied to the gyro case, the case fixed pickoffs sense the change of rotor attitude relative to the case and cause the caging loop to provide current to the torquers in such a sense as to reduce this change to zero. In an ideal strapdown gyro the torquer maintains the spin axis of the rotor aligned with the shaft spin axis and thus the rotor has the same angular velocities as the gyro case about the input axes.

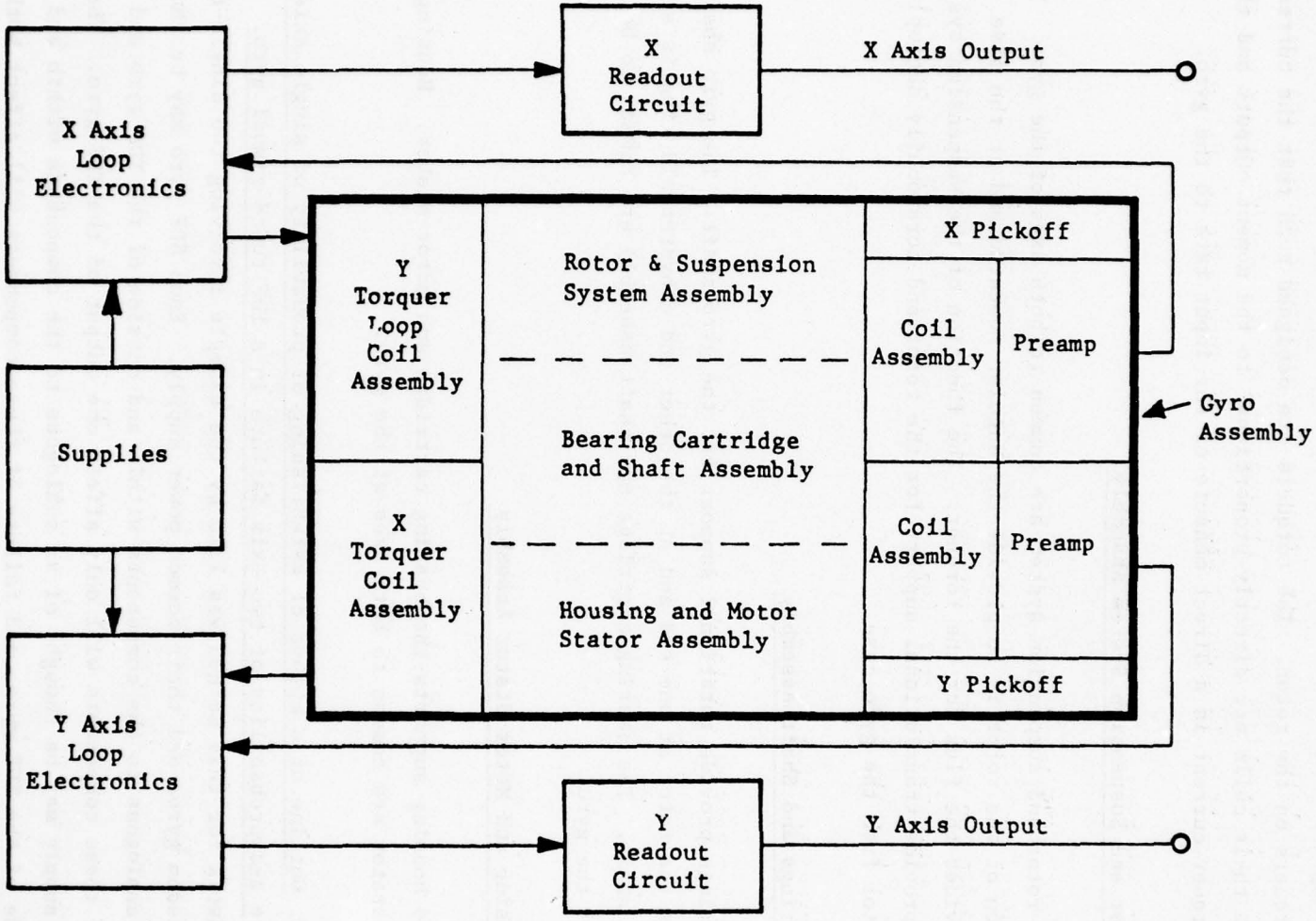

Figure 15. Gyro Assemblies and Gyro Associated Electronics

In order to satisfy this condition, the torquers must provide moments in accordance with the relation $\overline{M} = \overline{\omega} \times \overline{H}$, where $\overline{\omega}$ is the input angular rate, $\overline{H}$ is the angular momentum of the rotor, and $\overline{M}$ is the vector moment exerted by the torquers on the rotor. The torquers are designed such that the current through their coils are directly proportional to the moment outputs and thus the torquer current is a direct measure of the input rate to the gyro.

Rotor and Suspension System Assembly

The rotor and suspension system are common to both axes of the gyro. The function of the rotor is to provide the angular momentum and at the same time it provides the flux for the torquer. The function of the suspension system is to provide translational support for the rotor and torsionally decouple the rotor from the gyro case.

Bearings and Shaft Assembly

Bearings provide rotational support for the gyro shaft. The gyro shaft carries the rotor at one end and at the other end a hysteresis ring is attached to the shaft. The bearing cartridge and shaft assembly are common to both axes of the gyro.

Housing and Motor Stator Assembly

Gyro housing supports the bearing cartridge and motor stator. Housing and motor stator are common to both axes of the gyro.

4.2 Outline of a method of establishing of probability of single axis failure and probability of two axis failure in a TDF tuned-gimbal gyro. The groundwork for this method was laid by the example involving two single-degree-of-freedom gyros and their common power supply. Each SDF gyro may be thought of as analogous to the components within and outside of the TDF gyro and failure of these components will only affect one output of the TDF gyro. The power supply may be thought of an analogous to the components within and outside of the TDF gyro, and failure of these components will affect both

outputs of the TDF gyro. Figure 16 shows the reliability block diagram for the TDF tuned gimbal gyro and its associated electronics.

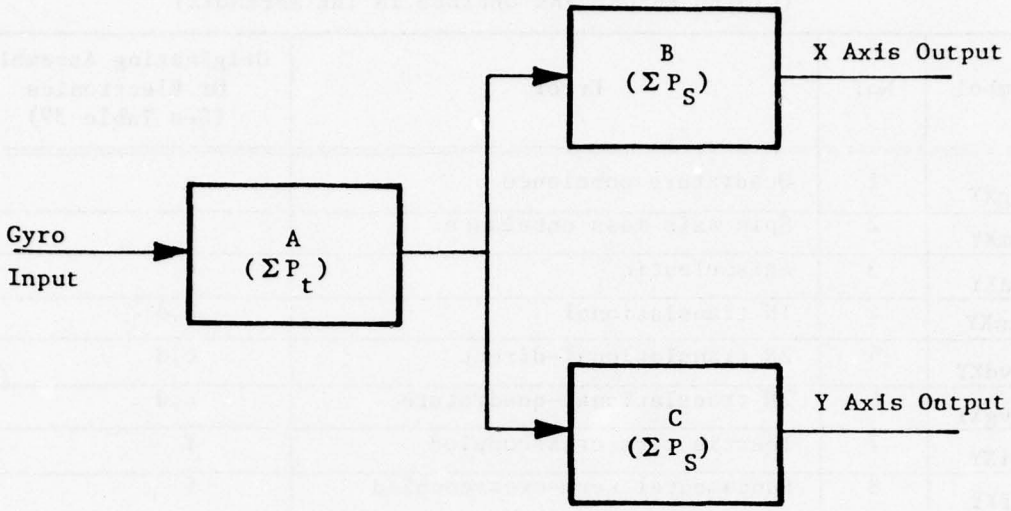

Figure 16. Reliability Block Diagram for the Two-Degree-Of-Freedom Tuned-Gimbal Gyro and its Associated Electronics

Using the indicated analogies we may write

$$P_1 = 2 \Sigma P_S$$

and

$$P_2 = \Sigma P_t + (\Sigma P_S)^2$$

Where P_1 denotes probability of failure of a single axis in the tuned-gimbal gyro and P_2 denotes the probability of failure of two axes in the tuned-gimbal gyro.

ΣP_S represents the sum of probabilities of failures of subassemblies that cause single axis failures.

ΣP_t represents the sum of probabilities of failures of subassemblies that cause two axis failures.

The error terms outlined in Table 38 are defined in the Appendices to this report.

TABLE 38. LIST OF ALL KNOWN ERRORS FOR THE TDF TUNED-GIMBAL GYRO (LISTED ERRORS ARE DEFINED IN THE APPENDIX)

Symbol	No.	Error	Originating Assembly Or Electronics (See Table 39)
M_{tgXY}	1	Quadrature unbalance	c
M_{tmXY}	2	Spin axis mass unbalance	c
M_{taXY}	3	Anisoelastic	c
M_{tnXY}	4	1N translational	c,d
M_{tvdXY}	5	2N translational-direct	c,d
M_{tvgXY}	6	2N translational-quadrature	c,d
M_{riXY}	7	Inertia term-crosscoupled	f
M_{rfXY}	8	Fundamental term-crosscoupled	f
M_{raXY}	9	Anisoinertia term	f
M_{rmXY}	10	Motor dynamics term	f,e
M_{rsXY}	11	Spin axis accel. coupling term	f
M_{rtXY}	12	Torquer axis misalignment	a
M_{rdXY}	13	Rotor damping term	c
M_{sdXY}	14	Direct spring rate term	b,f,d,g
M_{sqXY}	15	Quadrature spring rate term	b,f,d,e,g
M_{svdXY}	16	2N angular-direct	c,d,f
M_{svqXY}	17	2N angular-quadrature	c,d,f
M_{sbXY}	18	Bearing noise term	d
B_{1XY}	19	Motor voltage term	h,e
B_{2XY}	20	Motor frequency term	h
B_{3XY}	21	Pickoff voltage term	h,b
B_{4XY}	22	Pickoff frequency term	h
B_{5XY}	23	Internal magnetic term	e,a
B_{6XY}	24	External magnetic term	
B_{7XY}	25	Internal pressure term	e,a,b
B_{8XY}	26	Synchronous current term	f
SF_{XY}	27	Scale factor	h,e,d,a
B_{9XY}	28	G-sensitive temperature term	c
B_{10XY}	29	Non-g-sensitive temperature term	a,b,c,d,f

All the known errors in the tuned-gimbal gyros are listed in Table 38. Gyro subassembly or electronics that are most likely to produce the error are indicated against these errors. Table 39 lists the errors produced by gyro subassemblies and associated electronics

TABLE 39. ERRORS PRODUCED BY GYRO SUBASSEMBLIES AND ASSOCIATED ELECTRONICS

Gyro Subassemblies and Associated Electronics		Error Produced (See Table 38)
a	Torquer coil assembly	12,23,25,29,27
b	Pickoff coil assembly	14,15,21,25,29
c	Rotor and suspension system	1,2,3,4,5,6,13,16,17,28,29
d	Bearing assembly	4,5,6,14,15,16,17,18,27,29
e	Gyro housing assembly	10,15,19,23,25,27,29
f	Loop electronics	7,8,9,10,11,14,15,16,17,26, 29
g	Pickoff preamplifier	14,15
h	Voltage and power supplies	27
i	Readout circuits	

The method of establishing the probability of single axis and two axes failures shown in this section was used in the analysis of section 2.1 (to establish TDF gyro failure rates).

Tables 38 and 39 are included to indicate the relationship between failures and gyro subassemblies. The error terms listed in Table 38 are caused by the subassemblies listed in the last column. Reference the last column of Table 38 to the first column of Table 39, and the last column of Table 39 to the second column of Table 38.

SECTION V

CONCLUSIONS

1. The least amount of hardware possible to obtain fail-op/fail-op redundancy is four two-degrees-of-freedom strapdown gyros and four two-degrees-of-freedom accelerometers.

2. Single axis accelerometers can be used with two-degree-of-freedom gyros, but eight are required with four gyros to make a practical packaging arrangement. Therefore, two-degree-of-freedom accelerometers are much more desirable.

3. The most convenient arrangement for four TDF gyros and four TDF accelerometers is to mount them on the faces of a tetrahedron.

4. The orientation of the torquer axes for a TDF gyro and accelerometer for maximum sensitivity of failure detection and isolation depends on which has the highest probability of failure - one axis or both axes of the instrument. As the analysis shows, a higher probability for both axes to fail together, then the torquer axes should be orientated perpendicular to the parity equation line, as shown in Figure 10.

5. The least amount of hardware that can be mechanized for single-degree-of-freedom instruments is six gyros and six accelerometers. The most practical configuration is to mount a gyro and accelerometer on each face of a dodecahedron, as shown in reference V.

6. If it is required to disperse the sensors throughout the aircraft, because of survivability considerations, a six two-degree-of-freedom gyro and six two-degree-of-freedom accelerometer configuration, as shown in Figure 12, has the least amount of hardware that can be practically mechanized. The sensor axes alignment problem makes any reduction in hardware impractical for fail-op/fail-op redundancy.

AD-A061 449 INCOSYM INC CALABASAS CA F/G 17/7
FAILURE MODES AND REDUNDANCY ANALYSIS FOR THE MULTIFUNCTION INE--ETC(U)
MAR 78 R J CRAIG, J RUSSELL F33615-77-C-3015
UNCLASSIFIED AFFDL-TR-78-25 NL

2 OF 2
AD A061449

END
DATE FILMED
1-79
DDC

7. The mechanization using six two-degree-of-freedom gyros does not suffer from any ambiguity of failure isolation caused by either single or two axes failures.

8. If single axis instruments are used in a distributed configuration, then the sensor alignment problem will require that twelve gyros and twelve accelerometers will be required for a practical packaging arrangement that can maintain a fail-op/fail-op capability - assuming failure detection is to be performed by comparison of the instrument outputs.

9. A power supply should go with each channel of gyro/accelerometer combination. This means a power supply with each axis of SDF gyro/accelerometer and one with each TDF gyro/accelerometer combination. "Cross strapping" power supplies does not reduce size, weight and cost, and it relies in Built-in-Test for failure detection and isolation. Also, electrical shorts in any part of the system can cause a problem for all of the supplies at once, unless a complicated isolation mechanism is implemented.

10. Fast heating of gyros has caused a large degradation in relability because of stresses induced across their hermetic seals. Therefore, unheated gyros will be more appropriate for systems where reliability is critical and fast reaction required.

11. The reduction in the spin speed that has been implemented in strapdown tuned rotor gyros will improve their reliability.

12. The coupling of mass unbalance terms into the level navigation axes will tend to degrade the accuracy in a skewed axes array. The six TDF gyro-accelerometer mechanization shown in Section 3.3 has no mass unbalance coupling as the axes are not skewed.

REFERENCES

I Military Standardization Handbook. Reliability Prediction of Electronic Equipment, Military Handbook 217B, 20 September 1974, Department of Defense.

II "Failure Rate Data" from the Government and Industry Data Exchange Program.

III Investigation of Applications of Two-Degrees-Of-Freedom Dry-Tuned Gyroscopes to Strapdown Navigation Systems, Final Report, NASA CR-132419, April 1974, Teledyne Systems Company, Northridge, CA.

IV Preliminary Design of a Redundant Strapped Down Inertial Navigation Unit using Two-Degree-of-Freedom Tuned Gimbal Gyroscopes, Final Report, NASA CR-145305, October 1976, Litton Guidance and Control Systems, Woodland Hills, CA.

V "A Redundant Strapdown Inertial Reference Unit (SIRU)", Gerald P. Gilmore and Richard A. McKern; Journal of Spacecraft and Rockets, Vol. 9, No. 1, January 1972.

APPENDIX A

AN ANALYTICAL MODEL OF A DYNAMICALLY TUNED GYROSCOPE

ABSTRACT

Analytical model of a multigimbal elastically supported tuned gyroscope is derived and presented. The model is stated in mathematical form and simple block diagram form so that it can be readily used for servo synthesis and analysis, gyro error analysis, gyro test and calibration, compensation of gyro dynamic and static errors and basic gyro design. Examples illustrating use of the model are shown. Simplified derivation of equations for error moment associated with the multigimbal tuned suspension system is also presented.

SYMBOLS

a	Anisoelastic coefficient
a_x, a_y, a_z	Linear accelerations of gyro case resolved along the case-fixed coordinate set
a'_x, a'_y, a'_z	Linear accelerations of gyro rotor resolved along the case-fixed coordinate set
$A, B, C,$	Principal moments of inertia of gyro rotor
A_n, B_n, C_n	Principal moments of inertia of the nth gimbal about gimbal x_n, y_n, z_n axes respectively
B	Gyro bias
D	Damping coefficient - average of D_{no} and D_{ni}.
D_{no}, D_{ni}	Damping coefficients associated with the torsional flexures of the nth gimbal about the outer and inner axes respectively.
D_R	Damping coefficient associated with rotor to case the damping
F_m	Gyro figure of merit.
H	Angular momentum of gyro rotor at speed N

H_o	Angular momentum of gyro rotor at speed N_o
$j = \sqrt{-1}$	
K_{no}, K_{ni}	Torsional stiffness of flexures for the nth gimbal about the outer and inner axes
m	Spin axis mass unbalance coefficient
M	Moment
M_{nx}, M_{ny}	Moments acting on rotor along X_n and OA axis, respectively
n	Number of gimbals
N	Angular velocity of the motor synchronous speed vector
N_o	Gyro tuned angular velocity
P	Pendulosity
q	Quadrature coefficient
R_{1N}	Defined by Eq. (84).
R_{2N}	Defined by Eq. (79).
R_I	Defined by Eq. (56).

R_K	Defined by Eq. (57)
s	Laplacian Operator
SF_{xy}	Scale factor error
t	Time
α_n	Angle between X_n axis of the nth gimbal and X_r of the rotor
α_t	Motor torque angle
β	Phase angle of vibration in space domain
γ	Phase angle of vibration in time domain
$\frac{\delta K}{K_o}$	Per unit scale factor error defined in by Eq. (46).
δN	Difference between tuned speed and spin speed - defined by Eq. (52).
ϕ'_o	Amplitude of angular motion of gyro shaft resolved along case fixed coordinate set
ϕ_x, ϕ_y, ϕ_z	Components of angular displacement of the gyro case relative to inertial space, resolved along case fixed coordinate set

$\dot{\phi}_x, \dot{\phi}_y, \dot{\phi}_z$ Components of angular velocity of the gyro case relative to inertial space resolved along case fixed coordinate set

$\dot{\phi}'_x, \dot{\phi}'_y, \dot{\phi}'_z$ Components of angular velocity of gyro shaft relative to inertial space resolved along case fixed coordinate set

θ_x, θ_y Angular position of rotor relative to the gyro case resolved along case fixed coordinate set

φ_x, φ_y Angles defining attitude of shaft relative to rotor

ζ_x, ζ_y Misalignment angles of shaft axis relative to case fixed coordinate set

ζ_{xy} $= \zeta_x + j\zeta_y$

ζ_{tx}, ζ_{ty} Misalignment angles of torqueraxes relative to case fixed coordinate set

ω Angular velocity

ω_n Nutation Frequency

$\omega_{nx}, \omega_{ny}, \omega_{nz}$ Angular velocities of rotor defined by Eqs. (88), (89) and 90.

ω_{nxy} Defined by Eq. (91)

$\omega_x, \omega_y, \omega_z$ Components of absolute angular velocity of the nth gimbal resolved along gimbal fixed coordinate set

τ Gyro time constant defined by Eq. (53)

d, m_n, P_a, P_b, P_{gn}, P_r, q, q_x, q_y, x_r, y_{gn}, y_r, Δp, Δq are defined in reference 2.

INTRODUCTION

A model of a multigimbal, elastically supported, tuned gyroscope is a set of equations that describe static, dynamic and performance characteristics of the gyro.

Gyro model equations and model block diagram may be used for the following purposes:

a. Servo loop design and analysis

b. Analysis of gyro/servo loop errors induced by angular dynamic environments

c. Analysis of gyro errors induced by static and dynamic translational acceleration inputs

d. Gyro test

e. Gyro adjustments and calibrations

f. Compensation of gyro static and dynamic error characteristics

g. Basic gyro design.

Accuracy of the model is a function of understanding of the various phenomena involved and perhaps it is reasonable to assume that the complexity of the model is directly related to the accuracy. In order that the model be useful it must be simple to use and therefore a set of assumptions must be explicitely stated so that limitations in the accuracy of the model are clearly understood. One of the basic assumptions made in the subsequent presentations of the model is that it applies to a tuned gyro of the symmetric type. Symmetrical tuned gyro is defined as one in which rotor inertias, gimbal inertias and its associated torsional restraints are so selected as to yield the terms $\tau_{2(s)}$ and $F_{2(s)}$ both equal to zero. These terms are defined in Ref. [1], and it may be generally stated that the accuracy of the model is not affected by those terms provided gimbal inertias are small. Most inertial grade gyros fall into the category of the symmetrical type. When dealing with the non-symmetric type tuned gyros caution should be exercized in the use of the presented model for the purpose of servo

synthesis. Detailed discussions of a model representing the non-symmetric gyro is considered beyond the scope of this discussion.

The gyro model is presented in two forms: resolved form and vector form. The variables used with the resolved form are explicitely identified with the input axes of the gyro. For example: simplified gyroscopic equations stated in the resolved form are:

$$M_x = A\dot{\omega}_x + H\omega_y \tag{1}$$

$$M_y = A\dot{\omega}_y - H\omega_x \quad , \tag{2}$$

where the variables M_x and ω_x, M_y and ω_y are explicitely identified with the X and Y axis of the gyro respectively.

Variables used with the vector form are implicitely identified with the input axes of the gyro through an assumed relationship of the form stated by Eq. (3)

$$\xi_{XY} = \xi_X + j\xi_Y \quad . \tag{3}$$

The vector form of the simplified gyroscopic equations is stated by Eq. (4)

$$M_{XY} = A\dot{\omega}_{XY} - jH\omega_{XY} \quad , \tag{4}$$

where

$$M_{XY} = M_X + jM_Y$$

$$\omega_{XY} = \omega_X + j\omega_Y$$

$$\dot{\omega}_{XY} = \dot{\omega}_X + j\dot{\omega}_Y \tag{5}$$

Substituting of (5) into (4) and equating real and imaginary quantities yields the simple gyroscopic equations as stated by Eq. (1) and (2).

In performing the operations indicated in the previous paragraphs, it was noted that:

a. Single equation in the vector form together with the definitions provided by Eq. (3) contains the same information as two equations in the resolved form.

b. The real variable associated with the vector form may be thought of as a vector acting along the X axis of the gyro.

c. The imaginary variable associated with the vector form may be thought of as a vector acting along the Y axis of the gyro.

d. Multiplication of a variable by the operator j phase shifts this variable in space domain through a positive angle equal to $\pi/2$ radians.

Due to more compact notation, simplicity of expressions and ease of servo design the vector form is widely used throughout this discussion. The simplification afforded by this method is well illustrated by the model block diagrams shown in Figure 1 and 2.

The results of work contained in Ref. [1], combined with the definition of a symmetrical tuned gyro, serve as a basis of simplified derivation of the suspension related error moments in the multigimbal elastically supported, tuned gyroscope. This simplified derivation, where the rotor spin axis is assumed invariant relative to the inertial space, is presented in Appendix B. The equations thus determined represent contribution to errors by the suspension system and are stated by Eq. (42).

The section dealing with gyro sensitivities to translational accelerations, presented in Ref. [2], forms a basis for the portion of gyro errors associated with translational inputs. These errors are discussed in Appendix C and summarized by Eq. (71).

Rotor related moments, independent of the suspension systems used, are derived in Ref. [3]. These moments are discussed here in Appendix D and are stated by Eqs. (104) and (105).

GYRO MODELS

The behavior and characteristics of a multigimbal elastically supported tuned gyroscope are derived from the knowledge of the moments acting on the gyroscope due to all causes as discussed in Appendices B, C and D. Assuming that the typical criteria for the use of the principle of superposition are valid in this application, then the resultant torque-to-balance moment, M_{fXY}, that must be applied by the gyro torquer, is equal to the algebraic sum of the rotor-related moments, M_{nXY}, suspension-related moments, M_{sXY}, moment due to translational inputs, M_{tXY}, bias term, B_{XY} and scale factor error SF_{XY}. Thus,

$$M_{fXY} = M_{nXY} - M_{sXY} - M_{tXY} + B_{XY} - SF_{XY} \tag{6}$$

The negative sign used with the moments M_{sXY} and M_{tXY} indicates that these moments are generated within the gyro and equal but opposite moments must be applied by the gyro torquer in order to satisfy the torque-to-balance condition. The term torque-to-balance is used here to denote the condition in which the gyro torquer supplies torque such that the resultant of all torques applied to the rotor, measured relative to the gyro case, is equal to zero.

The terms in Eq. (6) are given in Eqs. (104), (42) and (71). The origin of the term B_{XY} will be discussed later. Substitute Eq.(104) into Eq. (6)

$$M_{fXY} = A(\ddot{\phi}_{XY} + \ddot{\theta}_{XY}) - jH(\dot{\phi}_{XY} + \dot{\theta}_{XY}) + M_{rXY} - M_{sXY} - M_{tXY} + B_{XY} - SF_{XY} \tag{7}$$

Define

$$\dot{M}_{eXY} = M_{rXY} - M_{sXY} - M_{tXY} + \beta_{XY} - SF_{XY} \tag{8}$$

Substituting Eq. (8) into Eq. (7), taking LaPlace transform and rearranging we obtain Eq. (9).

$$\Theta_{XY(s)} = \frac{M_{fXY(s)} - M_{eXY(s)} - A(s - j\omega_n)\dot{\phi}_{XY(s)}}{As(s - j\omega_n)} \tag{9}$$

where

$$\omega_n = \frac{H}{A} \tag{10}$$

Equation (9) is represented in block diagram form and is shown in Fig. A-1. The moment $M_{fXY(s)}$ may be considered to be the command torque, such as for example would be available from the output of the torque-to-balance caging loop where the gyro is used in strapdown mode. The moment, $M_{eXY(s)}$, may be thought of as the total error moment. For ease of reference, the components of this error moment are listed in Table A-1. Equations (56) and (57) define the vectors R_I and R_K and the relation between the rate of change of torque angle α_t, and $\dot{\phi}_Z$ is discussed in Reference [3].

The gyro model in the resolved form may be obtained in the following manner: multiply the numerator and the denominator of Eq. (9) by $(s + j\omega_n)$ and equate real and imaginary coefficients thus obtaining Eqs. (11) and (12)

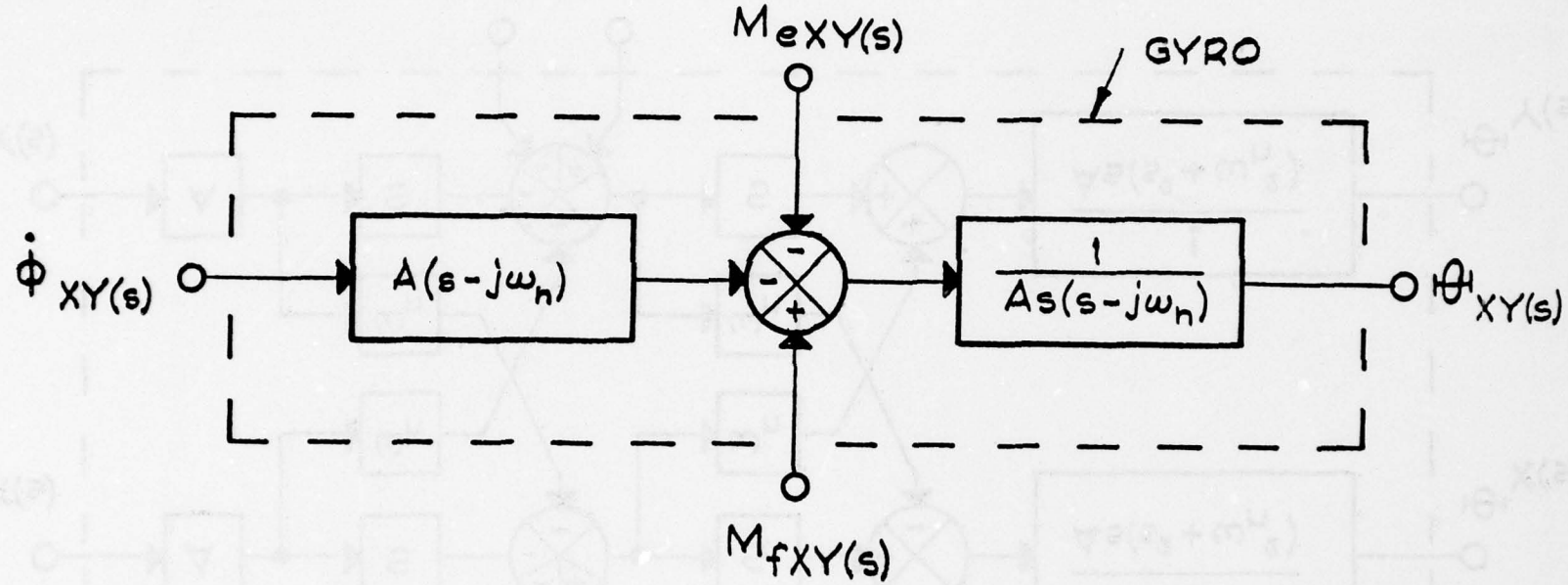

Figure A-1. Block Diagram of a TDF Elastically Supported Gyro - Vector Form

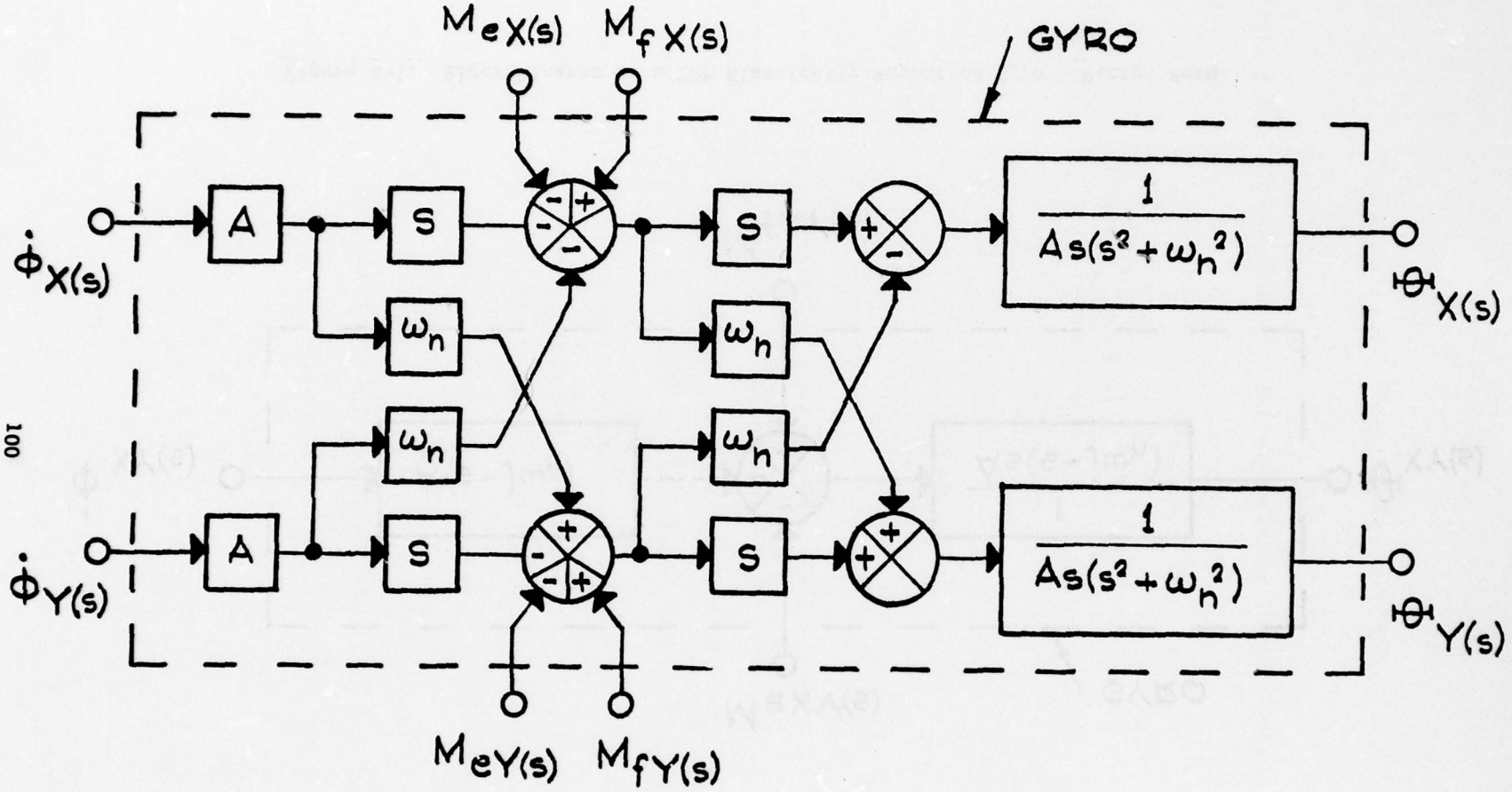

Figure A-2. Block Diagram of a TDF Elastically Supported Gyro - Resolved Form

TABLE A-1. COMPONENT OF THE ERROR MOMENT M_{eXY}

SOURCE	ERROR MOMENT	SYMBOL	EQUATION	FORM OF INPUT
TRANSLATIONAL INPUTS M_{tXY}	QUADRATURE UNBALANCE	M_{tqXY}	qa_{XY}	ARBITRARY
	SPIN AXIS MASS UNBALANCE	M_{tmXY}	$-jma_{XY}$	ARBITRARY
	ANISOELASTIC	M_{taXY}	$-jaa_{XY}a_z$	ARBITRARY
	1 N TRANSLATIONAL	M_{tnXY}	$HR_{1N}a'_z e^{jNt}$	ARBITRARY
			$.5jHR_{1N}a'_{z_0}e^{-j\gamma}\cdot e^{j(N-\omega)t}$	$a'_z = a'_{z_0}\sin(\omega t+\gamma)$
			$.5jHR_{1N}a'_{z_0}e^{-j\gamma}$	$a'_z = a'_{z_0}\sin(Nt+\gamma)$
	2 N TRANSLATIONAL	M_{tvXY}	$HR_{2N}\bar{a}'_{XY}e^{2jNt}$	ARBITRARY
			$5jHR_{2N}\bar{a}'_{XY_0}e^{-j(\beta+\gamma)}\cdot e^{j(2N-\omega)t}$	$a'_{XY} = a'_{XY_0}e^{j\beta}\sin(\omega t+\gamma)$
			$5jHR_{2N}\bar{a}'_{XY_0}e^{-j(\beta+\gamma)}$	$a'_{XY} = a'_{XY_0}e^{j\beta}\sin(2Nt+\gamma)$
ROTOR RELATED M_{rXY}	INERTIA TERM - CROSSCOUPLED COMP.	M_{riXY}	$jA[\dot{\theta}_{XY}\dot{\phi}_z+(\dot{\theta}_{XY}+\gamma_{XY})\ddot{\phi}_z]$	ARBITRARY
	FUNDAMENTAL TERM - CROSSCOUPLED COMP.	M_{rfXY}	$H(\dot{\theta}_{XY}+\gamma_{XY})\dot{\phi}_z$	ARBITRARY
	ANISOINERTIA TERM	M_{raXY}	$-j(C-A)\omega_{nz}\omega_{nxy}$	ARBITRARY
	MOTOR DYNAMICS TERM	M_{rmXY}	$jC\dot{\alpha}_t\omega_{nxy}$	ARBITRARY
	SPIN AXIS ACCEL. COUPLING TERM	M_{rsXY}	$-jC(\dot{\omega}_{nz}-\ddot{\alpha}_t)\theta_{XY}$	ARBITRARY
	TORQUER AXIS MISALIGNMENT TERM	M_{rtXY}	$H(\gamma_{ty}\omega_{nx}+j\gamma_{tx}\omega_{ny})$	ARBITRARY
	ROTOR DAMPING TERM	M_{rdXY}	$D_z\dot{\theta}_{XY}$	ARBITRARY
SUSPENSION RELATED M_{sXY}	DIRECT SPRING RATE	M_{sdXY}	$-\delta N\frac{H}{F_m}\theta_{XY}$	ARBITRARY
	QUADRATURE SPRING RATE	M_{sqXY}	$j\frac{H}{\tau}\theta_{XY}$	ARBITRARY
	2 N ANGULAR	M_{svXY}	$\frac{N_0H_0}{2F_m}\left\{\left[R_K+\left(\frac{N}{N_0}\right)^2R_I\right]\bar{\phi}'_{XY}-j\left[\frac{N}{N_0^2}R_I\right]\dot{\bar{\phi}}'_{XY}\right\}e^{jNt}$	ARBITRARY
			$-\frac{j\phi'_0N_0^2He^{-j(\beta+\gamma)}}{4NF_m}\left[R_K+\left(\frac{N}{N_0}\right)^2\left(\frac{\omega}{N}-1\right)R_I\right]e^{j(2N-\omega)t}$	$\phi'_{XY} = \phi'_0e^{j\beta}\sin(\omega t+\gamma)$
			$-\frac{j\phi'_0N_0H_0e^{-j(\beta+\gamma)}}{4F_m}(R_K+R_I)$	$\phi'_{XY} = \phi'_0e^{j\beta}\sin(2Nt+\gamma),\ N=N_0$
	BEARING NOISE	M_{sbXY}	$\left(\frac{H}{\tau N}-\frac{jH}{2F_m}\right)\dot{\phi}'_{XY}$	ARBITRARY
	BIAS TERM	B_{XY}		
	TORQUER SCALE FACTOR ERROR	SF_{XY}	$H\frac{\delta K}{K_0}\phi_{XY}$	ARBITRARY

$$\Theta_{X(s)} = \frac{(M_{fX(s)} - M_{eX(s)})\, s - (M_{fY(s)} - M_{eY(s)})\, \omega_n - A(s^2 + \omega_n^2)\, \dot{\phi}_{X(s)}}{As(s^2 + \omega_n^2)} \quad (11)$$

$$\Theta_{Y(s)} = \frac{(M_{fX(s)} - M_{eX(s)})\, \omega_n + (M_{fY(s)} - M_{eY(s)})\, s - A(s^2 + \omega_n^2)\, \dot{\phi}_{Y(s)}}{As(s^2 + \omega_n^2)} \quad (12)$$

The block diagram shown in Figure A-2 is based on Eqs. (11) and (12).

The term B_{XY} introduced in Equation (6) accounts for error torques which are not readily identifiable within the classification discussed in Appendices B, C and D. Among the major contributors to this bias error moment are: gyro internal pressure sensitivity bias, internal magnetic coupling sensitivity bias, external magnetic sensitivity bias, motor voltage sensitivity bias, pickoff voltage and frequency sensitivity bias, g-sensitive and non-g-sensitive temperature sensitive biases and all other biases sensitive to external environments.

Inspection of Table A-1 reveals presence of terms which are a function of the input angular rate to the gyro, $\dot{\phi}_{XY(s)}$, and the rotor to case pickoff angle, $\theta_{XY(s)}$. Normally, these terms are considered as constant errors and without appreciable loss in accuracy can be omitted from the transfer functions shown within the blocks in Figures A-1 and A-2. In cases when it is not desirable to make such an approximation, these terms can be readily moved in Figure A-1 so that the transfer function in the left hand block becomes

$$A\left[s - j\omega_n\left(1 - \frac{1}{2F_m}\right)\right] \tag{13}$$

and the transfer function in the right hand block becomes

$$\frac{1}{A\left(s + \frac{1}{\tau_n} - j\omega_n\right)\left(s + \frac{1}{\tau} + j\frac{\delta N}{F_m}\right)} \tag{14}$$

In arriving at Eqs. (13)and (14), the damping term associated with $\dot{\phi}_{XY}$ has been neglected,

$$\frac{1}{\tau_n} \simeq \frac{D_R}{A}\ , \tag{15}$$

and $\dot{\phi}_{XY}$ was assumed equal to $\dot{\phi}'_{XY}$.

ILLUSTRATIONS IN THE USE OF THE GYRO MODEL

Servo loop design and analysis.

There are two principal modes of mechanization of the elastically supported gyro. In one mode, the gyro is used as a two axis angular rate sensor (strapdown applications) and in the other mode the gyro is used to provide two axis angular reference for a stable element. In both these cases, the rotor to case angle is maintained at null by means of a control loop outside of the gyro. Block diagrams in Figures A-3 and A-4 show the two mechanizations. In the strapdown mechanization the transfer function, $S_{XY(s)}$, contains the functions representing the gyro pickoff, demodulator, shaping networks, (pulse electronics) and the gyro torquer. The input torque, $M_{fXY(s)}$, is oriented in such a direction as to keep $\Theta_{XY(s)}$ at null. In the stable element mechanization the transfer function, $P_{XY(s)}$, contains functions representing the gyro pickoff, (resolver), demodulator, shaping networks, gimbal torquers and the platform gimbals. The function of the servo, in this case, is to orient the gimbals in such a way so that $\Theta_{XY(s)}$ is maintained at null. Block diagrams as shown in Figures A-3 and A-4 form a basis of servo loop design and analysis. The use of complex method in servo loop design is discussed in Reference [4].

Gyro/servo loop errors induced by angular dynamic environments.

This type of errors can be obtained directly from the model shown in Figure A-3, by simply applying the desired inputs $\dot{\phi}_{XY}$ and $\dot{\phi}_Z$ and noting the behavior of the torque to balance moment M_{fXY}. The output from an ideal gyro/servo loop configuration is given by

$$M_{fXY} = -jH\dot{\phi}_{XY}. \tag{16}$$

Detailed discussion of these type of errors is presented in Reference [3].

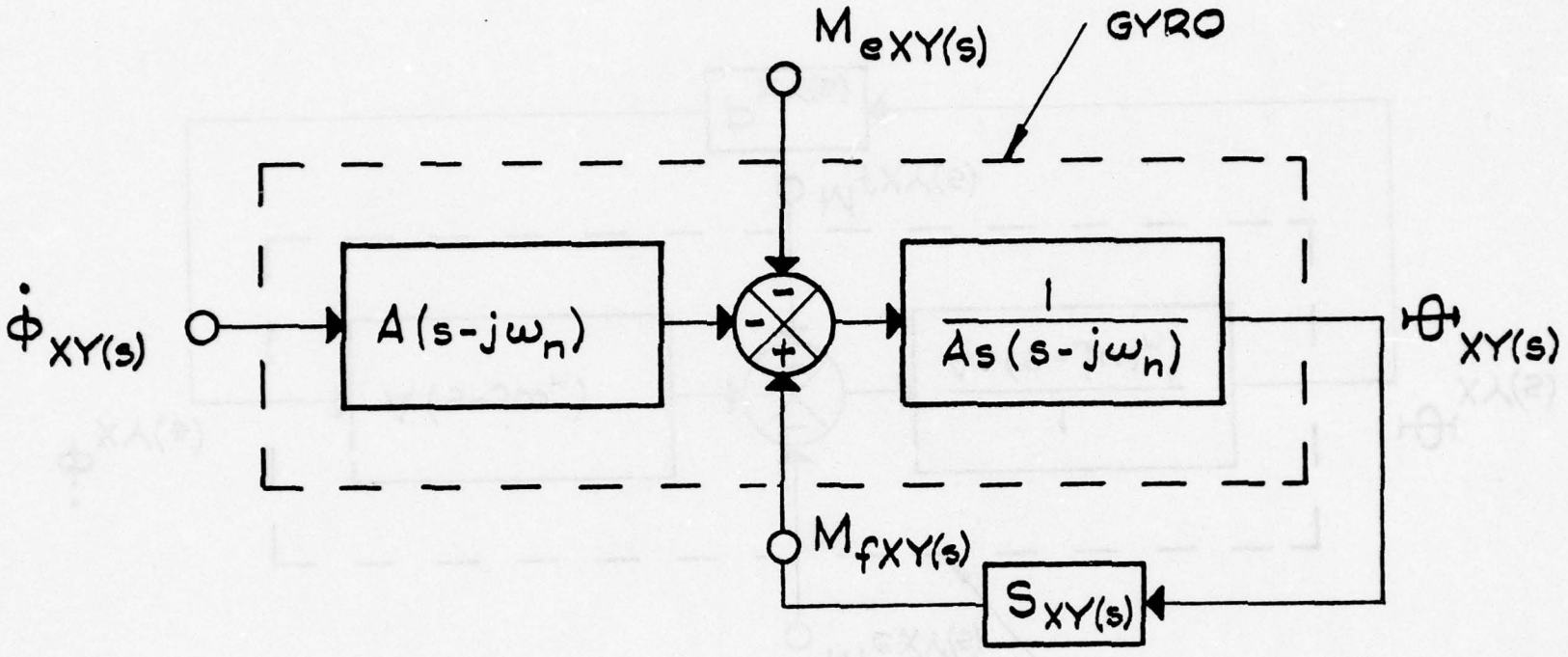

Figure A-3. Elastically Supported Tuned Gyro Mechanized in Strapdown Mode

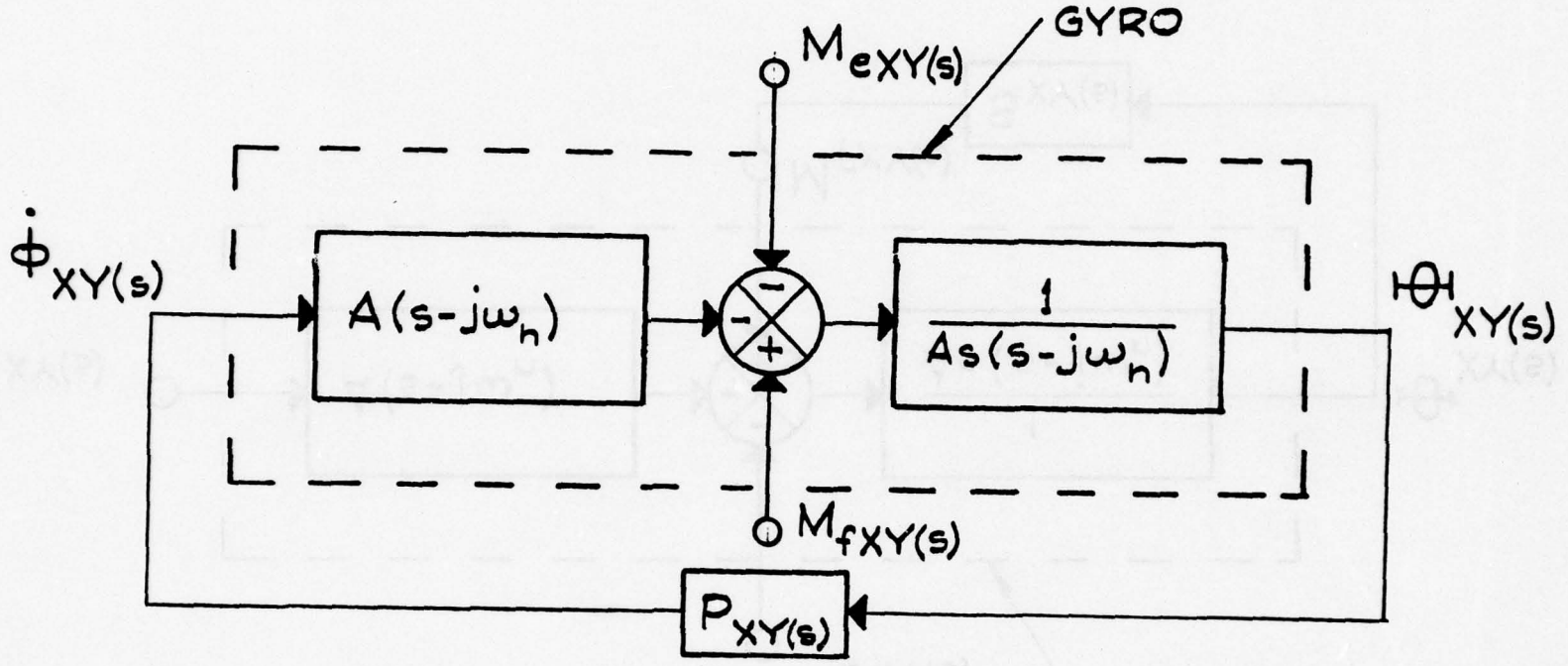

Figure A-4. Elastically Supported Tuned Gyro Mechanized in Stable Platform Mode

Use of gyro model for gyro test and adjustments.

Gyro-level testing for the static parameters is usually performed using constant inputs with the gyro mechanized in the strapdown mode. Under these conditions, and in the absence of angular input rates, the moment applied to the gyro via the gyro torquers is equal to the error moment; i.e.

$$M_{fXY} = M_{eXY} \tag{17}$$

Using Eq. (17) and the appropriate inputs to the gyro, all components of error moments due to translational inputs and all components of suspension related error moments can be isolated, measured and minimized provided that adjustment means are available for this purpose.

Compensation of gyro static and dynamic error characteristics.

From the block diagram of Figure A-3 we obtain

$$\dot{\phi}_{XY(s)} = \frac{M_{fXY(s)}}{A(s - j\omega_n)} - \frac{M_{eXY(s)}}{A(s-j\omega_n)} - s\theta_{XY(s)} \tag{18}$$

Inspection of Eq. (18) reveals that the true input angular rate vector, $\dot{\phi}_{XY(s)}$, can be computed from the knowledge of the feedback torque, $M_{fXY(s)}$, the error torque, $M_{eXY(s)}$, and the rate of change of the pickoff angle, $\theta_{XY(s)}$. It is interesting to note, that when the pickoff angle is available, the true computed angular input rate is independent of the characteristics of the transfer function, $S_{XY(s)}$.

Typically, the feedback torque is available in the integrated form either directly from the pulse rebalance loop or analog rebalance with an A/D conversion.

Integrating and rearranging Eq. (18) we obtain

$$\phi_{XY(s)} + \Theta_{XY(s)} = j\frac{M_{fXY(s)}}{sH} - j\frac{M_{eXY(s)}}{sH} + \frac{js}{\omega_n}\left(\phi_{XY(s)} + \Theta_{XY(s)}\right) \qquad (19)$$

The compensation block diagram, expressed in vector form and shown in Figure A-5 is based on Eq. (19). By normalizing of Eq.(19), one obtains two coupled compensation equations which are shown in the resolved form in Figure A-6. The inputs to the compensation processor, diagramatically depicted in Figure A-5, are the integrals of the vector moments, $\frac{M_{fXY(s)}}{s}$, applied to the gyro rotor by its torquers, rotor to case pickoff angles, $\Theta_{XY(s)}$, and the integral of the error vector moment, $\frac{M_{eXY(s)}}{s}$. The output of the compensation processor is the gyro input angle, $\phi_{XY(s)}$.

It is to be noted that the terms $\frac{M_{fXY(s)}}{s}$ and $\Theta_{XY(s)}$ may be directly obtained from the gyro outputs and typically are processed in an incremental form. The incremental value of the gyro input angle at the end of the n^{th} computational interval is normally based on the value of $\frac{M_{fXY(s)}}{s}$ and $\Theta_{XY(s)}$ for this interval and the correction terms are obtained from the previous computational interval. The correction terms are: integral of the error moment and the pseudoconing term which is of the form

$$\frac{js}{\omega_n}\left(\phi_{XY(s)} + \Theta_{XY(s)}\right).$$

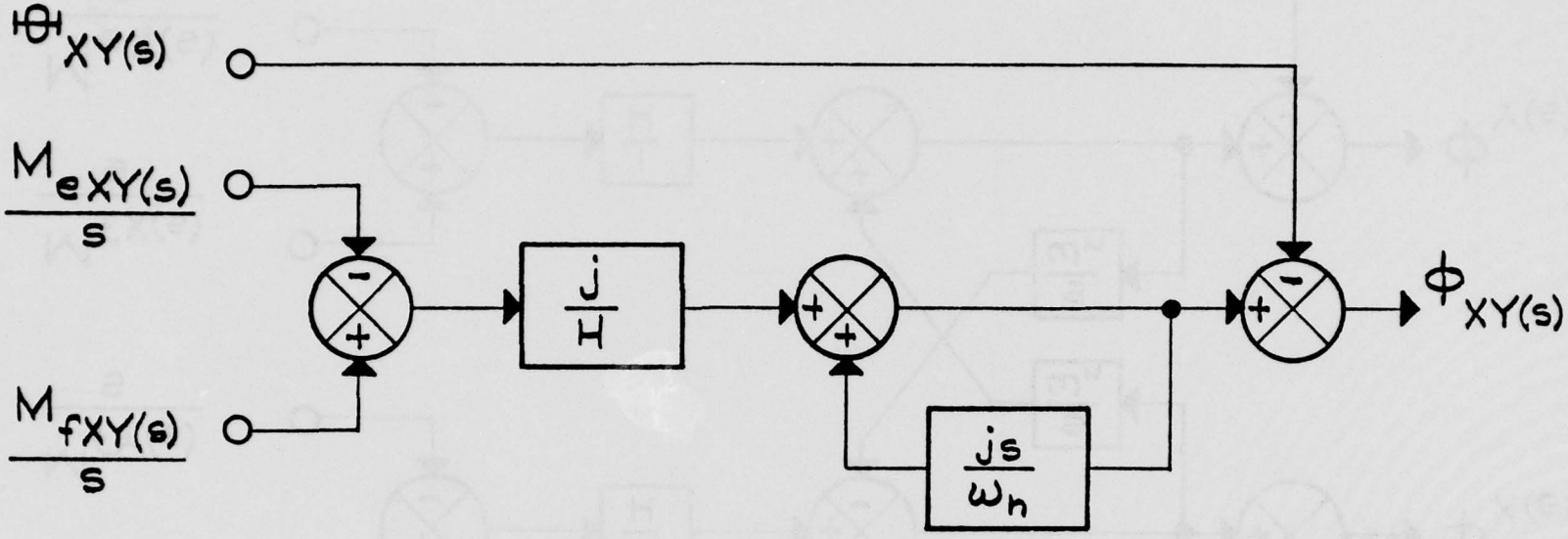

Figure A-5. Compensation Block Diagram - Vector Form
(Rate Integrated Output)

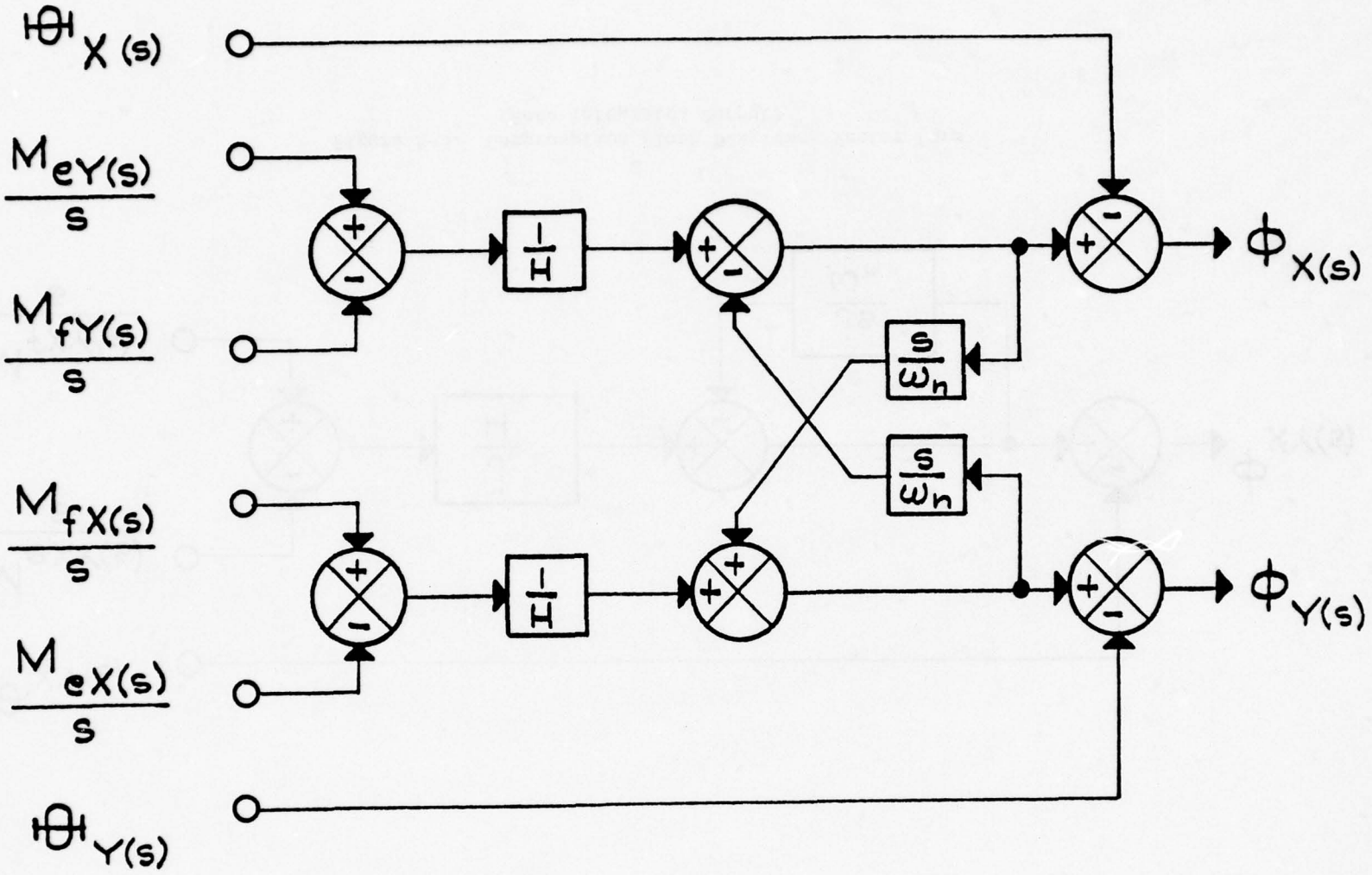

Figure A-6. Compensation Block Diagram - Resolved Form
(Rate Integrated Output)

APPENDIX B

DERIVATION OF SUSPENSION RELATED ERROR EQUATIONS

The derivation of the suspension related error equations presented here this paper are based on Refs. [1], [2] and [3].

The work contained in Ref. [1] was undertaken without specific assumptions as to the ratio of rotor to gimbal inertias. This approach, although very general and rigorous, yields results in a form whose usefulness is somewhat limited by its complexity. However, after the assumption was made in this reference that the gimbal inertias were very small relative to the rotor inertias, the unwieldy expressions became relatively simple. Since the validity of the simplified equations has been confirmed by experimental data, one may then undertake the derivation of the gyro suspension related error equations with an initial assumption that the rotor inertias are very much larger than the gimbal inertias. This assumption may be interpreted to mean that the instantaneous attitude of the rotor spin axis does not change as a function of small angular shaft motions about any axis perpendicular to the rotor spin axis. This approach is adopted here in arriving at the set of error moments, Eq. (42), caused by the multigimbal suspension system.

For ease of reference, four sets of rectangular right-handed coordinate frames will be used. All the sets have a common origin that is coincident with the effective center of torsional support established by rotor-to-shaft torsional elements. The reference sets are shown in Fig. B-1 and are defined as follows:

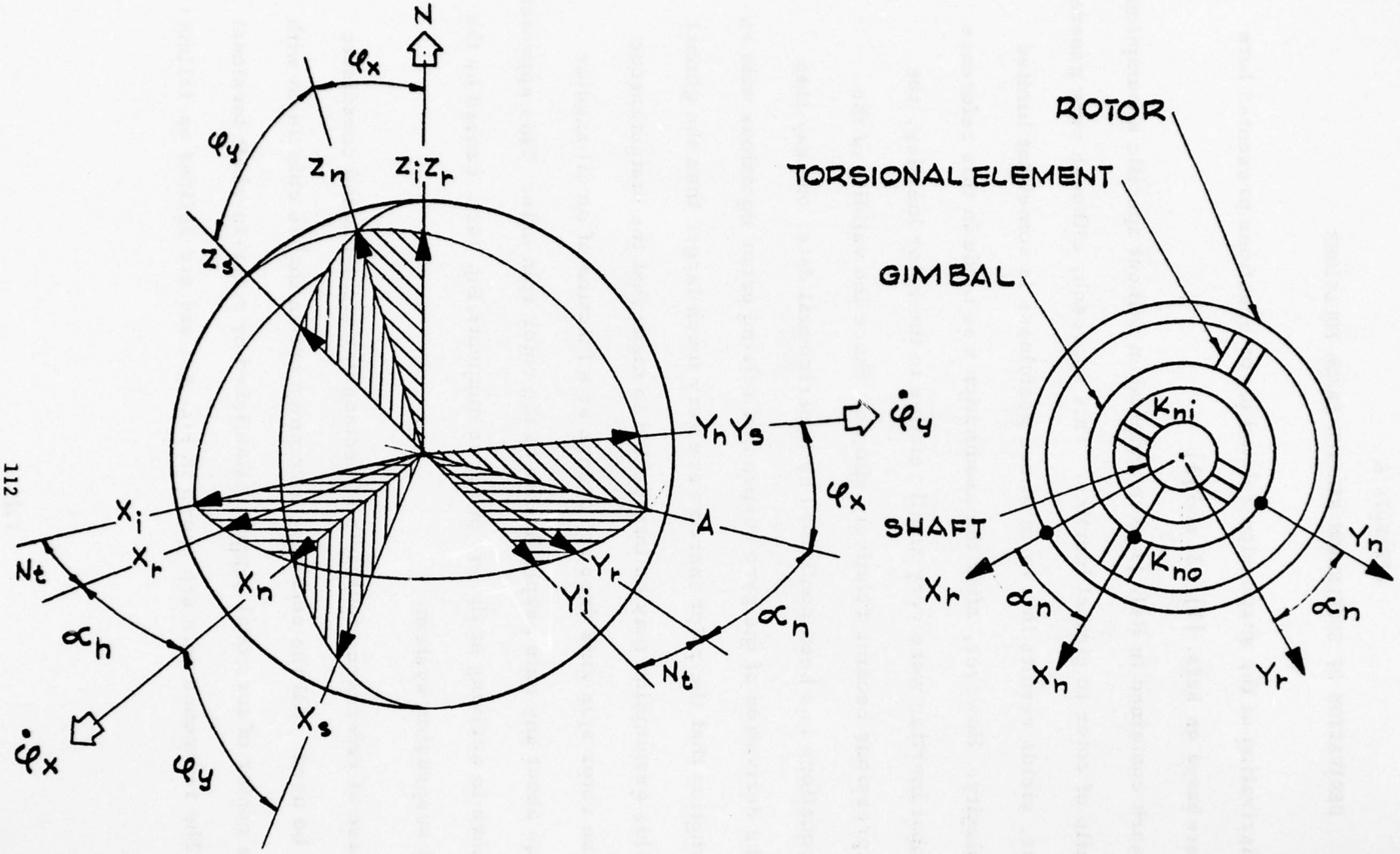

Figure B-1. Relative Attitudes of Shaft, n^{th} Gimbal and Rotor

i - set having coordinates $X_i Y_i Z_i$ fixed in the inertial space

r - set having coordinates $X_r Y_r Z_r$ fixed in the gyro rotor

s - set having coordinates $X_s Y_s Z_s$ fixed in the gyro shaft

n - set having coordinates $X_n Y_n Z_n$ fixed in the nth gimbal.

Next we define the relative angular attitudes of the reference sets. The rotor is assumed to spin about its Z_r axis and by the prior assumption this axis remains invariant relative to the inertial space. Assuming further that the axis Z_r is coincident with the axis Z_i, then at time t = 0 the sets i and r are aligned with each other and at any arbitrary time, t, the r-set is rotated about the Z_i axis through an angle Nt, where N is the rotor spin speed. When the Z_s axis is aligned with the Z_i axis, the n- and s-sets are coincident and both are rotated about the Z_i axis, relative to the r-set, through an angle α_n. Note, that the angle α_n relates the angular position of the n-th gimbal with respect to the rotor. The final attitude of the shaft is generated by rotations of the s-set first about the axis X_n, through an angle φ_x, and then about the axis Y_n through an angle φ_y. Since these angles are assumed to be small, the order of their rotations is not important.

Angular Velocity of the n-th Gimbal

The resultant angular velocity of the n-th gimbal is equal to the vectoral sum of rotor velocity relative to the inertial space and the n-th gimbal velocity relative to the rotor. Thus,

$$\underline{\omega_g} = \underline{N} + \underline{\varphi_x} \tag{20}$$

Resolution of (20) along the n- set yields

$$\omega_x = \varphi_x$$

$$\omega_y = N\varphi_x \tag{21}$$

$$\omega_z = N .$$

It is to be noted that $\dot{\varphi}_y$ does not contribute to gimbal angular velocities because the gimbal to rotor relative velocity about the Y_n axis is equal to zero.

Relationship Between Gyro Case Motions Relative to the Inertial Space and Shaft Motions in Spinning Coordinates

Assume instantaneous angular displacements of the gyro case relative to the inertial space about X_i and Y_i axes are ϕ_X and ϕ_Y respectively. The angular displacements are assumed to be small and therefore will be considered as vectors. Referring to Fig. B-1 we obtain the relationships expressed by (22) and (23)

$$\varphi_x = \phi_X \cos (Nt + \alpha_n) + \phi_Y \sin (Nt + \alpha_n) \tag{22}$$

$$\varphi_y = -\phi_X \sin (Nt + \alpha_n) + \phi_Y \cos (Nt + \alpha_n) . \tag{23}$$

Differentiate (22) and (23)

$$\dot{\varphi}_x = \dot{\phi}_X \cos (Nt + \alpha_n) - \phi_X N \sin (Nt + \alpha_n)$$

$$+ \dot{\phi}_Y \sin (Nt + \alpha_n) + \phi_Y N \cos (Nt + \alpha_n) \qquad (24)$$

$$\dot{\varphi}_y = -\dot{\phi}_X \sin (Nt + \alpha_n) - \phi_X N \cos (Nt + \alpha_n)$$

$$+ \dot{\phi}_Y \cos (Nt + \alpha_n) - \phi_Y N \sin (Nt + \alpha_n) \; . \qquad (25)$$

Moments Exerted on Rotor by the N-th Gimbal Dynamics, Torsional Elements and Damping

The total moment acting on the rotor will be considered to have two components: one along the X_n axis equal to M_{nx}, and the other acting along the OA axis and equal to M_{ny}.

As the gimbal is deflected through an angle φ_x and has an angular velocity, $\dot{\varphi}_x$, relative to the rotor, the moment acting on the rotor along the X_n axis is

$$M_{nx} = K_{no} \varphi_x + D_{no} \dot{\varphi}_x \qquad (26)$$

The moment M_{ny} may be obtained from the following consideration: the principle of equilibrium of moments applied to the gimbal demands that the resultant of all the external moments acting on the gimbal about the OA axis must be equal to the inertia moment of the gimbal about this axis. Thus,

$$-M_{ny} + K_{ni}\,\varphi_y + D_{ni}\,\dot{\varphi}_y = B_n\,\dot{\omega}_y - (C_n - A_n)\,\omega_z\,\omega_x \quad . \tag{27}$$

The inertia moment stated in the right hand side of Eq. (27) is equal to the Y component of the vectorial equation governing the dynamics of the nth gimbal: $M_g = \dot{H}\big]_g + \omega x H$, where $\dot{H}\big]_g$ denotes differentiation of the nth gimbal angular momentum relative to the nth gimbal coordinate reference set.

Rearranging (27) we obtain

$$M_{ny} = K_{ni}\,\varphi_y + D_{ni}\,\dot{\varphi}_y - B_n\,\dot{\omega}_y + (C_n - A_n)\,\omega_z\,\omega_x \tag{28}$$

Substitute (21), (22), (23) and (24) into (26) and (28)

$$M_{nx} = K_{no}\,(\phi_X \cos\beta_n + \phi_Y \sin\beta_n)$$

$$+ D_{no}\,(\dot{\phi}_X \cos\beta_n - \phi_X N \sin\beta_n + \dot{\phi}_Y \sin\beta_n + \phi_Y N \cos\beta_n) \tag{29}$$

$$M_{ny} = K_{ni}\,(-\phi_X \sin\beta_n + \phi_Y \cos\beta_n)$$

$$+ D_{ni}\,(-\dot{\phi}_X \sin\beta_n - \phi_X N \cos\beta_n + \dot{\phi}_Y \cos\beta_n - \phi_Y N \sin\beta_n)$$

$$- B_n N\,(\dot{\phi}_X \cos\beta_n - \phi_X N \sin\beta_n + \dot{\phi}_Y \sin\beta_n + \phi_Y N \cos\beta_n)$$

$$+ (C_n - A_n)\,N\,(\dot{\phi}_X \cos\beta_n - \phi_X N \sin\beta_n + \dot{\phi}_Y \sin\beta_n + \phi_Y N \cos\beta_n) \tag{30}$$

Noting that $e^{j\theta} = \cos\theta + j \sin\theta$ we obtain

$$\cos \beta_n = \frac{1}{2}\left(e^{j\beta_n} + e^{-j\beta_n}\right) \tag{31}$$

$$\sin \beta_n = \frac{1}{2j}\left(e^{j\beta_n} - e^{-j\beta_n}\right) \tag{32}$$

where

$$\beta_n = Nt + \alpha_n \,. \tag{33}$$

Substitute (31) and (32) into (29)

$$\begin{aligned} M_{nx} &= K_{no}\left[\phi_X \frac{1}{2}\left(e^{j\beta_n} + e^{-j\beta_n}\right) + \phi_Y \frac{1}{2j}\left(e^{j\beta_n} - e^{-j\beta_n}\right)\right] \\ &\quad + D_{no}\left[(\dot{\phi}_X + \phi_Y N)\frac{1}{2}\left(e^{j\beta_n} + e^{-j\beta_n}\right)\right. \\ &\qquad \left. + (-\phi_X N + \dot{\phi}_Y)\frac{1}{2j}\left(e^{j\beta_n} - e^{-j\beta_n}\right)\right] \\ &= \frac{K_{no}}{2}\left[(\phi_X - j\phi_Y)\, e^{j\beta_n} + (\phi_X + j\phi_Y)\, e^{-j\beta_n}\right] \\ &\quad + \frac{D_{no}}{2}\left[(\dot{\phi}_X + \phi_Y N + j\phi_x N - j\dot{\phi}_Y)\, e^{j\beta_n}\right. \\ &\qquad \left. + (\dot{\phi}_X + \phi_Y N - j\phi_X N + j\dot{\phi}_Y)\, e^{-j\beta_n}\right] \end{aligned} \tag{34}$$

Define

$$\phi_{XY} = \phi_X + j\phi_Y$$

$$\bar{\phi}_{XY} = \phi_X - j\phi_Y$$

$$\dot{\phi}_{XY} = \dot{\phi}_X + j\dot{\phi}_Y \qquad (35)$$

$$\bar{\dot{\phi}}_{XY} = \dot{\phi}_X - j\dot{\phi}_Y$$

Substitute (35) into (34)

$$M_{nx} = \frac{K_{no}}{2}\left[\bar{\phi}_{XY}\, e^{j\beta_n} + \phi_{XY}\, e^{-j\beta_n}\right]$$

$$+ \frac{D_{no}}{2}\left[(\bar{\dot{\phi}}_{XY} + j\,\bar{\phi}_{XY}\,N)\, e^{j\beta_n} + (\dot{\phi}_{XY} - j\,\phi_{XY}\,N)\, e^{-j\beta_n}\right] \qquad (36)$$

Substitute (31) and (32) into (30) and use (35)

$$M_{ny} = K_{ni}\left[-\phi_X \frac{1}{2j}\left(e^{j\beta_n} - e^{-j\beta_n}\right) + \phi_Y \frac{1}{2}\left(e^{j\beta_n} + e^{-j\beta_n}\right)\right]$$

$$+ D_{ni}\left[(-\dot{\phi}_X - \phi_Y N)\frac{1}{2j}\left(e^{j\beta_n} - e^{-j\beta_n}\right) + (-\phi_X N + \dot{\phi}_Y)\frac{1}{2}\left(e^{j\beta_n} + e^{-j\beta_n}\right)\right]$$

$$+ (C_n - A_n - B_n) N \left[(\dot{\phi}_X + \phi_Y N)\frac{1}{2}\left(e^{j\beta_n} - e^{-j\beta_n}\right)\right.$$

$$\left. + (-\phi_X N + \dot{\phi}_Y)\frac{1}{2j}\left(e^{j\beta_n} - e^{-j\beta_n}\right)\right]$$

$$= \frac{K_{ni}}{2}\left[\left(-\frac{\phi_X}{j} + \phi_Y\right) e^{j\beta_n} + \left(\frac{\phi_X}{j} + \phi_Y\right) e^{-j\beta_n}\right]$$

$$+ \frac{D_{ni}}{2}\left[\left(-\frac{\phi_X}{j} - \frac{\phi_Y N}{j} - \phi_X N + \dot{\phi}_Y\right) e^{j\beta_n} + \left(\frac{\dot{\phi}_X}{j} + \frac{\phi_Y N}{j} - \phi_X N + \dot{\phi}_Y\right) e^{-j\beta_n}\right]$$

$$+ (C_n - A_n - B_n) N \left[\left(\dot{\phi}_X + \phi_Y N - \frac{\phi_X N}{j} + \frac{\dot{\phi}_Y}{j}\right) e^{j\beta_n}\right.$$

$$\left. + \left(\dot{\phi}_X + \phi_Y N + \frac{\phi_X N}{j} - \frac{\dot{\phi}_Y}{j}\right) e^{-j\beta_n}\right]$$

$$= \frac{K_{ni}}{2}\left[j\bar{\phi}_{XY} e^{j\beta_n} - j\phi_{XY} e^{-j\beta_n}\right]$$

$$+ \frac{D_{ni}}{2}\left[(j\dot{\bar{\phi}}_{XY} - \bar{\phi}_{XY} N) e^{j\beta_n} + (-j\dot{\phi}_{XY} - \phi_{XY} N) e^{-j\beta_n}\right]$$

$$+ \frac{1}{2}(C_n - B_n - A_n) N \left[(\dot{\bar{\phi}}_{XY} + j\bar{\phi}_{XY} N) e^{j\beta_n} + (\dot{\phi}_{XY} - j\phi_{XY} N) e^{-j\beta_n}\right] \qquad (37)$$

Equivalent moments due to n gimbals acting on the rotor resolved along the inertially fixed 1-set are:

$$M_{sX} = \sum_{1}^{n} M_{nx} \cos \beta_n - \sum_{1}^{n} M_{ny} \sin \beta_n \tag{38}$$

$$M_{sY} = \sum_{1}^{n} M_{nx} \sin \beta_n + \sum_{1}^{n} M_{ny} \cos \beta_n \tag{39}$$

Multiply (39) by $j = \sqrt{-1}$ and add to (38)

$$M_{sXY} = \sum_{1}^{n} M_{nx} e^{j\beta_n} + j \sum_{1}^{n} M_{ny} e^{j\beta_n}$$

$$= \sum_{1}^{n} (M_{nx} + j M_{ny}) e^{j\beta_n} \tag{40}$$

Substitute (36) and (37) into (40)

$$M_{sXY} = \sum_{1}^{n} \left\{ \frac{K_{no}}{2} \left[\bar{\phi}_{XY} e^{2j\beta_n} + \phi_{XY} \right] \right.$$

$$\left. + \frac{D_{no}}{2} \left[(\dot{\bar{\phi}}_{XY} + j\bar{\phi}_{XY}{}^{N}) e^{2j\beta_n} + (\dot{\phi}_{XY} - j\phi_{XY}{}^{N}) \right] \right\}$$

$$+ j \sum_{1}^{n} \left\{ \frac{K_{ni}}{2} \left[j\bar{\phi}_{XY} e^{2j\beta_n - j\phi_{XY}} \right] \right.$$

$$\left. + \frac{D_{ni}}{2} \left[(j\dot{\bar{\phi}}_{XY} - \bar{\phi}_{XY}{}^{N}) e^{2j\beta_n} - (j\dot{\phi}_{XY} + \phi_{XY}{}^{N}) \right] \right.$$

$$+ \frac{1}{2}(C_n - B_n - A_n)\, N \left[(\bar{\dot{\phi}}_{XY} + j\bar{\phi}_{XY} N)\, e^{2j\beta_n} + (\dot{\phi}_{XY} - j\phi_{XY} N) \right] \Bigg\}$$

$$= \frac{1}{2} \sum_{1}^{n} \Bigg\{ K_{no} \left(\bar{\phi}_{XY}\, e^{2j\beta_n} + \phi_{XY} \right) + K_{ni} \left(-\bar{\phi}_{XY}\, e^{2j\beta_n} + \phi_{XY} \right)$$

$$D_{no} \left[(\bar{\dot{\phi}}_{XY} + j\bar{\phi}_{XY} N)\, e^{2j\beta_n} + (\dot{\phi}_{XY} - j\phi_{XY} N) \right]$$

$$+ D_{ni} \left[(-\bar{\dot{\phi}}_{XY} - j\bar{\phi}_{XY} N)\, e^{2j\beta_n} + (\dot{\phi}_{XY} - j\phi_{XY} N) \right]$$

$$+ (C_n - B_n - A_n)\, N \left[(j\bar{\dot{\phi}}_{XY} - \bar{\phi}_{XY} N)\, e^{2j\beta_n} + j\dot{\phi}_{XY} + \phi_{XY} N \right] \Bigg\}$$

$$= \frac{1}{2} \sum_{1}^{n} \Bigg\{ (K_{no} + K_{ni})\, \phi_{XY} + (K_{no} - K_{ni})\, \bar{\phi}_{XY}\, e^{2j\beta_n}$$

$$+ (D_{no} + D_{ni})(\dot{\phi}_{XY} - j\phi_{XY} N)$$

$$+ (D_{no} - D_{ni})\, (\bar{\dot{\phi}}_{XY} + j\bar{\phi}_{XY} N)\, e^{2j\beta_n}$$

$$+ (C_n - A_n - B_n)\, (j\dot{\phi}_{XY} + \phi_{XY} N)\, N$$

$$+ (C_n - A_n - B_n)\, N\, (j\bar{\dot{\phi}}_{XY} - \bar{\phi}_{XY} N)\, e^{2j\beta_n} \Bigg\}$$

$$= \frac{1}{2} \sum_{1}^{n} \left[K_{no} + K_{ni} - N^2 (A_n + B_n - C_n) \right] \phi_{XY}$$

$$- \frac{1}{2} \sum_{1}^{n} jN (D_{no} + D_{ni}) \phi_{XY}$$

$$+ \frac{1}{2} \sum_{1}^{n} \left\{ \left[(K_{no} - K_{ni}) + N^2 (A_n + B_n - C_n) + jN (D_{no} - D_{ni}) \right] \bar{\phi}_{XY} \right.$$

$$\left. - \left[jN (A_n + B_n - C_n) - (D_{no} - D_{ni}) \right] \dot{\bar{\phi}}_{XY} \right\} e^{2j\beta_n}$$

$$- \frac{1}{2} \sum_{1}^{n} \left[jN (A_n + B_n - C_n) - (D_{no} + D_{ni}) \right] \dot{\phi}_{XY} \qquad (41)$$

Equation (41) states the error moments related to the multigimbal suspension where the gyro shaft is subjected to an arbitrary angular input (small angles) and the attitude of the rotor spin axis is invariant relative to the inertial reference.

Assuming $D_{no} = D_{ni} = D$, the Eq. (41) may be written as

$$M_{sXY} = M_{sdXY} + M_{sqXY} + M_{svXY} + M_{sbXY} \tag{42}$$

with its components defined by Eqs. (43), (44), (45) and (46).

Direct spring rate moment:

$$M_{sdXY} = \frac{1}{2} \sum_{1}^{n} [K_{no} + K_{ni} - (A_n + B_n - C_n) N^2] \phi_{XY} \tag{43}$$

Quadrature spring rate moment:

$$M_{sqXY} = -jnDN\phi_{XY} \tag{44}$$

2N angular moment:

$$M_{svXY} = \frac{1}{2} \sum_{1}^{n} \left\{ [K_{no} - K_{ni} + (A_n + B_n + C_n) N^2] \bar{\phi}_{XY} - jN (A_n + B_n - C_n) \bar{\dot{\phi}}_{XY} \right\} e^{2j\beta_n} \tag{45}$$

Bearing noise moment:

$$M_{sbXY} = \left[nD - \frac{j}{2} \sum_{1}^{n} (A_n + B_n - C_n) N \right] \dot{\phi}_{XY} \tag{46}$$

Analysis of the components of suspension related error moments is presented in the following paragraphs.

The direct and quadrature spring rate moments constitute the errors referred to in Ref. 2. as the errors due to rotor offset angle. These moments produce steady drift rate errors when rotor to shaft angle has a constant non-zero value. Thus, let

$$\phi_{XY} = -\Theta_{XY} \tag{47}$$

and let us assume there exists a tuned spin speed equal to N_o such that

$$\sum_{1}^{n} (K_{no} + K_{ni}) - \sum_{1}^{n} (A_n + B_n - C_n) N_o^2 = 0$$

or

$$N_o = \left[\frac{\sum_{1}^{n} (K_{no} + K_{ni})}{\sum_{1}^{n} (A_n + B_n - C_n)} \right]^{1/2} \tag{48}$$

Substitute (47) and (48) into (43)

$$M_{sdXY} = -\frac{N_o^2 - N^2}{2} \sum_{1}^{n} (A_n + B_n - C_n)\, \Theta_{XY}$$

$$= -\frac{N_o^2 - N^2}{2N} \cdot \frac{H}{F_m} \cdot \Theta_{XY}$$

$$= -\delta N \frac{H}{F_m}\, \Theta_{XY} \tag{49}$$

where

$$H = CN \tag{50}$$

$$F_m = \frac{C}{\sum_{1}^{n} \left(A_n + B_n - C_n\right)} \tag{51}$$

$$\delta N = \frac{N_o^2 - N^2}{2N} \tag{52}$$

It is noted that the direct component of the spring moment is proportional to the square of spin speed.

Define gyro time constant

$$\tau = \frac{C}{nD} \tag{53}$$

Substitute (47), (50) and(53) into (44) and thus obtain a simple expression for the quadrature spring rate moment stated by Eq. (54)

$$M_{sqXY} = j\frac{H}{\tau}\Theta_{XY} . \tag{54}$$

The rectification effects caused by the 2N angular moment are produced by the shaft-to-rotor angular motions that occur at twice the frequency of spin. At these frequencies, the shaft angular motions may be different than those of the gyro case. To allow for this effect shaft angular motions,perpendicular to the spin axis, resolved along the inertial set and denoted ϕ'_{XY} will be used in place of ϕ_{XY} in Eq. (45).

Substituting from (33) into (45) and rearranging, we obtain

$$M_{svXY} = \frac{\sum_{1}^{n}(A_n + B_n - C_n)}{2}\left\{\left[\frac{\sum_{1}^{n}(K_{no} - K_{ni})\,e^{2j\alpha_n}}{\sum_{1}^{n}(A_n + B_n - C_n)} + N^2\frac{\sum_{1}^{n}(A_n+B_n-C_n)\,e^{2j\alpha_n}}{\sum_{1}^{n}(A_n+B_n-C_n)}\right]\bar{\phi}'_{XY}\right.$$
$$\left. - \left[jN\frac{\sum_{1}^{n}(A_n + B_n - C_n)\,e^{2j\alpha_n}}{\sum_{1}^{n}(A_n + B_n - C_n}\right]\dot{\bar{\phi}}'_{XY}\right\} e^{2jNt} \tag{55}$$

Let

$$R_I = \frac{\sum_{1}^{n}(A_n + B_n - C_n)\,e^{2j\alpha_n}}{\sum_{1}^{n}(A_n + B_n - C_n)} \tag{56}$$

$$R_K = \frac{\sum_{1}^{n} (K_{no} - K_{ni})\, e^{2j\alpha_n}}{\sum_{1}^{n} (K_{no} + K_{ni})} \tag{57}$$

Substitute (48), (51) and (56) into (55)

$$M_{svXY} = \frac{C}{2F_m} \left\{ \left[N_o^2 \frac{\sum_{1}^{n} (K_{no} - K_{ni})\, e^{2j\alpha_n}}{\sum_{1}^{n} (K_{no} + K_{ni})} + N^2 R_I \right] \bar{\phi}'_{XY} - [jNR_I]\, \dot{\bar{\phi}}'_{XY} \right\} e^{2jNt} \tag{58}$$

Substitute (50) and (57) into (58)

$$M_{svXY} = \frac{N_o H_o}{2F_m} \left\{ \left[R_K + \left(\frac{N}{N_o}\right)^2 R_I \right] \bar{\phi}'_{XY} - \left[j \frac{N}{N_o^2} R_I \right] \dot{\bar{\phi}}'_{XY} \right\} e^{2jNt} \tag{59}$$

Let the angular motion of the gyro shaft resolved along the i-set be

$$\phi'_X = \phi'_o \sin(\omega t + \gamma) \cos\beta \tag{60}$$

$$\phi'_Y = \phi'_o \sin(\omega t + \gamma) \sin\beta \tag{61}$$

Combining (60) and (61) into vector form we obtain

$$\begin{aligned} \phi'_{XY} &= \phi'_o e^{j\beta} \sin(\omega t + \gamma) \\ &= \phi'_o e^{j\beta} \frac{1}{2j} \left(e^{j(\omega t+\gamma)} - e^{-j(\omega t+\gamma)}\right) \end{aligned} \tag{62}$$

Take conjugate of (62)

$$\bar{\phi}'_{XY} = \phi'_o e^{-j\beta} \frac{j}{2} \left(e^{-j(\omega t+\gamma)} - e^{j(\omega t+\gamma)}\right) \tag{63}$$

Differentiate (62)

$$\dot{\phi}'_{XY} = \phi'_o \omega e^{j\beta} \cos(\omega t + \gamma) \tag{64}$$

$$= \phi'_o \omega e^{j\beta} \frac{1}{2} \left(e^{j(\omega t+\gamma)} + e^{-j(\omega t+\gamma)}\right)$$

Take conjugate of (64)

$$\bar{\dot{\phi}}'_{XY} = \phi'_o \omega e^{-j\beta} \frac{1}{2} \left(e^{j(\omega t+\gamma)} + e^{-j(\omega t+\gamma)}\right) \tag{65}$$

Substituting (63) and (65) into (59) and neglecting terms involving $e^{j(\omega t+\gamma+2\beta_n)}$, as these terms represent error moments at a frequency equal to $N + \omega$, Eq. (59) becomes

$$M_{svXY} = -\frac{j\phi'_o N_o^2 H e^{-j(\beta+\gamma)}}{4NF_m} \left[R_K + \left(\frac{N}{N_o}\right)^2 \left(\frac{\omega}{N} - 1\right) R_I\right] e^{j(2N-\omega)t} \tag{66}$$

When $N = N_o$ and $\omega = 2N_o$, Eq. (66) reduces to Eq. (67)

$$M_{svXY} = -\frac{j\phi'_o N_o H_o e^{-j(\beta+\gamma)}}{4F_m} [R_K + R_I] \tag{67}$$

Bearing noise moment consists of two components: one due to damping and the other due to gimbal inertias. Typically, this moment does not give rise to rectification effects but it provides a mechanism by means of which the bearing generated noise couples into the rotor and thus may account for the "torquer trace" noise in gyros operated in torque-to-balance mode.

Substituting (50) and (53) into (46) the expression for the bearing noise moment becomes

$$M_{sbXY} = \left(\frac{H}{\tau N} - \frac{jH}{2F_m}\right) \dot{\phi}_{XY} . \tag{68}$$

APPENDIX C

ERROR MOMENTS ASSOCIATED WITH TRANSLATIONAL ACCELERATION INPUTS

The origins of error moment due to translational acceleration inputs are discussed in Reference [2]. Equation (68) of Reference [2] states the moment acting on the rotor relative to the gyro case fixed reference coordinate set when accelerations a_{XY} and a_Z are present. For ease of reference Eq. (68), supplemented with the error moment due to anisoelastic effects, is expressed here by Eq. (69).

$$M_{tXY} = (q - j\Delta p)\, a_{XY} + (\Delta q + jp)\, \bar{a}_{XY} e^{2jNt} + (p_a + jp_b)\, a_Z e^{jNt} - ja\, a_{XY} a_Z \tag{69}$$

Substitution of Eq. (61) of Reference [2] into Eq. (69) results in Eq. (70)

$$\begin{aligned} M_{tXY} = {} & \frac{q_x + q_y}{2}\, a_{XY} \\ & - j\left(P_r + \frac{1}{2} \sum_1^n P_{gn}\right) a_{XY} \\ & + \left[\frac{q_x - q_y}{2} + \frac{j}{2}\left(Md + \sum_1^n P_{gn} e^{2j\alpha_n}\right)\right] \bar{a}_{XY} e^{2jNt} \\ & - \left[M(y_r - jx_r) + \sum_1^n m_n y_{gn} e^{j\alpha_n}\right] a_Z e^{jNt} \\ & - jaa_{XY} a_Z \cdot \end{aligned} \tag{70}$$

Equation (70) states the error moment associated with arbitrary translational acceleration inputs a_{XY} and a_Z, to the gyro rotor. This equation may be written as:

$$M_{tXY} = M_{tqXY} + M_{tmXY} + M_{tvXY} + M_{tnXY} + M_{taXY} \quad . \tag{71}$$

The components of Eq. (71) are discussed in the following paragraphs and are defined by Eqs. (72), (73), (74), (77), (78), (80), (82), (83), and (85).

Quadrature moment:

$$M_{tqXY} = \frac{q_x + q_y}{2} a_{XY}$$

$$= qa_{XY} \tag{72}$$

The quadrature components, q, is a function of geometry of torsional elements and thus it is a very stable gyro error parameter.

Spin axis unbalance moment:

$$M_{tmXY} = -j\left(P_r + \frac{1}{2}\sum_{1}^{n} P_{gn}\right) a_{XY}$$

$$= -jma_{XY} \quad . \tag{73}$$

The spin axis unbalance coefficient, m, is a function of rotor and gimbal pendulosities and thus it is somewhat less stable than the quadrature coefficient.

2N translational moment:

$$M_{tvXY} = \left[\frac{q_x - q_y}{2} + \frac{j}{2} \left(Md + \sum_{1}^{n} P_{gn} e^{2j\alpha_n} \right) \right] \bar{a}'_{XY} e^{2jNt}$$

$$= [HR_{2N}] \bar{a}'_{XY} e^{2jNt} \tag{74}$$

The rectification effects caused by the 2N translational moment are produced by effective accelerations of rotor and gimbals occurring at twice the frequency of spin. The actual accelerations of rotor and gimbals may be different than those of the gyro case. This situation may occur when some of the structural frequencies of the gyro are close to the 2N. To allow for these effects a'_{XY} instead of a_{XY} is used in Eq. (74).

Let the accelerations of the gyro rotor and gimbals resolved along the gyro case fixed set be

$$a'_{XY} = a'_{XYo} e^{j\beta} \sin(\omega t + \gamma)$$

$$= a'_{XYo} e^{j\beta} \frac{1}{2j} \left(e^{j(\omega t+\gamma)} - e^{-j(\omega t+\gamma)} \right) \tag{75}$$

Take conjugate of Eq. (75) and substitute it into Eq. (74)

$$M_{tvXY} = HR_{2N} \bar{a}'_{XYo} e^{-j\beta} \frac{j}{2} \left(e^{-j(\omega t+\gamma)} - e^{j(\omega t+\gamma)} \right) e^{2jNt} \tag{76}$$

Neglecting terms involving $e^{j[(2N+\omega)t+\gamma]}$, as these terms are associated with moments at frequency equal to $2N + \omega$, Eq. (76) becomes

$$M_{tvXY} = \frac{jHR_{2N}\,\bar{a}'_{XYo}\,e^{-j(\beta+\gamma)}}{2}\; e^{j(2N-\omega)t} \tag{77}$$

when

$\omega = 2N$, Eq. (77) becomes

$$M_{tvXY} = \frac{jHR_{2N}\,\bar{a}'_{XYo}\,e^{-j(\beta+\gamma)}}{2}\,, \tag{78}$$

where

$$HR_{2N} = \frac{q_x - q_y}{2} + \frac{j}{2}\left(Md + \sum_{1}^{n} P_{gn}\, e^{2j\alpha n}\right) \tag{79}$$

1N Moment:

This moment is due to combination of radial unbalance of rotor and gimbal and acceleration along the gyro spin axis.

$$M_{tnXY} = -\left[M\,(y_r - jx_r) + \sum_{1}^{n} m_n y_{gn}\, e^{j\alpha_n}\right] a_Z\, e^{jNt}$$

$$= [HR_{1N}]\, a'_Z\, e^{jNt} \tag{80}$$

Let $a'_Z = a'_{Zo} \sin(\omega t + \gamma)$

$$= a'_{Zo}\frac{1}{2j}\left(e^{j(\omega t+\gamma)} - e^{-j(\omega t+\gamma)}\right) \tag{81}$$

Substitute (81) into (80) replacing a_Z with a'_Z (for reasons similar to that stated in paragraph following Eq. (74)) and neglect components at frequency $\omega + N$.

$$M_{tnXY} = [HR_{1N}]\, a'_{Zo}\, \frac{j}{2}\, e^{-(\omega t+\gamma)}\, e^{jNt}$$

$$= \frac{jHR_{1N}}{2}\, a'_{Zo}\, e^{-j\gamma} \cdot e^{j(N-\omega)t} \tag{82}$$

when

$\omega = N$, (82) becomes

$$M_{tnXY} = \frac{jHR_{1N}}{2}\, a'_{Zo}\, e^{-j\gamma} \quad , \tag{83}$$

where

$$HR_{1N} = -\left[M(y_r - jx_r) + \sum_{1}^{n} m_n y_{gn}\, e^{j\alpha n}\right] \tag{84}$$

Anisoelastic Moment:

$$M_{taXY} = -ja\, a_{XY} a_Z \tag{85}$$

APPENDIX D

ROTOR RELATED MOMENTS

Consider a tuned-gimbal gyro in which the rotor is supported by a perfect suspension system. A perfect suspension system may be defined as one which in any environment provides translational support for the rotor without imposing upon it error moments discussed in Appendix B.

Moments acting on such perfectly supported rotor, resulting from angular motion of the gyro case, are derived in the Appendix of Reference [3] and are presented here by Equations (86), (87), (88), (89) and (90).

$$M_{nX} = A\dot{\omega}_{nx} + H\omega_{ny} + (C - A)\,\omega_{ny}\omega_{nz} - C\dot{\alpha}_t\omega_{ny}$$

$$+ \circledR_Y C(\dot{\omega}_{nz} - \ddot{\alpha}_t) - \zeta_{ty}H\omega_{nx} + D_R\dot{\circledR}_X \tag{86}$$

$$M_{nY} = A\dot{\omega}_{ny} - H\omega_{nx} - (C - A)\,\omega_{nx}\omega_{nz} + C\dot{\alpha}_t\omega_{nx}$$

$$- \circledR_X C(\dot{\omega}_{nz} - \ddot{\alpha}_t) + \zeta_{tx}H\omega_{ny} + D_R\dot{\circledR}_Y \quad , \tag{87}$$

where

$$\omega_{nx} = \dot{\phi}_X + \dot{\circledR}_X - (\circledR_Y + \zeta_y)\,\dot{\phi}_Z \tag{88}$$

$$\omega_{ny} = \dot{\phi}_Y + \dot{\circledR}_Y + (\circledR_X + \zeta_x)\,\dot{\phi}_Z \tag{89}$$

$$\omega_{nz} = \dot{\phi}_Z + \zeta_y\dot{\phi}_X - \zeta_x\dot{\phi}_Y \tag{90}$$

Equations (86) and (87) are based on Eqs. (A. 16) and (A. 17) of Reference [3] where M_{sx} and M_{sy} are considered to be equal to $D_R\dot{\Theta}_X$ and $D_R\dot{\Theta}_Y$ respectively, thus accounting for rotor to case damping effects. In arriving at Eqs. (88), (89) and (90) products of small quantities were neglected. Multiply (89) by $j = \sqrt{-1}$ and add to (88)

$$\omega_{nxy} = \dot{\phi}_{XY} + \dot{\Theta}_{XY} + j(\Theta_{XY} + \zeta_{xy})\,\dot{\phi}_Z \quad . \tag{91}$$

Differentiate (91)

$$\dot{\omega}_{nxy} = \ddot{\phi}_{XY} + \ddot{\Theta}_{XY} + j\dot{\Theta}_{XY}\dot{\phi}_Z + j(\Theta_{XY} + \zeta_{xy})\,\ddot{\phi}_Z \quad . \tag{92}$$

Multiply (87) by $j = \sqrt{-1}$ and add to (86)

$$M_{nXY} = A\dot{\omega}_{nxy} - jH\omega_{nxy} - j(C - A)\,\omega_{nz}\omega_{nxy} + jC\dot{\alpha}_t\omega_{nxy}$$

$$- jC(\dot{\omega}_{nz} - \ddot{\alpha}_t)\Theta_{XY} + D_R\dot{\Theta}_{XY} + H(-\zeta_{ty}\omega_{nx} + j\zeta_{tx}\omega_{ny}) \quad . \tag{93}$$

Substituting (91) and (92) into (93) we obtain (94)

$$M_{nXY} = M'_{riXY} + M_{riXY} + M'_{rfXY} + M_{rfXY} + M_{raXY} + M_{rmXY}$$

$$+ M_{rsXY} + M_{rtXY} + M_{rdXY} \tag{94}$$

The terms contained in Eq. (94) are defined by Eqs. (95) through (103).

Inertia term - direct component:

$$M'_{riXY} = A(\ddot{\phi}_{XY} + \ddot{\Theta}_{XY}) \quad . \tag{95}$$

Inertia term - crosscoupled component:

$$M_{riXY} = jA[\dot{\Theta}_{XY}\dot{\phi}_Z + (\dot{\Theta}_{XY} + \zeta_{xy})\ddot{\phi}_Z] \quad . \tag{96}$$

Fundamental term - direct component:

$$M'_{rfXY} = -jH(\dot{\phi}_{XY} + \dot{\Theta}_{XY}) \quad . \tag{97}$$

Fundamental term - crosscoupled component:

$$M_{rfXY} = H(\Theta_{XY} + \zeta_{xy})\dot{\phi}_Z \quad . \tag{98}$$

Anisoinertia term:

$$M_{raXY} = -j(C - A)\omega_{nz}\omega_{nxy} \quad . \tag{99}$$

Motor Dynamics term:

$$M_{rmXY} = jC\dot{\alpha}_t\omega_{nxy} \quad . \tag{100}$$

Spin Axis Accel. Coupling term:

$$M_{rsXY} = -jC(\dot{\omega}_{nz} - \ddot{\alpha}_t)\Theta_{XY} \quad . \tag{101}$$

Torquer Axis Misalignment terms:

$$M_{rtXY} = H(\zeta_{ty}\omega_{nx} + j\zeta_{tx}\omega_{ny}) \quad . \tag{102}$$

Rotor Damping term:

$$M_{rdXY} = D_R \dot{\Theta}_{XY} \quad . \tag{103}$$

Equation (94) may be written as

$$M_{nXY} = A(\ddot{\phi}_{XY} + \ddot{\Theta}_{XY}) - jH(\dot{\phi}_{XY} + \dot{\Theta}_{XY}) + M_{rXY} \quad , \tag{104}$$

where the term M_{rXY} may be defined as the rotor related error moment and is given by Eq. (105).

$$M_{rXY} = M_{riXY} + M_{rfXY} + M_{raXY} + M_{rmXY} + M_{rsXY} + M_{rtXY} + M_{rdXY} \quad . \tag{105}$$

REFERENCES

(1) R.J.G. Craig, "Theory of Operation of an Elastically Supported, Tuned Gyroscope", IEEE Trans. on Aerospace and Electronic Systems, Vol. AES-8, No. 3, May 1972.

(2) R.J.G. Craig, "Theory of Errors of Multigimbaled, Elastically Supported, Tuned Gyroscope", IEEE Trans. on Aerospace and Electronic Systems, Vol. AES-8, No. 3, May 1972.

(3) R.J.G. Craig, "Dynamically Tuned Gyros in Strapdown Systems", Conference Proceedings No. 116, North Atlantic Treaty Organization Advisory Group for Aerospace Research and Development, Florence, Italy, 2-5 October 1972.

(4) J.S. Lipman, "Application of the Complex Method to Transform Analysis of Spinning Systems with Rotating Nonsymmetries", presented at the Joint Automatic Control Conf. of the American Automatic Control Council, University of Michigan, Ann Arbor, June 26-28, 1968.

☆U.S.Government Printing Office: 1978 — 657-002/160